MARGARET LOCKHART DICKSON

EXPERIMENTAL AND THEORETICAL INVESTIGATIONS OF A FERROUS/ASCORBATE COMPLEX

THESIS

SUBMITTED FOR THE DEGREE

OF

MASTER OF SCIENCE IN CHEMISTRY

VICTORIA UNIVERSITY OF WELLINGTON

NEW ZEALAND

1966

PREFACE

This thesis is concerned with a field of research which has become of great importance in the last few years, namely the study of metal-ion complexes of biological significance. The topic is one which could have important results in the study of biochemical reactions in vivo.

The author wishes to thank the following: Dr E. Sullivan for his supervision of the thesis, Dr R.M. Golding for helpful discussions on Crystal Field calculations, the Applied Mathematics Division and Chemistry Division, Department of Scientific and Industrial Research, for the use of facilities, and her fiancé, John Bailey, for typing the thesis so well, initiating her into the field of theoretical chemistry and in particular for moral support.

CONTENTS

INTRODUCTION

The importance of trace metal ions in biological processes has been known for some time, but the role of chelating molecules in the human body is a comparatively new and interesting field of research [1]. Among the important complexes occuring in the body are haemoglobin, containing iron, and vitamin B-12, containing cobalt, both essential to human health. Other well-known naturally occuring complexes include cytochrome oxidase, containing both iron and copper, and chlorophyll, containing magnesium.

The transition metal ions of the First Transition Series are well-known for their ability to form complexes with suitable ligands, and in particular with chelate ligands which can seize the metal ion like a claw (chele means claw in Greek). Many of these complexes have been characterized experimentally, and their properties interpreted by theoretical calculations. However, the complexes arising from biological systems are much more difficult to study, partly because of their greater size and special properties.

In this thesis, a system containing ferrous ions and ascorbate ions is considered. Ferrous ion and ascorbic acid (or vitamin C) are both important in human beings, and need

to be assimilated from our daily food. Haemoglobin, which is a ferrous complex of porphyrin associated with a globular protein, is responsible for the transport of oxygen from the lungs around the body. A deficiency of iron leads to anaemia. Vitamin C, found in fresh fruit and vegetables, is necessary to prevent scurvy-like symptons such as abnormal tooth structure, anorexia, anaemia and predisposition to some infectious diseases. As the vitamin is readily oxidized, its content may be very small in cooked, canned or dried foods.

These two important substances are considered to form a complex, the ascorbate ions chelating to the ferrous ion at pH 7, which is the physiological pH of the body. The usual techniques of physical chemistry are used in an attempt to characterize the complex, both in solution and as an isolated solid, using mainly spectroscopic methods.

The gathering of experimental evidence then enables suitable theoretical calculations to be performed, on both the considered complex and its component species, in an attempt to gain an understanding of the complex. With large biological molecules, it is possible to do only semi-empirical type calculations at present, as the size of the calculation is limited by the size and speed of the computer available. As these factors are improved, it is hoped that biological

systems will be studied by more rigorous methods.

Although the biochemical significance of this complex has not been considered in this thesis, this investigation is a step on the way to discovering more about those complexes which are of biological importance.

Chapter I LITERATURE SURVEY

In 1954, Udenfriend and his coworkers [2] described a reaction system, composed of ascorbic acid, oxygen and ferrous ions, which hydroxylated aromatic compounds to give products with phenolic properties. Previous studies on the metabolism of drugs in the body had shown that compounds of aromatic nature were hydroxylated in the body to yield substances with phenolic properties. For example, aniline gave p-aminophenol and o-aminophenol [3], and quinoline gave 3-hydroxyquinoline [4]. These compounds yielded identical products when acted on by Udenfriend's reaction system. The abundance of ascorbic acid and ferrous compounds in animal tissues suggested that ascorbic acid might be used in biological hydroxylations of both naturally occuring and foreign compounds with aromatic character [5]. The use of ascorbic acid system as a synthetic hydroxylating agent was proposed: the hydroxyl group generated, being electrophilic, would hydroxylate aromatic or heterocyclic rings at electronegative sites.

The properties of this hydroxylating system were reviewed by Mason [6], who suggested that the system would serve as a model for mixed function oxidases, in particular phenylalanine hydroxylase. A mixed function oxidase is

defined as an enzyme which catalyses the consumption of one molecule of oxygen per molecule of substrate, one atom of this oxygen molecule appearing in the product, the other being reduced. The model system showed (i) a characteristic dependence upon a reducing agent and oxygen, (ii) the introduction of molecular oxygen as hydroxyl into aromatic systems, and (iii) electrophilic properties. By studying the simpler model system, it was hoped to be able to explain the mechanism of the enzyme reaction.

At first, it was suggested that the hydroxylating intermediate was the hydroxyl radical. However, further examination of the products formed in the reaction showed that the hydroxyl radical was not the hydroxylating species when oxygen was the oxidant [7]. Another suggestion was that the intermediate was the cation OH^+, although it was doubtful if this existed in aqueous solution. More recent proposals have been the formation of an intermediate complex between the ferrous ion and ascorbic acid. These will now be discussed in detail.

Hamilton and his coworkers [8] performed experiments using the model system and a simple saturated hydrocarbon, cyclohexane, to investigate the Udenfriend reaction. In the presence of oxygen, the model ascorbic acid system produced both cyclohexanol and cyclohexanone. When either

the oxygen or the ascorbic acid was omitted in the experiment, no products were formed. Hydrogen peroxide was used in another two of the experiments to test for the participation of hydroxyl. When oxygen was absent, no products resulted, whereas with oxygen present the products obtained included some not obtained in the Udenfriend reaction. From these experiments, it was concluded that the model system did not involve hydroxyl radical as the oxidizing agent.

The phenylalanine hydroxylase had been shown to require a cofactor, tetrahydropteridine (A), for enzymatic conversion to tyrosine [9], which had structural features similar to the enediol structure of ascorbic acid (B). On identification of the cofactor, 2,4,5-triamino 6-hydroxy pyrimidine (C) was suggested as a model system, this giving similar reaction products to the ascorbic acid system, and being closer in structure to the cofactor.

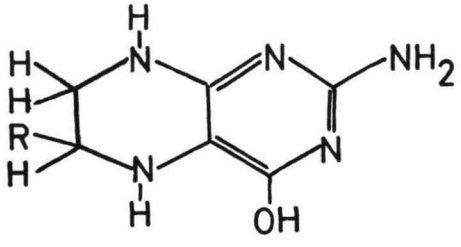

A

phenylalanine hydroxylase cofactor

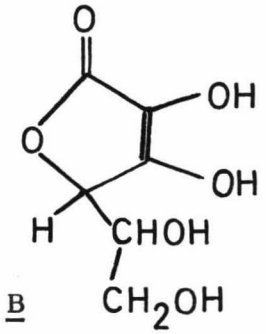

B

ascorbic acid

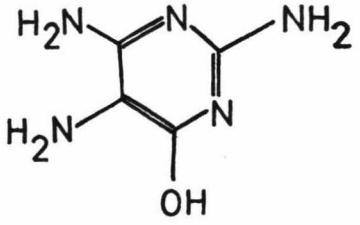

C

2,4,5-triamino 6-hydroxy pyrimidine

Both the model and enzymatic systems were supposed to react by the following mechanism [10]:

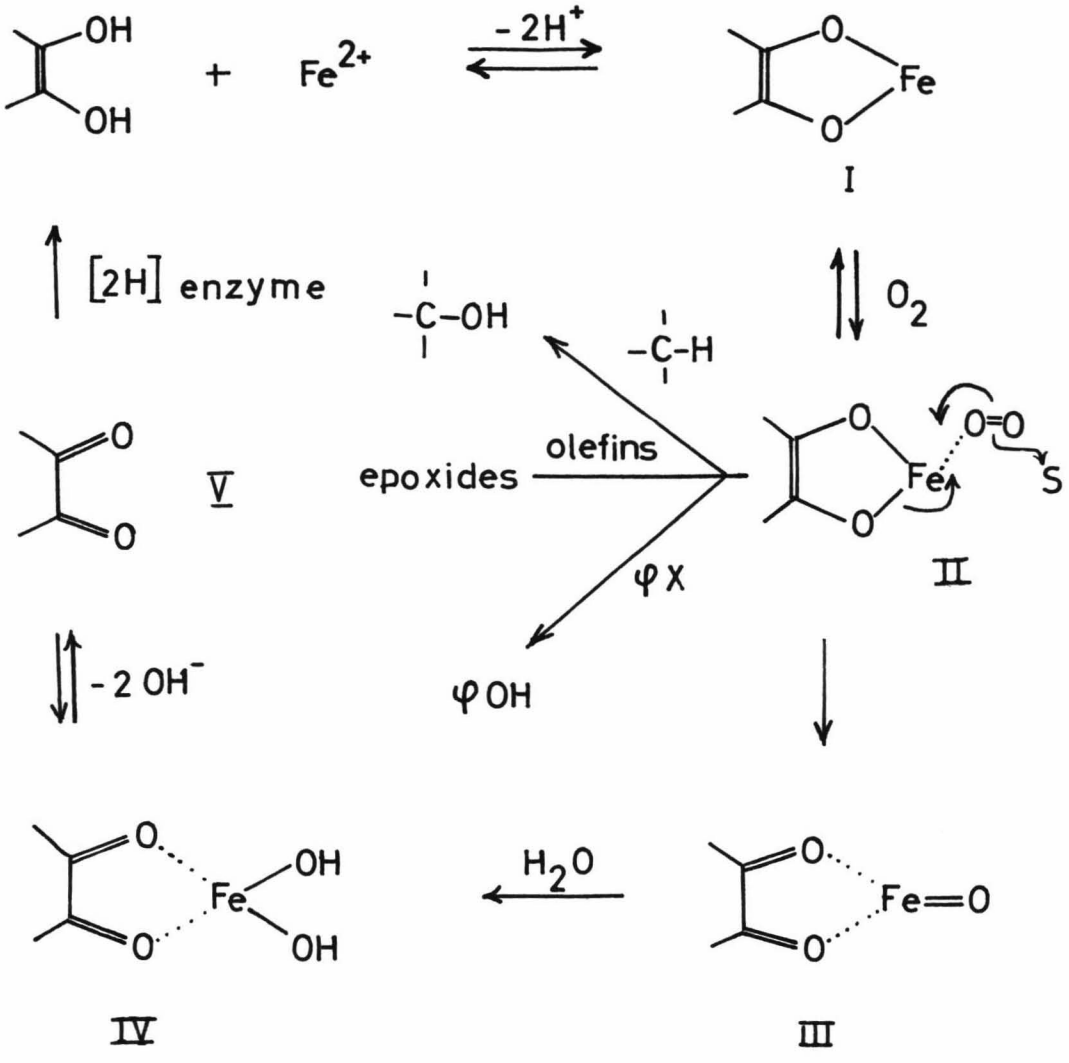

This mechanism is shown for the ascorbate reaction, but one of the oxygens in the ene-diol could be replaced by N-R as in the cofactor with little change in the mechanism.

Hamilton explains this, as follows: "The enediol structure, ferrous ion and oxygen could be in equilibrium with a complex such as II, which is proposed as the actual oxidizing agent. By a shift of electrons, as shown, an oxygen atom with six electrons could be transferred from II to an organic substrate if at the same time the enediol complex is oxidized to the dicarbonyl complex, III. It is not proposed that II would generate a free oxygen atom, but in the presence of a substrate molecule, complex II could act as an "oxenoid" species (named in analogy to the carbenoid species which can transfer a divalent carbon during reaction [11]). The formation of phenols, alcohols and epoxides by reaction with II with appropriate substrates should occur in a way analogous to the formation of methyl compounds and cyclopropanes by reaction of carbenes or carbenoid species with similar substrates [11]. The transformation of II to III is an overall four-electron oxidation and requires that the enediol be oxidized at the same time as the substrate is oxidized. This is observed for phenylalanine hydroxylase [9]. Complex III would be expected to add water to give IV which should be in equilibrium with ferrous ion, hydroxyl ion and the dicarbonyl compound V. In the model system, the ferrous ion could recycle but during the oxidation the ascorbic acid would be oxidized to dehydroascorbic acid and could not recycle.

However, in the enzymatic reaction the oxidized cofactor would have to be reduced back to the tetrahydropteridene level so that it could recycle. This would explain the requirement for a reducing agent in oxidations by mixed-function oxidases.

Several variations of the proposed mechanism can be envisaged. One possibility is that the enediol, ferrous ion, and oxygen form a complex such as VI which by a shift of electrons and a proton as shown, could presumably transfer an oxygen atom to an organic substrate (S) and form a complex VII. Such a reaction would be subject to general acid and

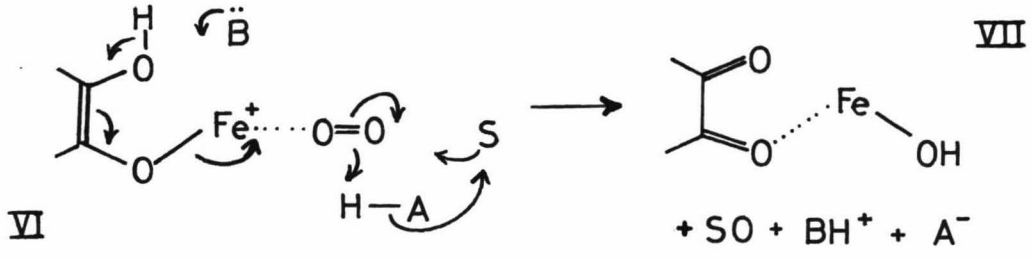

general base catalysis, which could partially explain why the enzyme reaction proceeds more rapidly than the model reaction. Also, if such a mechanism were true, then it would not be necessary for both groups to complex with the metal ion and vinylogous enediols might also be reactants".

The important feature of this mechanism is that a metal ion must form a complex with molecular oxygen and some system capable of oxidation by two electrons such as an enediol.

The metal ion's function would seem to be to form an electronic link between the enediol and the oxygen [7], as well as probably allowing the conversion of the triplet oxygen (two unpaired electrons) to a singlet species (no unpaired electrons). Radical or diradical intermediates would not be necessary in the reaction of complex II with the substrate.

A similar mechanism has been postulated for the catalytic auto-oxidation of ascorbic acid by cupric ion, by Weissburger and his coworkers [12]. The cupric ion forms a chelate with

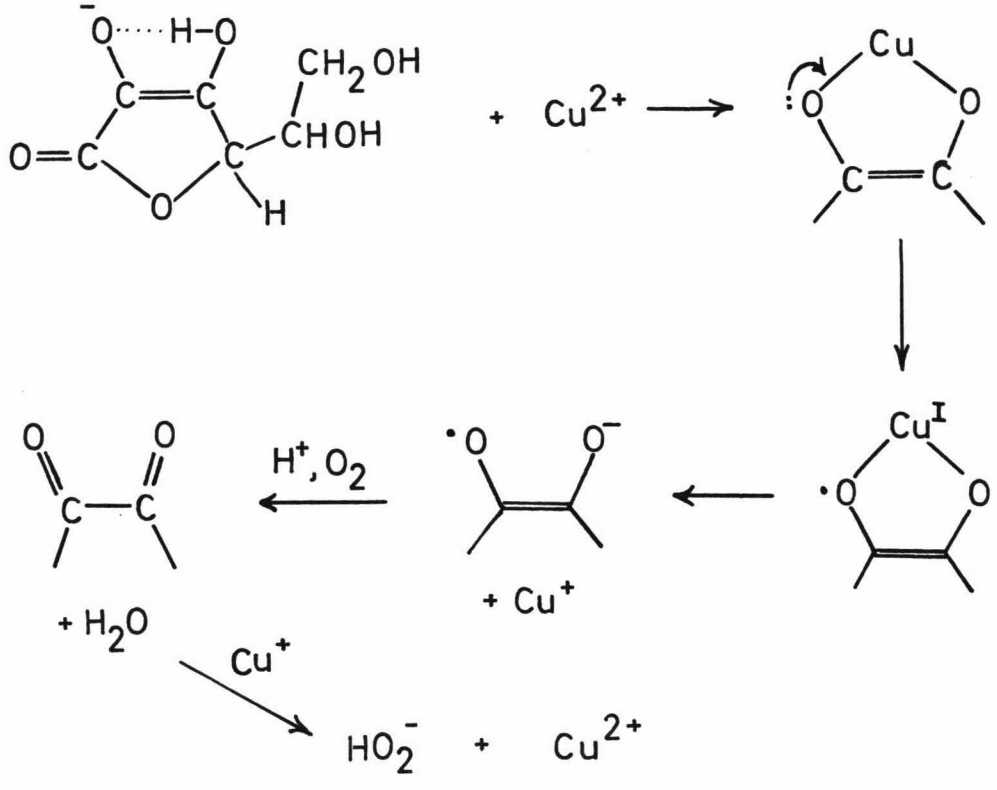

the ascorbate ion, which by an electron shift to the metal acquires a semiquinone structure. Dissociation then takes place, since monovalent copper does not have a strong affinity for oxygen donors. Both the cuprous ion and the semiquinone are oxidized by oxygen. The catalytic effect of cupric ion increases the rate of oxidation of ascorbic acid ten thousand fold [13].

However, iron has a greater significance in biological systems than any other transition metal cation, mainly on account of its abundance, so the main reaction to be studied in this thesis is that of ferrous ions with ascorbic acid.

Chapter 2 PRELIMINARY INVESTIGATION

2.1 Introduction

Before starting to investigate the formation of a complex in the Udenfriend reaction, it was decided to find out as much information as possible about the component species of the model enzyme system, namely ascorbic acid and ferrous sulphate. Some of their properties, obtained from the literature, are given in this chapter, while others will be discussed in the relevant section in chapter 3.

The investigation and discovery of a complex, together with a few of its properties, is discussed.

2.2 Ascorbic Acid [14]

L-Ascorbic acid (vitamin C) has FW 176.12, and is represented as shown [14]. It crystallizes as white needles or plates, mp 190-192°C. 1 gm dissolves in 3 mls water, in 50 mls absolute alcohol and in 100 mls glycerol. It is insoluble in benzene, ether, petroleum ether, and most organic solvents. Having two assymmetric carbon centres, it gives a specific rotation, $[\alpha]_D^{20}$,

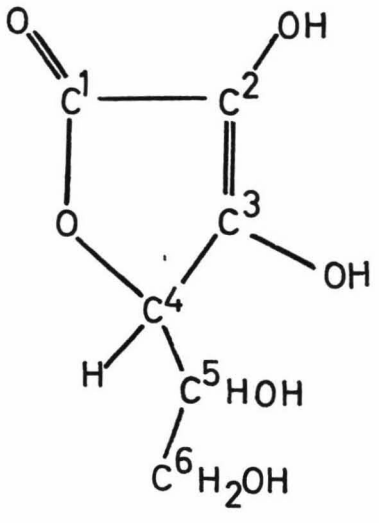

of $+21^{\circ}$ in water and $+48^{\circ}$ in methanol. The D-form differs only in the configuration about C-4. In aqueous solution, the H atom of the enol group at C-3 dissociates, yielding a solution with a pH of about 3. It behaves as a monobasic acid, forming salts containing one monovalent metal atom or its equivalent. In alkaline solution, the H of the enol group on C-2 dissociates and may be replaced by a metal ion. The acidic dissociation constants, $pK_1 = 4.17$ and $pK_2 = 11.57$, show that it is a comparatively strong acid. At neutrality, the absorption maximum in the UV spectrum occurs at 265 mμ, with a small band between 350 and 400 mμ , but shifts towards shorter wavelengths with decreasing pH.

The crystals are stable in air for years, but in solution ascorbic acid is easily oxidized, the instability increasing with increasing pH. Mild oxidation with air, H_2O_2 or $FeCl_3$ converts it to dehydroascorbic acid. Above pH 5, this readily undergoes rearrangement to diketogulonic acid.

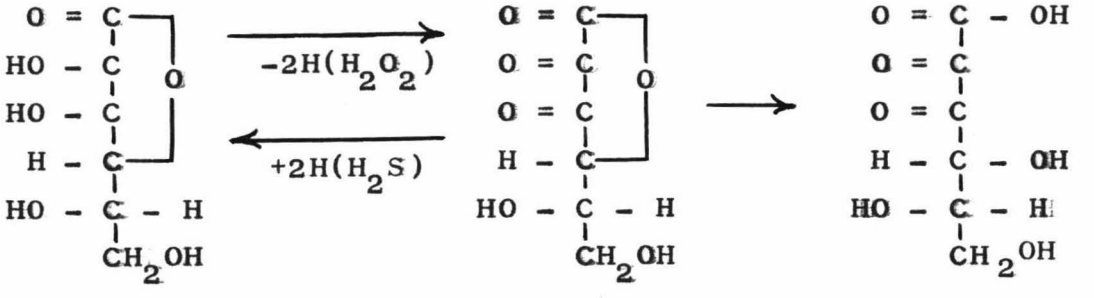

L-Ascorbic Acid | Dehydroascorbic Acid | Diketogulonic Acid

Once the lactone ring is opened, the molecule is readily oxidized and may be degraded to oxalic acid. Hence ascorbic acid is a strong reducing agent. Oxidation of ascorbic acid by molecular oxygen is catalysed by Cu^{2+} and Ag^{+} ions. The ease of oxidation is reduced by use of an inert atmosphere (N_2 or CO_2), storage at low temperatures and absence of light.

Further properties, such as the NMR spectra of ascorbic acid and its sodium salt, will be discussed in section 3.5.

2.3 Ferrous Sulphate [15]

Ferrous sulphate heptahydrate (green vitriol, copperas), $FeSO_4.7H_2O$, has FW 278.03. It crystallizes from solution at ordinary temperatures as blue-green monoclinic crystals, mp 64°C, density (15°C) 1.899 gm/cc. It is very soluble in water, dissolving nearly half its weight in cold water, and nearly its own weight in boiling water, but solubility data is conflicting. It is soluble in glycerol, insoluble in alcohol, acetone, methyl and ethyl acetate. The UV spectrum shows a strong maximum at 950 mμ and a weak maximum at 1070 mμ, which gives ferrous sulphate its characteristic blue-green colour.

The green crystals are efflorescent in dry air and oxidize in moist air forming a brown coating of basic ferric sulphate. It is said that the green colour is due to the

presence of a basic salt and when free from this salt, the crystals are bluish-white and stable in air. In acid or neutral solutions at room temperature, ferrous sulphate is oxidized fairly slowly by air. Passing air into a 0.1 N solution at 25°C oxidizes 0.03 % per hour. The oxidation is more rapid in alkaline solution and is accelerated by an increase in temperature and exposure to light. The rate is reduced by a high concentration of chlorides and sulphates of sodium, potassium and magnesium, as these decrease the solubility of oxygen.

X-ray studies show that the 7 H_2O are not symmetrically located nor equivalent to one another in their structural relations to other constituents. On heating, the tetra and monohydrates are formed at 56.6 and 65.0°C, the last H_2O being driven off at a much higher temperature to give the white anhydrous salt.

Further properties, such as the Mössbauer spectrum and magnetic susceptibility, will be discussed in sections 3.7 and 3.8.

2.4 The Ferrous/Ascorbate Complex

As Hamilton [10] had postulated that a complex was possibly formed between ferrous ion and ascorbic acid in the presence of oxygen, the logical step was to try and

characterize it. After several attempts, a beautiful purple solution was obtained when ferrous sulphate was added to a solution of ascorbic acid which had previously been neutralized to pH 7 by addition of sodium hydroxide solution, i.e. to sodium ascorbate solution. This purple solution was rather unstable in the presence of air, gradually becoming lighter in colour and finally becoming a yellow solution of possibly oxidized ascorbic acid and ferrous sulphate.

Preliminary investigation of the UV spectrum suggested that for efficacious production of the complex, a ratio of 3 moles of sodium ascorbate to 1 mole of ferrous sulphate would be suitable. A detailed discussion of this is given in section 3.3. The purple solution could be conveniently prepared by dissolving known amounts of solid ferrous sulphate and solid sodium ascorbate in the solvent, usually water.

To demonstrate the effect of oxygen on the complex, the following experiments were performed:

(1) A small foil bucket containing sodium ascorbate and ferrous sulphate was suspended by a cotton thread in a gas bubbler. Nitrogen was passed through water below the bucket in the bubbler for about an hour. Then, the cotton was released to lower the bucket into the water. Only a faint tinge of purple was noticed in the water. After a quarter of an hour, the nitrogen flow was stopped and air passed through.

Immediately, a deep purple solution was obtained.

(2) This purple solution was then used for the next experiment. Half of it was placed in a beaker and left open to the atmosphere. Nitrogen was again passed through the remaining solution in the bubbler. After several hours, the solution in the beaker had become much fainter, whereas that in the bubbler was still purple. The former became yellow after 24 hours; but as long as the nitrogen was passed through, the purple solution remained purple.

These experiments clearly indicated the important role oxygen had in the system, as had been shown by Hamilton et al [8]. Oxygen was necessary to form the complex, but excess oxygen destroyed the complex. For experimental work, it was thus necessary to have conditions such that the complex was stable for long enough to carry out the experiments.

The next step was to isolate a solid complex. Great difficulty was experienced in attempting to obtain a pure solid species. The first method of obtaining the solid was to remove the water from the purple solution containing 3 moles of sodium ascorbate and 1 mole of ferrous sulphate, by using a rotary vacuum evaporator. A black shiny mass of solid was obtained after drying in a vacuum desiccator. This method was convenient but any by-products or impurities would also be left in the solid.

Another method of preparation was then tried. 1 mole of Analar $FeSO_4.7H_2O$ and 3 moles of the sodium salt of L-Ascorbic acid were added to a sufficient volume of methanol to dissolve the solids. Nitrogen was passed through the resulting purple solution which was warmed gently in a water bath for several hours. Precipitation was effected by the addition of isopropanol. The flocculent blackish precipitate was filtered off and placed in a vacuum desiccator to dry. The solid obtained was a black-purple powder.

Unfortunately, neither of these methods produced a crystalline complex, nor apparently a pure species. Analysis figures on the sample prepared by the first method, obtained from Dr Campbell of Otago University, showed that there was a considerable amount of sulphur present:

C 26.45 % H 3.75 % S 4.14 % .

The ratio C:H:S was calculated as 17:29:1 or 1:1.70:0.06 (18:31:1). No other analysis figures were obtained. The formula assumed from this was $NaFe(C_6H_7O_6)_3.Na_2SO_4.xH_2O$, where x is about 4 or 5, i.e. some water was present either as water of hydration loosely bound to the complex or absorbed from the atmosphere by the solid.

The solid was soluble in water and in methanol, yielding a purple solution, but insoluble in acetone, chloroform, benzene and carbon tetrachloride. On heating, it started to

decompose at 68°C becoming shiny and black, and melted at about 80°C. This large range of melting would suggest that the solid contained some water. The solid complex was apparently stable provided it was kept in a desiccator.

To characterize the solid, infrared (IR) spectra were run of the solids made by each method and these were compared with the spectra for ferrous sulphate and sodium ascorbate as given in the literature [16]. The spectra for the two solids were to all appearances much the same, one being given in figure 2.1. The bands were assigned using tables of IR frequencies for characteristic bands [17]. The sulphate band, occuring in the region 1050-1200 cm^{-1}, obliterated much of the portion of the graph where ascorbic acid bands are expected. However, there were two bands, one at 1620 cm^{-1}, the other at 1725 cm^{-1}, which could correspond to the C=C and C=O stretching frequencies. The large band at 3500-2500 cm^{-1} could be due both to water present (3200-3500 cm^{-1}) and to the OH stretching frequency from the bonding of the hydroxyl group to the iron atom forming a chelate compound (2500-3200 cm^{-1}). The bands marked with crosses were those arising from the solvent, nujol.

After consideration of the experimental techniques being used to characterize the complex, it was decided not to continue to try to isolate a pure crystalline solid.

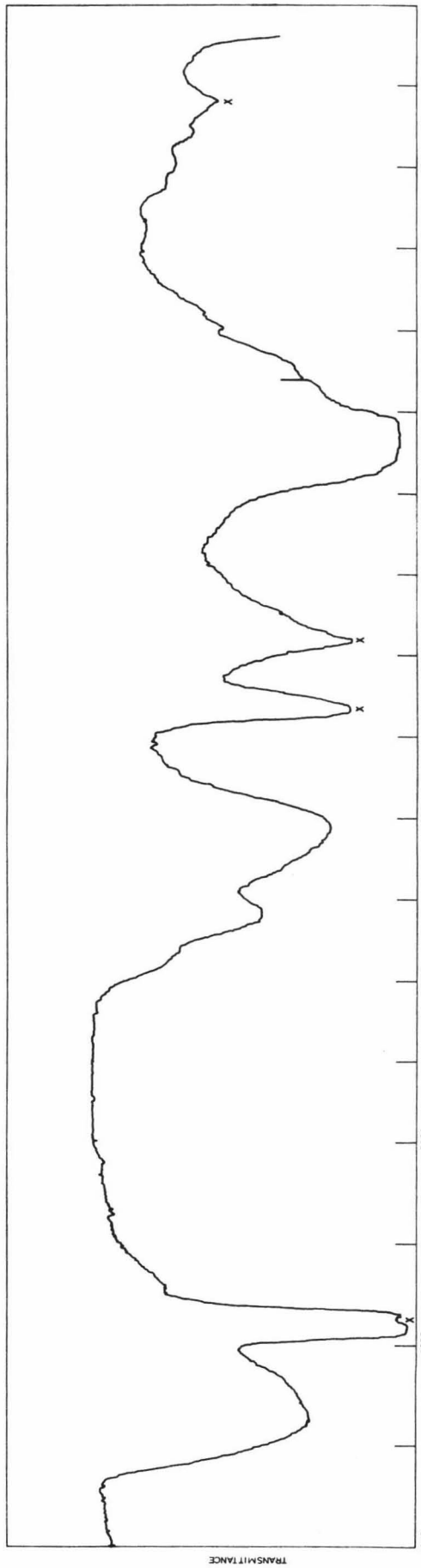

I.R. SPECTRUM OF FERROUS/ASCORBATE COMPLEX

FIGURE 2-1

Because of the nature of the ferrous sulphate/ascorbic acid system, it may not have been possible to isolate a pure ferrous/ascorbate complex. However, if the complex is of importance in biological systems, its significant reactions and properties would be those in aqueous solution, and the unavailability of a pure solid would be of little consequence.

Chapter 3 EXPERIMENTAL STUDIES

3.1 Introduction

To characterize the ferrous/ascorbate complex, as many modern physical techniques as possible were used. Following Hamilton[8], the oxidation of cyclohexane by the complex was studied using gas chromatography to analyse the products. This is a highly sensitive method of detecting small amounts of products of organic reactions. The presence of a coloured solution immediately suggests an investigation of its visible and ultraviolet (UV) spectrum. The requirement of a neutralized ligand solution for the formation of the complex led to an investigation of its pH dependence. From the variation of the pH of both the ligand and complex solution, information about the stability of the complex can be obtained. For hydrogen-containing species, nuclear magnetic resonance (NMR) spectroscopy is a useful analytical method. When this species is bound as a ligand to a paramagnetic transition metal ion, temperature-dependent shifts of the proton resonance peaks are sometimes observed. The proton NMR spectra of ascorbic acid, sodium ascorbate and the complex were all studied.

Electron spin resonance (ESR) spectroscopy can be used to study transition metal ions under certain conditions determined by the electronic properties of the molecule.

However, the presence of a paramagnetic metal ion does not necessarily mean that an ESR spectrum will be obtained at room temperature. Since iron is a Mössbauer nucleus, detailed information about the environment of the iron atom can be provided by Mössbauer spectroscopy. Complementary to this, magnetic susceptibility also gives information about the iron atom, from the deviations of the magnetic moment from the spin-only value. More information can also be obtained by a temperature-dependent study of the complex using the last two techniques.

These methods and their results are now discussed individually in the rest of this chapter.

3.2 Oxidation Reactions

Hamilton and his coworkers [8] reported the use of the model ascorbic acid system as an oxidizing agent for the oxidation of cyclohexane to cyclohexanol and cyclohexanone. Their experimental conditions were:

1.1 millimoles ascorbic acid, 0.04 millimoles ferrous ion in a heterogeneous mixture containing 31.5 mls of 0.058 M acetate buffer (pH 4.5), 30 mls of acetone and 5 mls of cyclohexane. The mixture was shaken under an atmosphere of air for 2 hours. The products, analysed by gas chromatogra-

phy, gave a yield of 2.1 mg of cyclohexanol and 0.7 mg of cyclohexanone.

To investigate whether the ferrous/ascorbate complex could be used in this oxidation process, the following experiments were carried out. A mixture of

15 mls Analar acetone

15 mls distilled water

and 2.5 mls cyclohexane (spectroscopic grade)

was used, to which was added

(1) and (2): approximately 0.1 gm of ferrous/ascorbate complex,

(3) approximately 0.1 gm of ferrous sulphate plus a large excess of sodium ascorbate.

Oxygen was bubbled through solution (1) for 2 hours; solutions (2) and (3) were shaken in air for 2 hours.

The products were analysed using a Perkin-Elmer vapour fractometer model 154 gas chromatograph. The samples were injected with a syringe, using 2 μl of liquid. The attenuation was kept low to enable the peaks to be observed, which led to trailing effects from the large solvent peak. A mixture of cyclohexane, cyclohexanol and cyclohexanone was used as a standard. The syringe was cleaned with acetone and injected to ensure there was no residue.

All three solutions gave a cyclohexanol peak, but the

cyclohexanone peak was rather difficult to detect since it was masked by the tail of the solvent peak. The solutions became brown and finally yellow.

The experiments were then repeated, under the following conditions. To the above mixture was added

(1) 0.160 gms ferrous/ascorbate complex

(2) 0.1100 gms sodium ascorbate and 0.0055 gms ferrous sulphate

(3) 0.1020 gms ferrous sulphate and excess sodium ascorbate, more being added at frequent intervals.

All solutions were shaken in air for at least 2 hours.

These solutions were analysed by gas chromatography, all three giving cyclohexanol and cyclohexanone peaks. The conditions of the gas chromatograph, such as temperature and gas flow, had been adjusted so that the cyclohexanone peak could be obtained distinct from the solvent peak. The chromatogram obtained for one of the solutions, together with that for the standard, is shown in figure 3.1. Solution (3) gave the greatest yield, remaining purple for several hours after solution (1) had become yellow. Solution (2) also remained purple longer than solution (1).

These results imply that the ferrous/ascorbate complex can be used to oxidize cyclohexane. However, better results are obtained if the complex can be formed during the oxidation

CONCENTRATION OF CYCLOHEXANOL (A)
AND CYCLOHEXANONE (B)

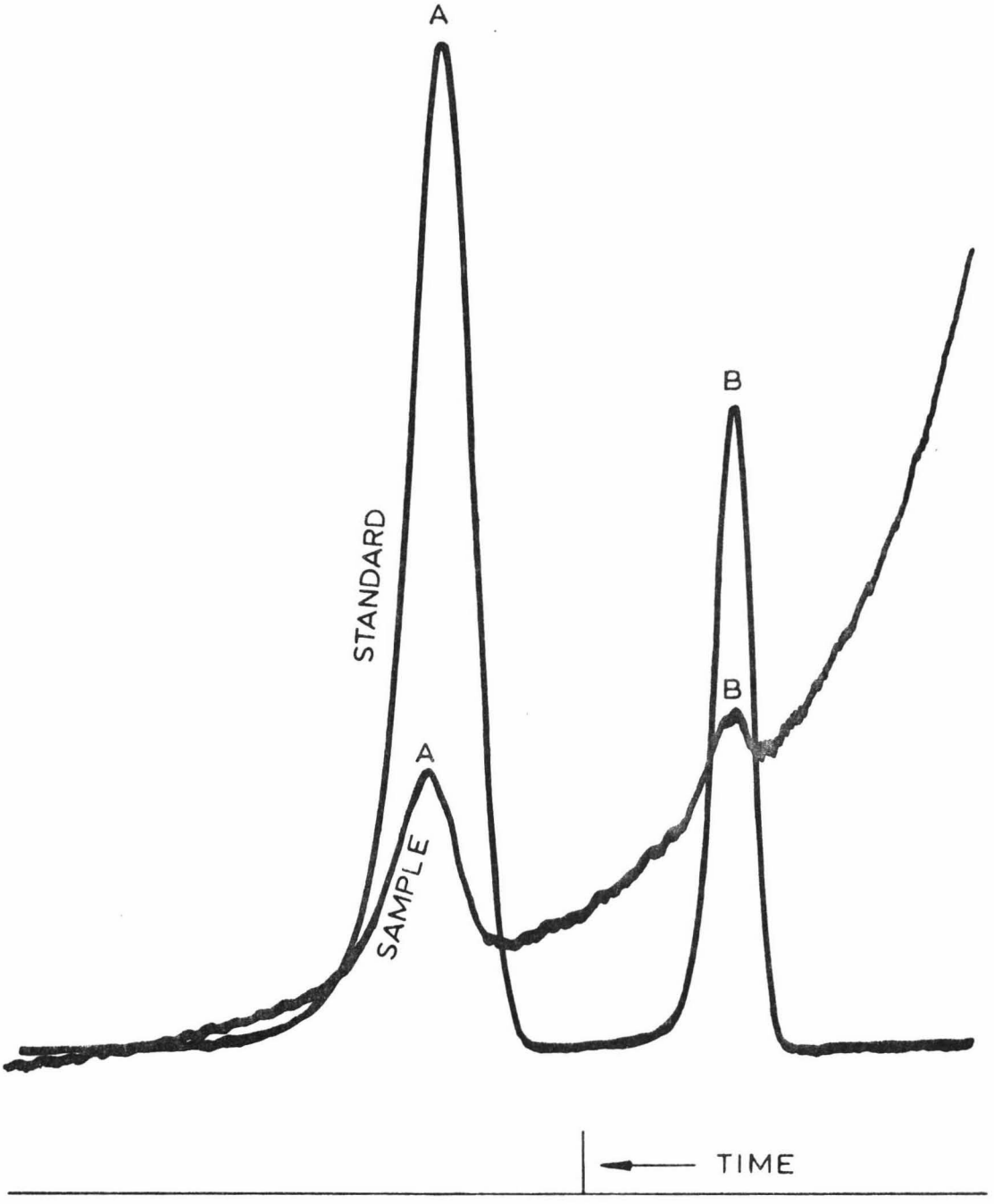

GAS CHROMATOGRAM

FIGURE 3·1

process: in the presence of excess sodium ascorbate the complex will form until all the sodium ascorbate is used up, provided that the ferrous ion has not been oxidized. Initially the ferrous ion appears to cycle to form more complex, since those experiments in which excess sodium ascorbate was added gave more products, but the process apparently cycles for only a finite time. As long as there is sufficient ferrous ion and sodium ascorbate to form the complex, more cyclohexanol should be formed.

3.3 UV and Visible Spectra

The absorption spectrum of the ferrous/ascorbate complex was measured in the regions 400-1200 mμ and 360-220 mμ, using a Beckman DK2 spectrophotometer. A weak absorption band had its maximum at 553 ± 2 mμ (figure 3.2) and a strong absorption band had its maximum at 265 ± 2 mμ (figure 3.3). Comparison with the value for the maximum of ferrous sulphate and sodium ascorbate showed that the latter maximum corresponded to the ascorbic acid absorption associated with the conjugated α-β unsaturated ketone system [14]. Consequently, the remaining experiments were concentrated in the visible region, 400-750 mμ.

In figure 3.2, the various plots correspond to different

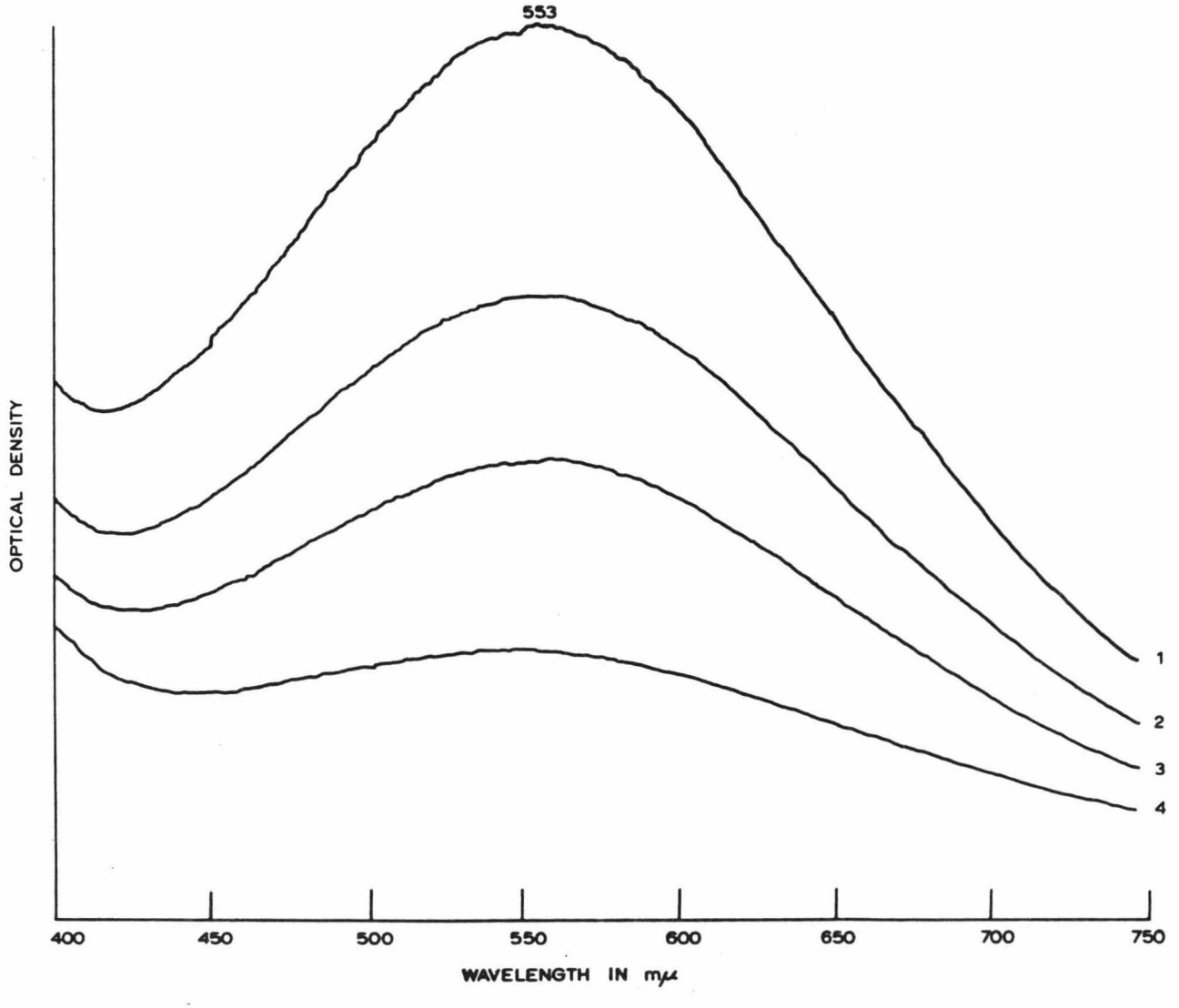

U.V. SPECTRUM OF FERROUS ASCORBATE COMPLEX SOLUTION

FIGURE 3·2

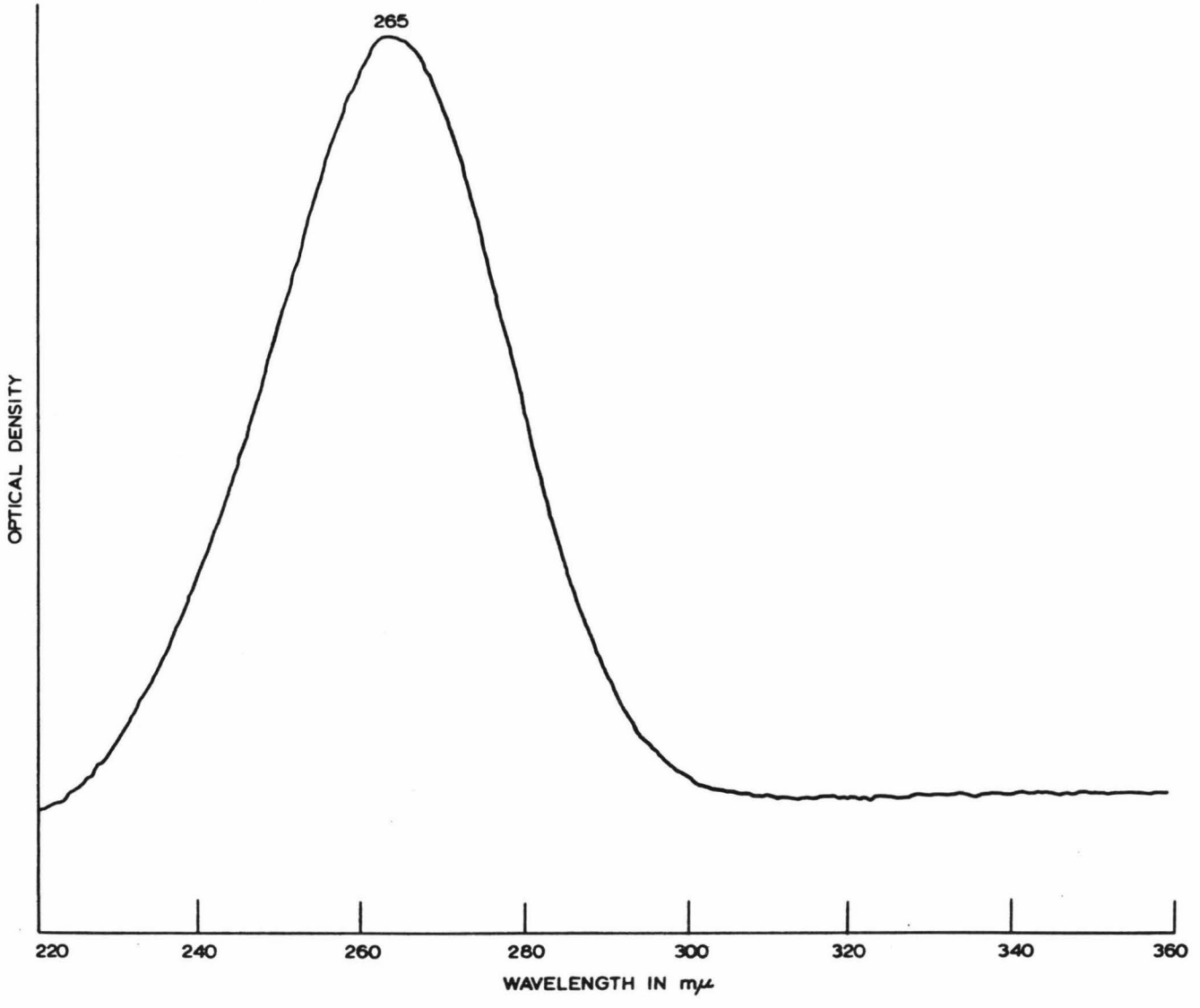

U.V. SPECTRUM OF SODIUM ASCORBATE SOLUTION

FIGURE 3·3

times. The optical density of the purple solution slightly increased after preparation, then gradually decreased, the solution becoming lighter in colour. This change in optical density was associated with the appearance of a streaming of darker solution from the surface of the liquid in the cell, seemingly because of oxidation by air. Shaking the solution also altered the optical density.

An estimate of the molar extinction coefficient, ϵ , at the band maximum was obtained from a Beer-Lambert Law plot. Because the oxidation of the ferrous/ascorbate solution seemed to vary with concentration, the question of the verification of the Beer-Lambert Law was difficult. In figure 3.4 a set of results are plotted at two concentrations (A and B), together with the line obtained for the less concentrated solution if there was no oxidation and the Beer-Lambert Law could be applied rigorously (C). An estimate of the extinction coefficient is 100-120 litre.mole^{-1}.cm^{-1}.

The intensity of the absorption band can be measured in terms of the oscillator strength, f [18],

$$f = 4.32 \times 10^{-9} \int_{\nu_2}^{\nu_1} \epsilon \, d\nu$$

i.e. the oscillator strength is the area under the band stretching from frequency ν_1 to ν_2 (in cm^{-1}) in a plot of extinction coefficient against frequency.

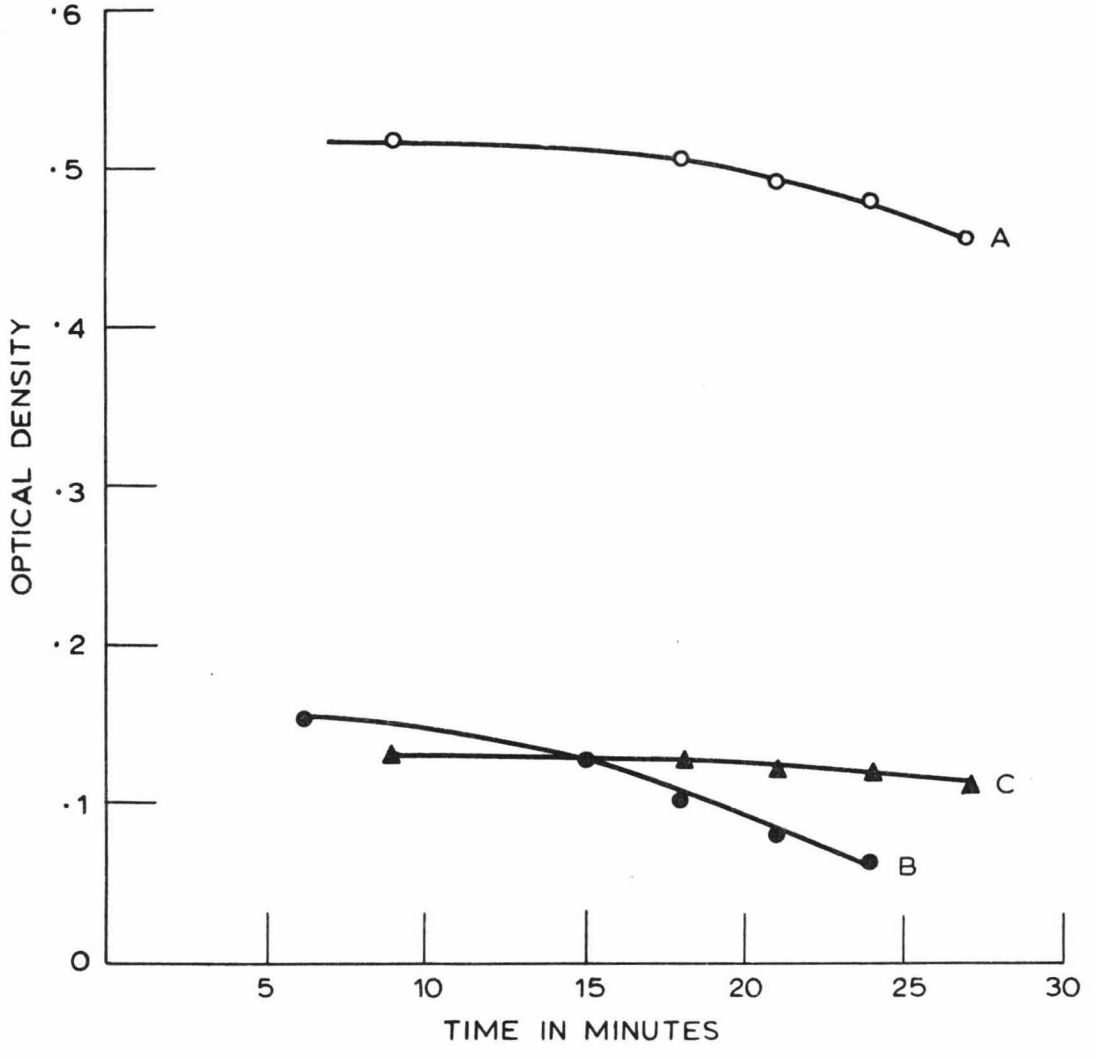

GRAPH TO VERIFY BEER'S LAW

FIGURE 3·4

For approximate calculations, the absorption bands of complex solutions are assumed to have Gaussian shapes, expressed analytically by

$$\epsilon = \epsilon_o \exp[-\alpha(\nu - \nu_o)^2]$$

where α is a constant

ϵ_o is the extinction coefficient at the maximum absorption

ν_o is the frequency at the maximum absorption.

The area under the curve is therefore approximated to $\epsilon_o \Delta\nu$, where $\Delta\nu$ is the width of the band at half height. This is a convenient approximation, and sufficiently accurate, if the band does not show fine structure. Hence the oscillator strength can be given by

$$f = 4.32 \times 10^{-9} \times \epsilon \times \Delta\nu$$
$$\div 4 \times 10^{-3}$$

on substituting the above value of ϵ, and the estimated value of $\Delta\nu$ from figure 3.2.

The spectrum of the yellow solution, obtained after the ferrous/ascorbate solution had been left standing in air, was also measured; the onset of an absorption was apparent about 400 mμ.

To determine the number of ligands co-ordinated to the metal ion, i.e. the number of ascorbate ligands co-ordinated

to the ferrous ion, the Method of Continuous Variations (or Job's Plot) [19] was used. Firstly, the spectra of solutions containing ferrous sulphate and sodium ascorbate in the ratios of 1:1, 1:2, 1:3 were measured in the visible region. As these all gave the same maximum (at 553 mμ), it was assumed that only one complexing species was present in solution or could be detected in the visible region. Accordingly the Job's Plot method was applicable.

Initially, a plot was done at three wavelengths, namely 430, 550 and 600 mμ. These were chosen as being wavelengths at which the ferrous/ascorbate complex solution and the component solutions had appreciable differences in optical densities. The component solutions used were:

$$0.01\ M\ FeSO_4$$

and $$0.01\ M\ C_6H_7O_6Na,$$

these being prepared immediately prior to commencing the experiment to minimize errors through oxidation of the solutions by air. Mixed solutions were prepared one at a time, containing x mls of sodium ascorbate solution and (10-x) mls of ferrous sulphate solution where x ranged from 4 to 9 mls. Each solution was shaken well for a given time. Readings of the optical density were taken on a Beckman DU spectrophotometer at a set time, a further set of readings being taken after a fixed time. This procedure was carried out

for each solution, i.e. for each value of x. The optical densities of the component solutions were also measured.

From the graphs obtained by plotting the above results, the maximum appeared to lie in the region of 7-8 mls of sodium ascorbate. As the errors involved in each reading were large, the drawing of straight lines through the points was somewhat arbitrary.

To clarify these results, a more accurate Job's Plot was done at 550 mμ over the range of solutions x = 6.0 to 9.0 mls, in steps of 0.5 mls, using a Unicam SP500 spectrophotometer. The optical density was measured at two minute intervals for about ten minutes, in an attempt to average the errors in timing. The component solutions used were:

0.02 M $FeSO_4$

and 0.02 M $C_6H_7O_6Na$,

the mixed solutions being prepared as previously, prior to taking the readings.

The errors involved arose mainly from the slow oxidation of the ferrous/ascorbate solution as well as the component solutions. The errors in taking the readings on the spectrophotometer and in preparing the component solutions were considered to be negligible compared with those arising from the gradual oxidation of the ferrous/ascorbate solution.

The results obtained were averaged over the time

interval involved; these average values of optical density, together with their deviation with time, are shown plotted against the value of x in figure 3.5. The maximum, obtained by drawing two straight lines through the experimental points, is at x = 7.5 mls. Using Job's formula

$$n = \frac{x}{10-x} ,$$

where n is the number of co-ordinated ligands, and on substituting 7.5 for x, it was calculated that there are three ascorbate ligands bound to each ferrous ion. Accordingly, the species present in solution is a 1:3 complex, and can be prepared by using one mole of ferrous sulphate and three moles of sodium ascorbate.

3.4 pH Measurements

In section 2.4, it was noted that the ferrous/ascorbate complex was prepared by adding ferrous sulphate to a solution of sodium ascorbate of pH 7. On addition of acid, the purple solution became colourless, whereas with alkali, the solution turned brown and gave a precipitate, probably of iron hydroxide. The effect of pH on the ferrous/ascorbate solution was then investigated.

The pH measurements were carried out using a Radiometer pH meter 22, with glass and calomel electrodes. This was

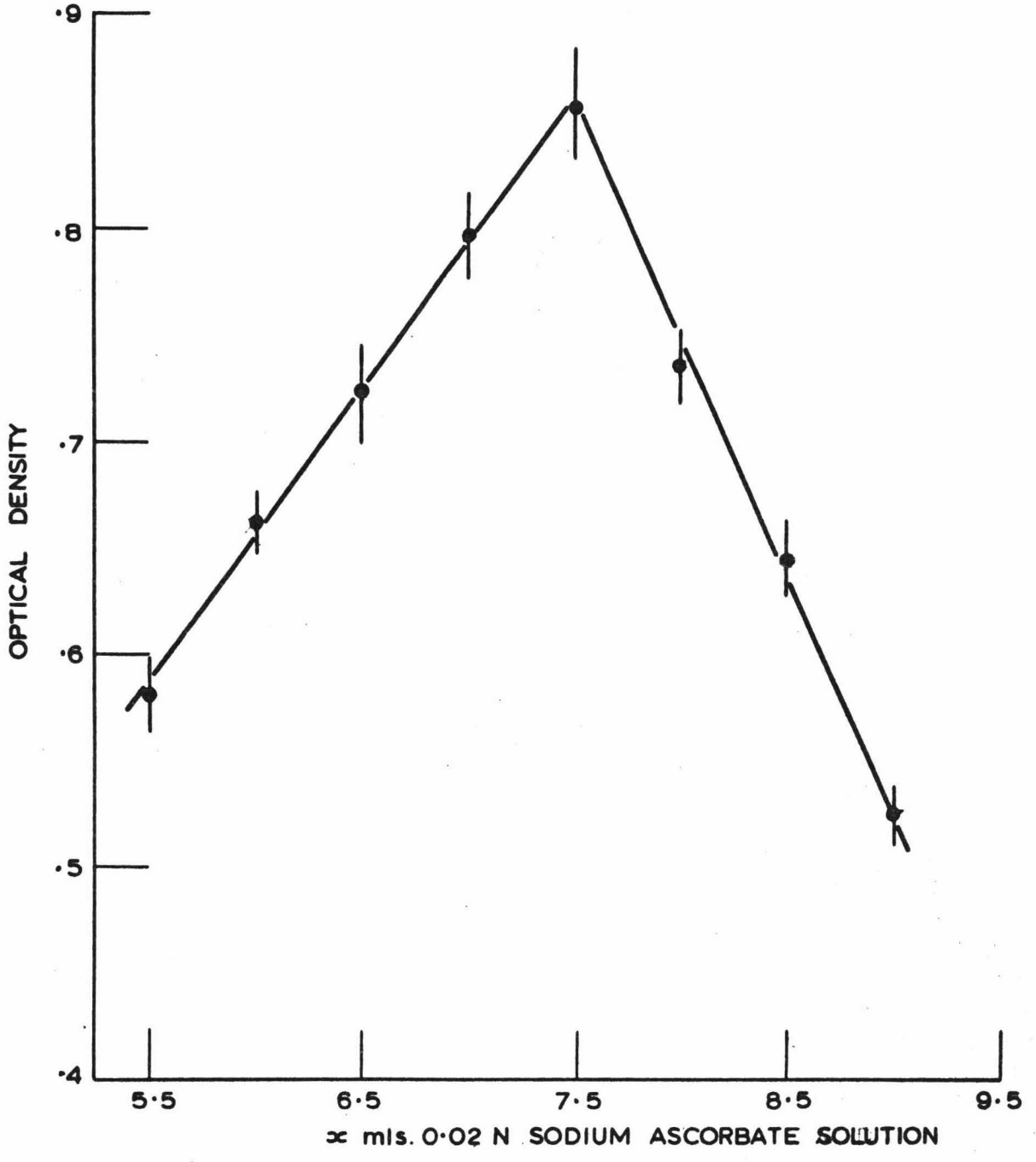

JOB'S PLOT AT 550 mμ

FIGURE 3·5

calibrated with a potassium hydrogen phthalate buffer of known pH, the pH being read to ±0.02 pH units. The titrations were carried out using a burette, containing a standard solution of approximately 0.1 N sodium hydroxide, the volume being read to ±0.05 mls. Constant temperature was maintained by using a double-walled beaker, with water flowing through the space between the two walls. Each solution to be titrated was prepared immediately prior to doing the experiment.

The experiment was carried out in two stages. A solution of known concentration of ascorbic acid was titrated with the sodium hydroxide solution until a pH of about 11 was reached, after which the glass electrode is not accurate. Then a solution of the same concentration of ascorbic acid with a known amount of ferrous sulphate added was titrated until a pH of about 7.5 was reached, when precipitation occured.

This experiment was carried out using two different concentrations:

(1A) 25 mls of 0.1 M ascorbic acid solution

(1B) solution (1A) plus 0.232 gms of ferrous sulphate

(2A) 100 mls of solution, 0.002 M in nitric acid and 0.02 M in ascorbic acid

(2B) solution (2A) plus 0.056 gms of ferrous sulphate.

During the titration of solutions (B), the colourless solutions changed through various shades of blue and violet to purple at pH 5.8-6.4. Above pH 7, the solutions became brown and started to precipitate. Readings of the pH could no longer be taken accurately as this precipitation caused the pH to vary. The ascorbic acid solutions (A) became yellow as the pH rose above 8; once again the pH varied somewhat, probably due to the oxidation of the solution.

Graphs of pH against mls of 0.1 N sodium hydroxide solution added are shown. Figure 3.6 shows the graph obtained for ascorbic acid solution. The neutralization point is at pH 7 showing that ascorbic acid does act as a monobasic acid. By noting the pH of the half-neutralization point [20], an estimate of the acid dissociation constant pK_1 is 4.15 $\pm$ 0.05, which is in good agreement with the literature value quoted in section 2.2 as 4.17.

Figure 3.7 is the graph obtained for solutions (1), and figure 3.8 is that for solutions (2). In the latter, the lower curve has been displaced to allow comparison to be made between the two plots. The two plots are almost identical up to pH 6, when the plot for the ferrous/ascorbate solutions curves away. An estimate of the stability of the complex can be made from the differences between these two curves [21].

As the plots differed only above pH 6, and readings of

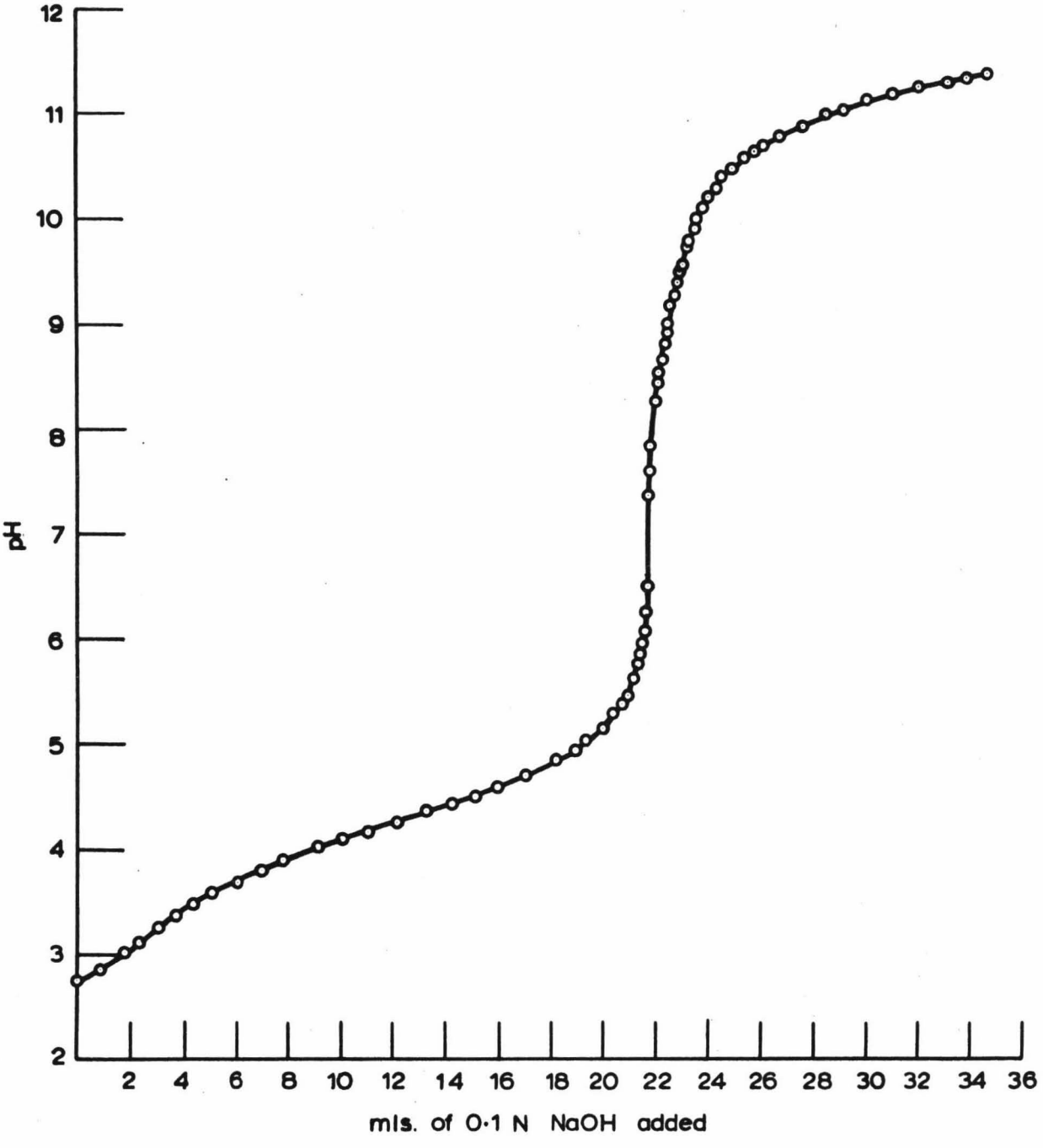

GRAPH OF pH AGAINST mls OF SODIUM HYDROXIDE ADDED TO A SOLUTION OF ASCORBIC ACID

FIGURE 3·6

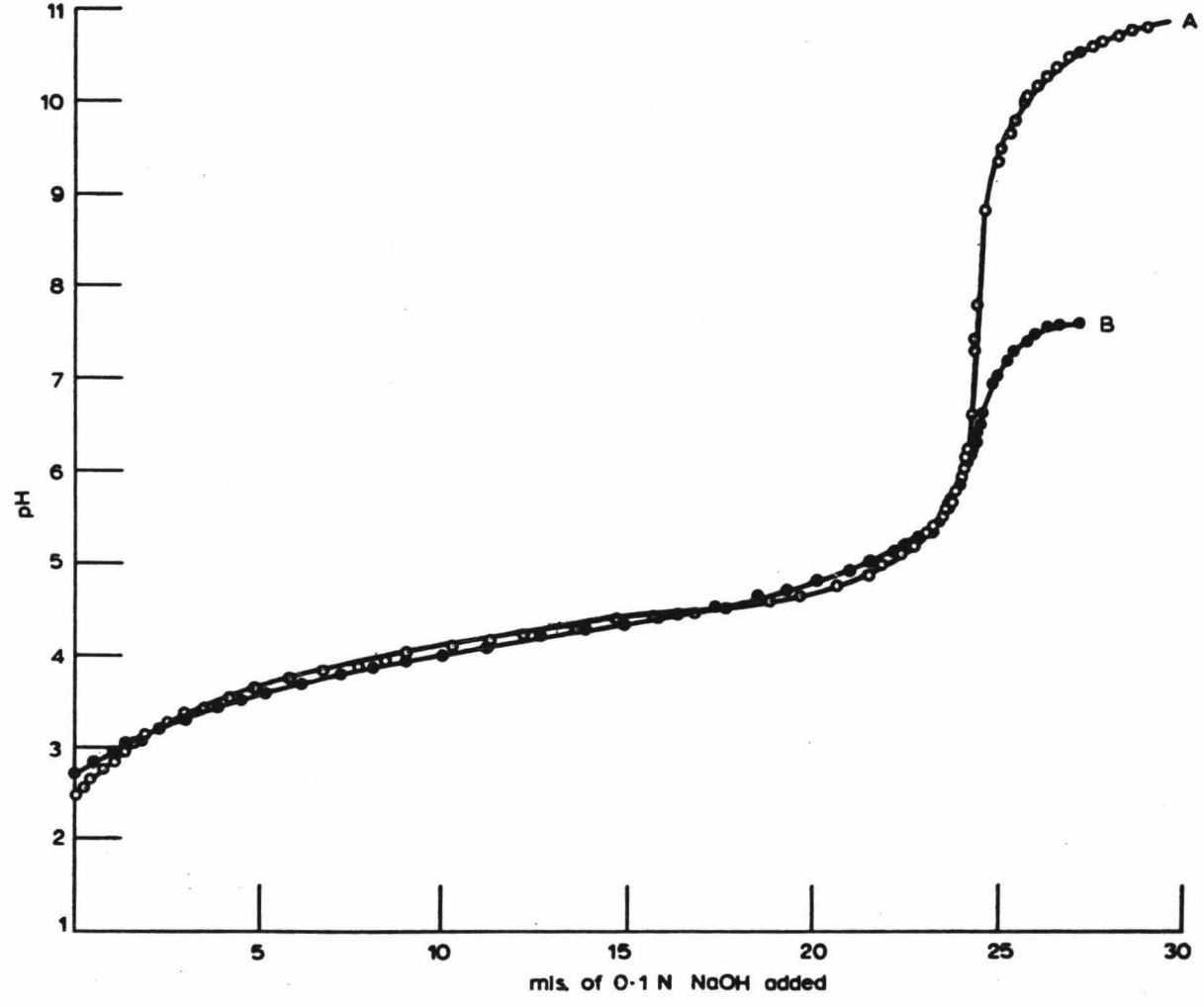

GRAPH OF pH AGAINST mls. OF SODIUM HYDROXIDE ADDED - TO A SOLUTION CONTAINING ASCORBIC ACID (A); TO A SOLUTION CONTAINING ASCORBIC ACID AND FERROUS SULPHATE (B)

FIGURE 3·7

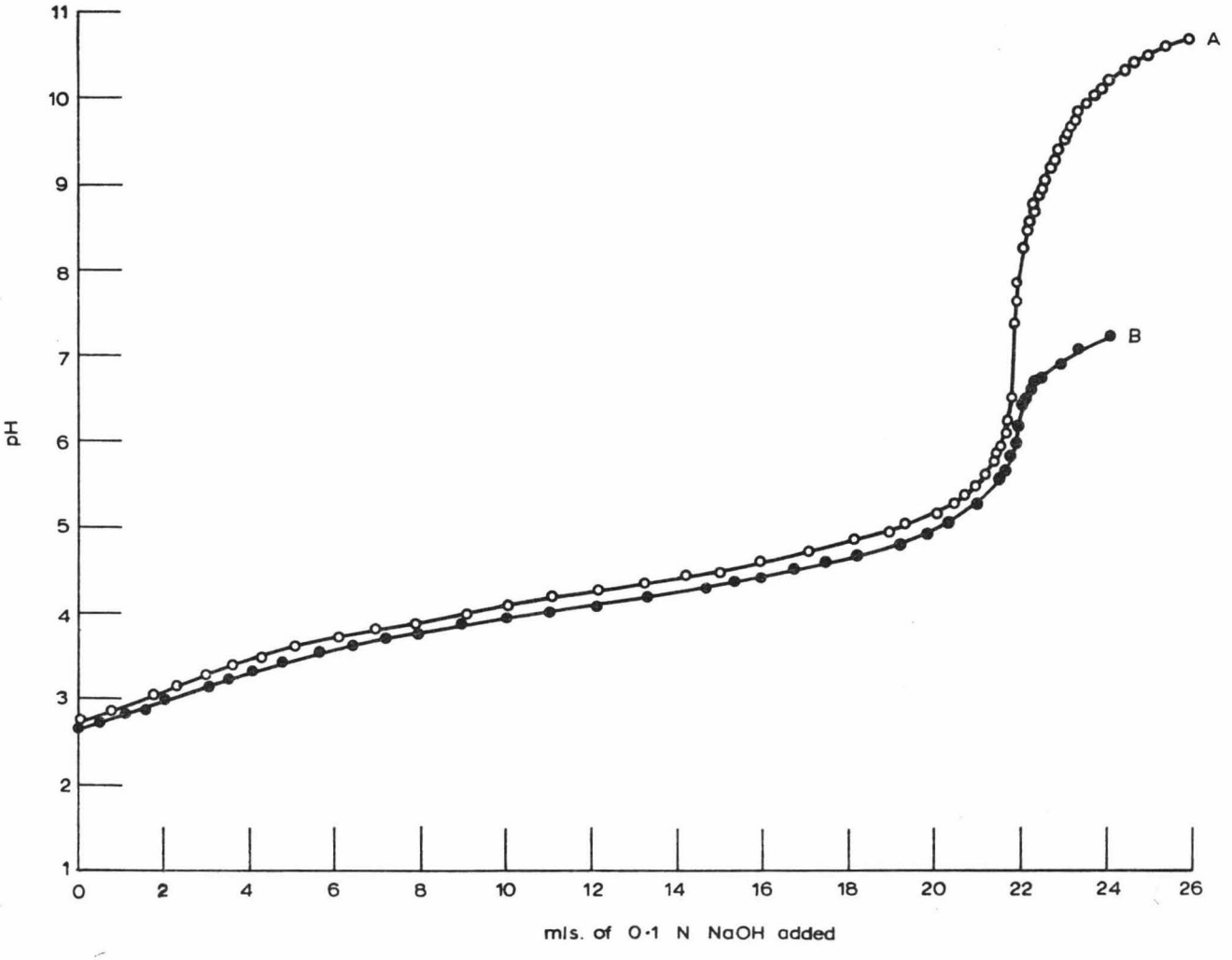

GRAPH OF pH AGAINST mls. OF SODIUM HYDROXIDE ADDED - TO A SOLUTION CONTAINING ASCORBIC ACID AND NITRIC ACID (A); TO A SOLUTION CONTAINING ASCORBIC ACID NITRIC ACID AND FERROUS SULPHATE (B)

FIGURE 3·8

pH were not accurate above pH 7, this left only a very few readings which could be used in calculating the stability constant. Furthermore, the limitations in the methods used to calculate stability constants [22] did not appear to make such a calculation worthwhile. Consequently no attempt was made to compute the stability constant for the complex. However, the complex would not be expected to be very stable, because the differences in the plots are not great [21].

3.5 NMR Spectra

A proton NMR spectrum of ascorbic acid and its sodium salt was initially run on a Varian DP60 High Resolution NMR spectrometer at Chemistry Division, Department of Scientific and Industrial Research, using D_2O (deuterated water) as the solvent. A small amount of 3-(trimethylsilyl)-propanesulphonic acid sodium salt was added as an internal reference, and the relative positions of the peaks obtained by the audio side band method [23] using a frequency of 350 c/s to reflect the spectrum and in particular the reference peak. The spectrum of the ferrous ascorbate complex was then done under the same conditions.

Later an opportunity arose to run the spectra under considerably improved resolution, on a Varian DA60I spectrometer at Chemistry Division. This instrument has the facility

of "locking" on to one particular resonance peak in the spectrum, thus leading to considerably improved stability and resolution. A few drops of acetone were added to the D_2O solution and the acetone peak was used to "lock" on to. The previously used internal reference was not found to be suitable since its solubility in D_2O was not sufficient to give a large enough peak to "lock" on to. With this system, the portion of the spectrum containing the peaks (about 100 c/s) was spread over 50 cm of chart.

The spectrum of ascorbic acid obtained initially is shown in figure 3.9, while that obtained later is shown in figure 3.9A. The peak positions in c/s measured from the high-field singlet is given in table 3.1 for both ascorbic acid and its sodium salt.

Table 3.1 Positions of Peaks in NMR Spectra

Spectra from DA60I.

Peaks in c/s ($\pm$0.2 c/s) from high-field singlet.

Peak	Ascorbic Acid	Sodium Ascorbate
doublet	-7.9	-8.1
	-6.1	-5.9
singlet	0.0	0.0
doublet	9.6	7.7
	11.4	9.6

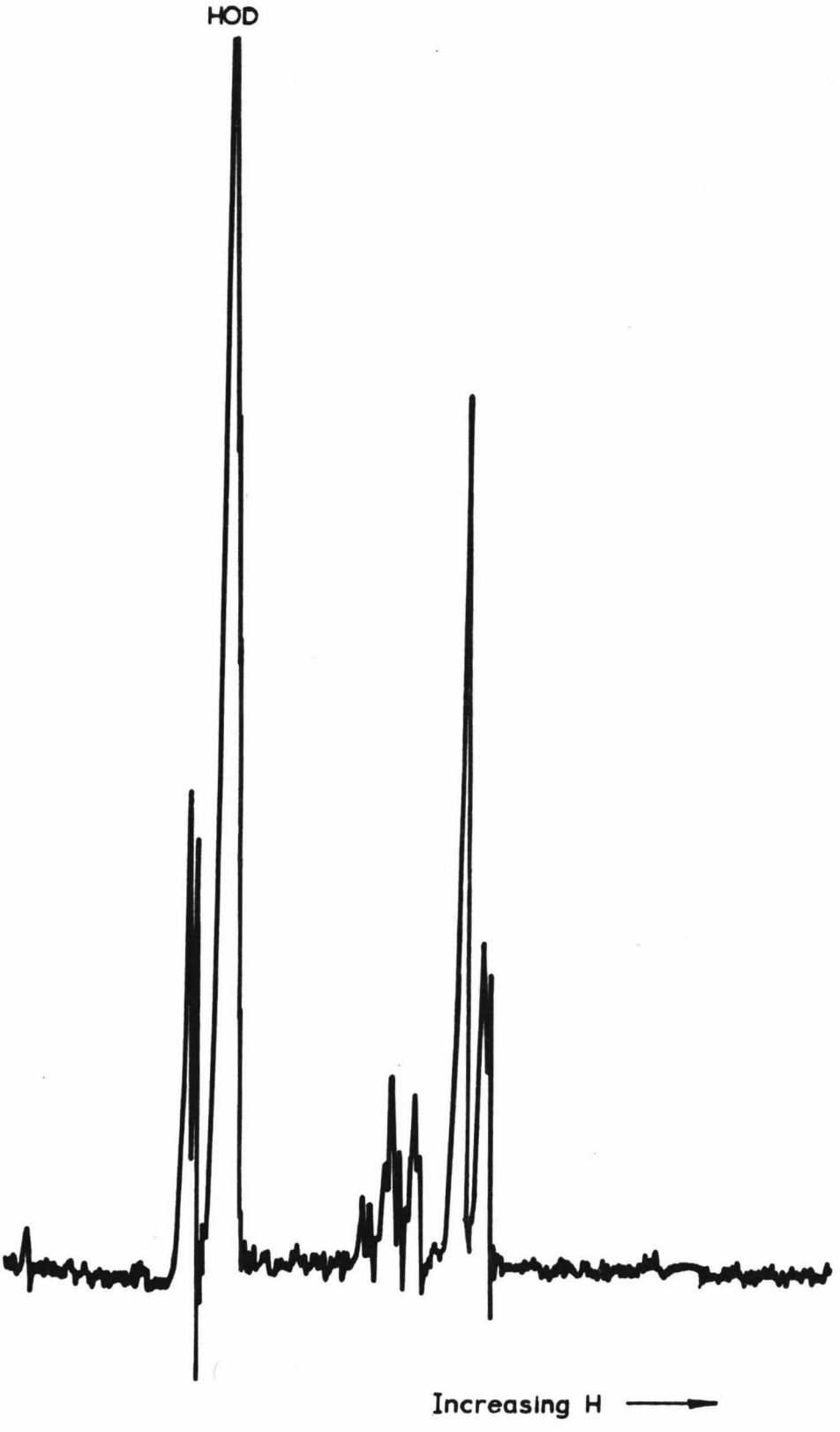

N.M.R. SPECTRUM OF ASCORBIC ACID IN D_2O

FIGURE 3·9

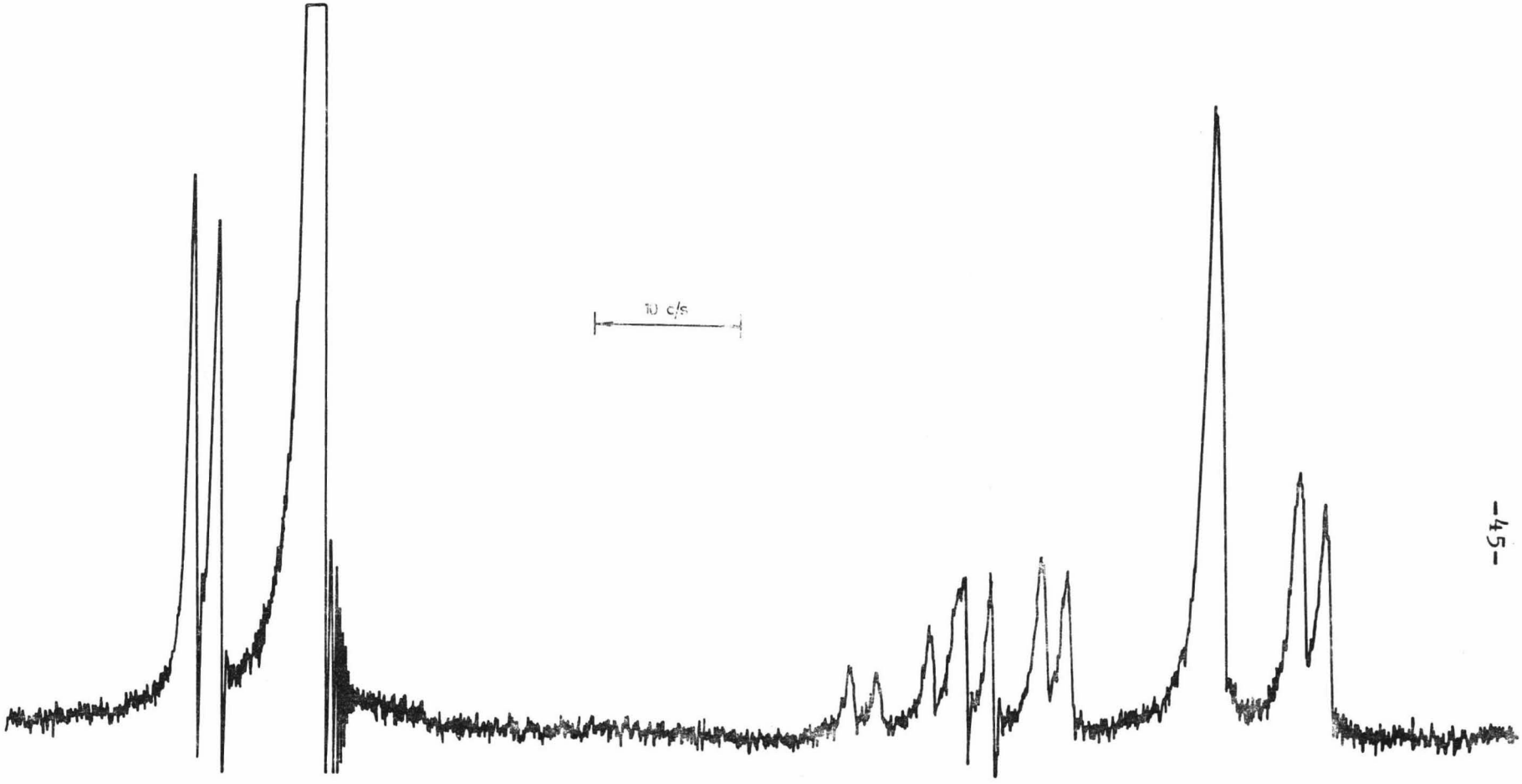

N.M.R. SPECTRUM OF ASCORBIC ACID UNDER HIGH RESOLUTION

FIGURE 3·9A

multiplet	14.9	12.6
	16.7	14.7
	17.1	15.6
	19.1	17.3
doublet	22.6	20.6
	24.5	22.5
doublet (X)	68.0	41.5
	69.8	43.4
HOD	61.5	60.4

The HOD peak arises from the interchange of the H on the four hydroxyl groups and the D in the D_2O. The rest of the spectrum is due to the hydrogens situated on C-4, C-5 and C-6 [see section 2.2]. An interpretation of this spectrum, together with deduced values for the coupling constants and chemical shifts, is given in chapter 5. The spectrum obtained for ascorbic acid is similar to that given in the NMR spectra catalogue [24].

Except for one notable feature, the spectra of sodium ascorbate and ascorbic acid are almost identical. The low-field doublet at 69 c/s in the latter has shifted to 42 c/s in the former, a shift of 27 c/s. The slight difference of about 2 c/s in some of the other peaks is not as significant as this comparatively large shift of the low-field doublet (labelled X in table 3.1). This will also be interpreted in chapter 5.

The spectrum of the ferrous/ascorbate complex consisted of three broad peaks in the same regions as the peaks in the sodium ascorbate spectrum. The HOD peak was very broad, almost masking the neighbouring doublet. This broadening effect arose from the presence of a paramagnetic ion, high spin ferrous ion, which substantially reduced the proton relaxation times [25]. Even the addition of one crystal of ferrous sulphate to the sodium ascorbate solution was sufficient to broaden the peaks so that the multiplet structure about 15 c/s was no longer in distinct peaks.

A temperature-dependence study was attempted on the complex solution, but no conclusive results were obtained. The large peak at low field shifted with increasing temperature, but this was probably due to the HOD peak, which is temperature-dependent [26]. The broad nature of the peaks also made it difficult to measure the positions of the peaks with enough accuracy to tell if a temperature-dependent shift had occured.

However, as the ascorbic acid spectrum had not previously been characterized using theoretical techniques, it was thought to be relevant to interpret this spectrum and the associated spectrum of sodium ascorbate. The theoretical interpretation of these two spectra is given in chapter 5.

3.6 ESR Spectrum

An ESR spectrum of the ferrous/ascorbate complex was run on a Varian ESR spectrometer at the University of Sydney, New South Wales. The spectrum obtained showed the characteristic spectrum of manganese [27]. The presence of manganese was confirmed by an emission spectrograph, done by Dr Sullivan (Analar $FeSO_4.7H_2O$ contains 0.03 % of manganese impurities).

Because of spin-lattice relaxation times, ESR spectra are rarely observed for high spin ferrous compounds at room temperature. By reducing the temperature to liquid hydrogen or liquid helium temperatures, it is possible to reduce spin-lattice relaxation so that an ESR spectrum may be detected. This is discussed by Figgis [28].

3.7 Mössbauer Spectra

Mössbauer spectra of the ferrous/ascorbate complex were run on the Mössbauer spectrometer at Victoria University of Wellington, by Dr R. Bailey. The sample used, containing approximately 0.025 gm of iron per square centimeter of sample, was prepared by the second method given in section 2.4. Mössbauer spectroscopy does not depend critically on the amount of solid present, provided there is sufficient iron present. The use of a pure crystalline solid was not

essential because the sample was powdered to ensure a homogeneous mixture.

The spectrum obtained at room temperature, shown in figure 3.10, has two fairly broad peaks with minima at 87 and 145 channels. Using conversion factors obtained from a calibration spectrum of sodium nitroprusside, the quadrupole splitting ΔE_Q and chemical shift δ_{ss} with reference to stainless steel were calculated [29] as

$$\Delta E_Q = 2.53 \pm 0.10 \quad \text{mm/sec}$$

$$\delta_{ss} = 1.12 \pm 0.10 \quad \text{mm/sec.}$$

Using the correlation diagram [29], it is seen that these values correspond to the iron being in a high spin ferrous state. Comparison with the values given for $FeSO_4.7H_2O$, namely

$$\Delta E_Q = 3.20 \quad \text{mm/sec}$$

$$\delta_{ss} = 1.31 \quad \text{mm/sec}$$

shows that ΔE_Q depends on the ligands surrounding the iron atom.

The temperature-dependence of the Mössbauer spectrum was also considered. At low temperatures, the spectrum peaks became somewhat sharper and the value of ΔE_Q increased. Values obtained at 195°K (dry ice/alcohol mixture) were

$$\Delta E_Q = 2.87 \pm 0.10 \quad \text{mm/sec}$$

$$\delta_{ss} = 1.09 \pm 0.10 \quad \text{mm/sec.}$$

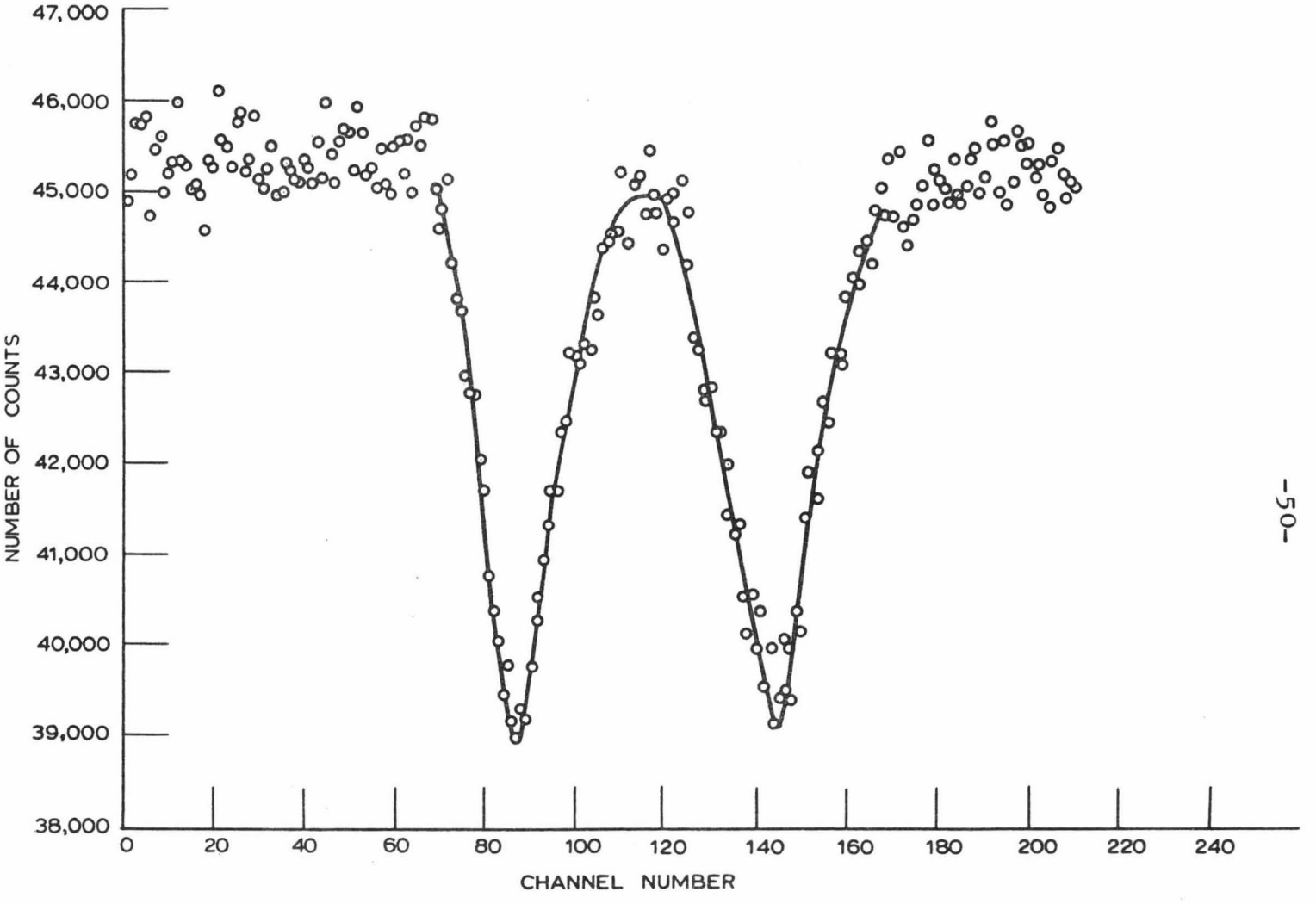

MÖSSBAUER SPECTRUM OF FERROUS/ASCORBATE COMPLEX AT ROOM TEMPERATURE

FIGURE 3·10

Within the experimental error, the chemical shift is independent of temperature. An interpretation of these values of ΔE_Q is given in section 4.7.

3.8 Magnetic Susceptibility Measurements

Magnetic susceptibility measurements on the ferrous/ascorbate complex at various temperatures were carried out at the Tala Institute of Fundamental Research, Bombay, India. The sample used was made in the same preparation as that used in the Mössbauer experiments, but, unlike in Mössbauer spectroscopy, impurities could lead to large errors in a determination of the magnetic moment. As discussed in section 2.4, the molecular weight and composition of this complex were not known accurately.

The results obtained for the gram susceptibility χ_g at various temperatures are given in table 3.2 [p.53]. A plot of $1/\chi_g$ against T (in ^oK) is strictly linear, with intercept at -9^oK, i.e. the Curie-Weiss Law [30],

$$\chi_g = \frac{C}{T + \theta} \quad ,$$

where C is the Curie constant, is obeyed with a Weiss constant θ of 9^oK.

The molar susceptibility χ_M^{cor} is then calculated using the formula

$$\chi_M^{cor} = [\chi_g \times MW] + \chi_d$$

where χ_d is the correction for the diamagnetism of the molecule, calculated empirically from Pascal's constants [31]

$$\chi_d = [290 + 13x]\ 10^{-6} \text{ c.g.s. units}$$

where x is the number of water molecules in the complex. In calculating χ_M^{cor}, two molecular weights have been considered, 854 (obtained from the formula given in section 2.4 with x = 6) and 900 (to account for impurities).

The magnetic moment was then calculated [30] from

$$\mu_{eff} = 2.84\sqrt{\chi_M^{cor}\ T}$$

assuming the Curie Law (i.e. $\theta = 0$) and

$$\mu_{eff} = 2.84\sqrt{\chi_M^{cor}\ (T + \theta)}$$

assuming the Curie-Weiss Law. The magnetic moments obtained for these four possibilities are given in table 3.2.

It is interesting to note that μ_{eff} for MW = 854 and MW = 900 differ by an approximately constant amount, namely 0.14 Bohr magnetons, for both the Curie and Curie-Weiss Laws. The ratio of the μ_{eff}'s is approximately the square root of the ratio of the MWs, the only other contributing factor being the correction for diamagnetism which is small. The Curie-Weiss values show less variation with temperature than the corresponding Curie values.

Although the experimental errors were not given for these values, the actual measurements would involve some error as well as those arising from impurities and the

uncertainty in the molecular weight. The range of these latter errors can be seen in the values quoted in table 3.2.

Table 3.2 Magnetic Susceptibility and Magnetic Moment for Various Temperatures

T	χ_g cgs units x 10^6	$\frac{1}{\chi_g}$ x 10^{-4}	μ_{eff} in Bohr magnetons Curie Law		Curie-Weiss Law	
			MW 854	MW 900	MW 854	MW 900
84	41.94	2.385	4.95	5.08	5.21	5.35
96.5	37.53	2.665	5.02	5.16	5.25	5.39
112	32.75	3.053	5.06	5.20	5.26	5.40
134	27.54	3.631	5.08	5.22	5.25	5.39
166	22.52	4.440	5.12	5.26	5.26	5.40
222.5	17.39	5.751	5.23	5.37	5.33	5.48
288	13.57	7.375	5.27	5.41	5.35	5.50
295	13.14	7.612	5.25	5.39	5.33	5.48

[The value for room temperature (288°K) was obtained by interpolation of the results plotted on the graph of $1/\chi_g$ against T].

On comparing with the "spin-only" value of 4.9 [30], these values of μ are found to correspond to the presence of four unpaired electrons, thus confirming that the iron atom in the complex is in a high-spin ferrous state.

The value quoted for $FeSO_4.7H_2O$ is 5.22 Bohr magnetons [32]. These values lie within the experimental range for ferrous compounds, 5.1 - 5.7 quoted by Figgis and Lewis [32].

An interpretation of these results is given in section 4.7.

Chapter 4 CRYSTAL FIELD CALCULATIONS

4.1 Introduction

From the experimental results discussed in chapter 3, certain features of the ferrous/ascorbate complex have been characterized. These are now discussed in terms of the Crystal Field model for transition metal ion complexes.

Magnetic susceptibility and Mössbauer studies have shown that iron is in a high spin ferrous state with configuration d^6. UV studies have shown the complex to have three ascorbate ligands surrounding it, presumably bound via the oxygen atoms on C-2 and C-3 to form a bidentate chelate group.

The majority of ferrous complexes have their ligands arranged around the central metal ion at the vertices of an octahedron; these are said to have octahedral crystal fields and belong to the symmetry point group O_h. Because the ascorbate ligands are asymmetrical, the ferrous/ascorbate complex will have only C_3 symmetry, and this is further reduced if free rotation about single bonds is allowed. However, if the principle of local symmetry is applied, the complex can be approximated to D_3 in the first instance and even to O_h symmetry. This principle states [33] that it is the immediate surroundings which are the most important in the assessment of the symmetry of the environment of the

metal ion. The atoms bonded to the metal ion are all oxygen atoms, giving O_h symmetry; these are further bonded to carbon atoms which form a five-membered ring with the ferrous ion, thus giving D_3 symmetry, as shown.

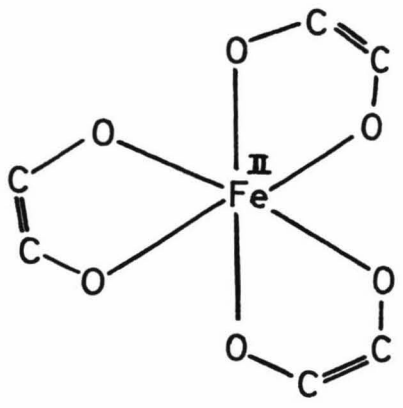

Therefore, in this crystal field calculation, the model assumed for the complex is that of a bidentate complex with D_3 symmetry. To calculate the eigenstates for a transition metal ion in a crystal field of D_3 symmetry, the crystal field potential V_{D_3} has to be known. The crystal field potentials for O_h and D_3 symmetry are [34]

$$V_{O_h} = r^4[A\ Y_4^0 + B(Y_4^4 + Y_4^{-4})]$$

$$V_{D_3} = C\ r^2\ Y_2^0 + r^4[D\ Y_4^0 + E(Y_4^3 + Y_4^{-3})]$$

where the constant term, which shifts all crystal field eigenstates by the same amount, has been omitted, A, B, C, D and E are constants, and Y_n^m is a normalized spherical harmonic.

The use of V_{D_3} immediately presents a problem. Whereas for V_{O_h}, the crystal field eigenfunctions can be expressed in terms of just one crystal field parameter $Dq \sim \langle r^4 \rangle / a^5$

[$\langle r^m \rangle$ is the average value of r^m for the 3d wave function, a is the metal-ligand distance], for V_{D_3} (and also for V_{D_4}) two crystal field parameters are needed, namely $\langle r^4 \rangle / a^5$ and $\langle r^2 \rangle / a^3$. This latter parameter gives the contribution from the low symmetry components of the crystal field.

The problem arises in relating these two parameters, i.e. in calculating the ratio $\langle r^2 \rangle / \langle r^4 \rangle$. To do this, the radial wave function $R_{3d}(r)$ must be accurately known. Self-consistent field wave functions are available for d^6 iron, but only for the free atom. It is not known how appropriate these would be for an iron atom in a molecule.

To overcome this problem, a different approach is made. The formula for the crystal field potential for D_3 is taken as

$$V_{D_3} = V_{O_h} + \text{low symmetry component}$$
$$= V_{O_h} + \text{term in } r^2 Y_2^0.$$

Transforming the last term with equivalent operators [35] yields constant$[L_z^2 - L(L+1)]$. Hence the D_3 potential is taken as

$$V_{D_3} = V_{O_h} + \sum_i \delta \, 1_{iz}^2$$

where δ, the distortion parameter measuring the extent of the lowering of the symmetry from octahedral to trigonal, is regarded as an adjustable parameter.

Furthermore, from mathematical group theory, the effect on the octahedral crystal field eigenstates of lowering the symmetry about the metal ion from O_h to D_3 can be predicted [36]. For example,

O_h	to	D_3
E	goes into	E
T_1	" "	$A_2 + E$
T_2	" "	$A_1 + E$.

The above crystal field potential $V_{D_3} = V_{O_h} + \sum \delta 1_{iz}^2$ does indeed lead to the appropriate splitting of the octahedral crystal field eigenstates [see section 4.4].

This approach considerably simplifies the mathematics, as well as overcoming the problem of unknown parameters. By calculating values of ΔE_Q and μ as a function of δ and comparing these values with those obtained experimentally, a value of δ can be deduced.

Some physical properties are more sensitive to contributions from the low symmetry components than are others. For example, Mössbauer spectroscopy is highly sensitive, magnetic susceptibility moderately sensitive, whereas UV spectroscopy is hardly sensitive at all [37]. Hence in the interpretation of the UV spectrum, the "distortion" is of negligible effect, and the model used is that of a crystal field of octahedral symmetry.

For calculating ΔE_Q and μ, the ion is assumed to be in a crystal field of trigonally distorted octahedral symmetry. Allowance for spin-orbit coupling is also made. The calculations are performed by treating the spin-orbit coupling interaction and the trigonal distortion as perturbations on the octahedral crystal field ground state, $^5T_2$, for high spin d^6 ions. The eigenstates for transition metal ions in crystal fields of octahedral symmetry have been characterized in great detail by Griffith [38]. Mixing of any excited states such as ^5E into the ground state, through spin-orbit coupling, is neglected. The magnetic moment μ and quadrupole splitting ΔE_Q are calculated by using the appropriate Hamiltonians with the crystal field eigenstates, for various ratios of distortion parameter and spin-orbit coupling constant. Temperature dependence is also considered. Comparison with experimental results then enables an estimation of the contribution to the crystal field from the low symmetry components, i.e. the degree of distortion in the ferrous/ascorbate complex.

From this, a prediction of the temperature dependence of μ and ΔE_Q can be made and a correlation made between μ and ΔE_Q.

4.2 Interpretation of Visible Spectrum

To interpret the visible spectrum of the ferrous/ascorbate complex, i.e. to explain the values of λ_{max}, ϵ and f obtained in section 3.3, it is necessary to know the energy levels of the complex. The calculation of the energy levels for a d^6 system, making allowance for both interelectronic interactions and crystal fields of medium strengths is a difficult exercise in quantum mechanics. However, calculations of this type for d^n configurations in crystal fields of octahedral symmetry have been carried out, and presented in the form of Tanabe-Sugano diagrams, for certain values of the Racah parameters (the parameters of interelectronic interaction), B and C [39]. The diagram for d^6 is shown in figure 4.1, together with the value of γ = C/B used in its calculation. The energy levels E are plotted along the vertical axis, and the crystal field strength Δ along the horizontal axis, both being in units of B.

The Racah parameter values required for Fe^{2+} differ from those for Co^{3+}, being γ = 4.1 and B = 1060 cm^{-1} (for Co^{3+}, γ = 4.808 and B = 1065 cm^{-1}). Unfortunately it is not possible to indicate how changes in γ will alter the diagram, though it has been stated [40] that the diagrams do not seem to be sensitive to the ratio γ. However, transitions between terms of the same multiplicity depend only on B,

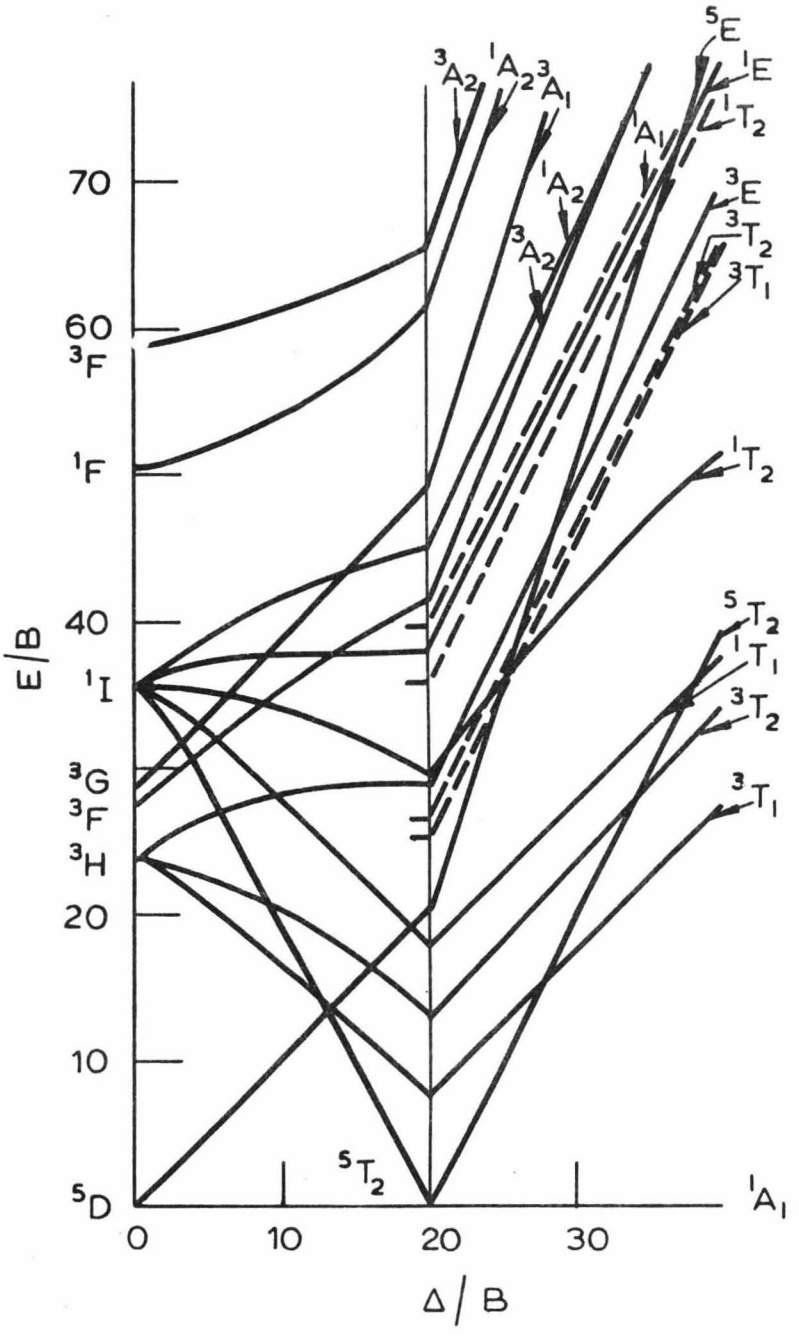

TANABE - SUGANO DIAGRAM FOR d^6, WITH $\gamma = 4 \cdot 808$

FIGURE 4·1

and the energies for these particular transitions are therefore independent of γ.

These diagrams have been calculated for d^n configurations in crystal fields of octahedral symmetry. Provided that the low symmetry crystal field component present in the complex is small compared with the main octahedral crystal field component, the distorted octahedral complex can be treated as a perturbed octahedral complex. This has been discussed in section 4.1.

With these assumptions, it is now possible to characterize the visible spectrum of the complex using the method outlined by Figgis [41]. The purple solution results from an absorption band at 553 mμ = 18,100 cm^{-1} ($\epsilon \doteqdot 110$, $f \doteqdot 4 \times 10^{-3}$). These values of ϵ and f are of the right order of magnitude for a d-d transition. Furthermore, Mössbauer and magnetic moment studies have shown that the $^5T_2$ term is the ground state. Hence, by the selection rule that transitions are spin allowed only between terms of the same multiplicity, the band is assigned to the d-d transition

$$^5T_2 \longrightarrow {}^5E$$

which has an energy of Δ. Hence the value of Δ is 18,100 cm^{-1}.

The values of ϵ and f are higher than the corresponding values for $Fe(H_2O)_6^{2+}$, which has a weak band at 10,000 cm^{-1}

(ϵ= 1.1, f = 1.6 x 10^{-5}) [42]. Band intensities for other complexed ions are often much higher than for the corresponding aquo ion. This has been attributed to the lowest electronic levels occuring at higher energies in the free water molecule than in most other ligands [43], preventing much "intensity stealing". The ascorbate ligand has an absorption band at 265 mμ = 37,700 cm^{-1}, which will cause the d-d band to "intensity steal" and hence have higher ϵ and f values.

From this interpretation of the visible spectrum using the Tanabe-Sugano diagram, a value of the crystal field parameter, Δ, has been obtained. However, as there is only one observed d-d transition, it is not possible to calculate the Racah parameters for the iron atom in the complex.

4.3 Wave Functions and Spin-orbit Interaction Calculation

From an interpretation of the UV spectrum, using the Tanabe-Sugano diagram for d^6, a value for the crystal field parameter Δ has been deduced, in section 4.2. Since this Δ for the complex is less than Δ_c, the critical value of Δ at the cross-over point [see figure 4.1], the excited states are sufficiently high in energy that spin-orbit interaction will not lead to a significant mixing of any excited states into the ground state. Consequently, in these calculations,

only the wave functions for the ground state need be considered.

The ground state for high spin d^6 $^5T_2$ can be represented by $t_2^4(^3T_1)e^2(^3A_2)$ [44]. From Griffith [45] the basis wave functions can be determined from the functions for t_2^4 and e^2, in terms of the complex d orbitals, i.e.

$$|^3T_1\ 1\ 1\rangle = -|1^+ -1^2 \xi_1^+\rangle$$

$$|^3T_1\ 1\ -1\rangle = -|1^2 -1^+ \xi_1^+\rangle$$

$$|^3T_1\ 1\ 0\rangle = |1^+ -1^+ \xi_1^2\rangle$$

$$|^3A_2\ 1a_2\rangle = |\theta^+ \epsilon^+\rangle$$

where e.g. 1^+ $(m_1 m_s)$ has $m_s = +\frac{1}{2}$, $m_1 = 1$

$$\xi_1 = \frac{1}{\sqrt{2}}[|2\rangle - |-2\rangle]$$

$$\epsilon = \frac{1}{\sqrt{2}}[|2\rangle + |-2\rangle]$$

$$\theta = |0\rangle$$

$$\xi_1^2 = \xi_1^+ \xi_1^-$$

and $|m_1\rangle$ is a short-hand notation for the complex d wave function having angular dependence $e^{im_1\phi}$. Therefore it follows that

$$|^5T_2\ -1\ 2\rangle = -|1^2 -1^+ \xi_1^+ \theta^+ \epsilon^+\rangle$$

$$|^5T_2\ 0\ 2\rangle = |1^+ -1^+ \xi_1^2 \theta^+ \epsilon^+\rangle$$

$$|^5T_2\ 1\ 2\rangle \quad = -\ |1^+ -1^2 \xi_1^+ \theta^+ \epsilon^+\rangle$$

where the notation $|^5T_2\ M_L\ M_S\rangle$ will be explained later. Using the spin angular momentum one-electron step operators the complete basis set of wave functions for d^6 may be obtained from the terms listed above. As an example of the use of the step operators, the basis function $|^5T_2\ -1\ 1\rangle$ is derived from that for $|^5T_2\ -1\ 2\rangle$:-

$$\begin{aligned}
|^5T_2\ -1\ 1\rangle &= S_-|^5T_2\ -1\ 2\rangle \\
&= S_-|1^2 -1^+ \xi_1^+ \theta^+ \epsilon^+\rangle \\
&= -\tfrac{1}{2}\,[|1^2 -1^- \xi_1^+ \theta^+ \epsilon^+\rangle + |1^2 -1^+ \xi_1^- \theta^+ \epsilon^+\rangle \\
&\quad + |1^2 -1^+ \xi_1^+ \theta^- \epsilon^+\rangle + |1^2 -1^+ \xi_1^+ \theta^+ \epsilon^-\rangle\,].
\end{aligned}$$

The 15 basis wave functions obtained are given in table 4.1 [tables 4.1 - 4.12 are in Appendix I].

The effect of spin-orbit interaction is calculated by considering the Hamiltonian for spin-orbit interaction,

$$\begin{aligned}
H_s &= \sum_i \zeta\, l_i . s_i \\
&= \sum_i \zeta\, [l_{iz}s_{iz} + l_{ix}s_{ix} + l_{iy}s_{iy}] \\
&= \sum_i \zeta\, [l_{iz}s_{iz} + \tfrac{1}{2}(l_{i+}s_{i-} + l_{i-}s_{i+})]
\end{aligned}$$

where ζ is the spin-orbit coupling constant

l_i is the one-electron orbital angular momentum operator

s_i is the one-electron spin angular momentum operator and the i summation is over the six d electrons.

The 15x15 matrix, whose elements are $\langle \psi_i | H_s | \psi_j \rangle$, where the ψ_i are the basis wave functions, is then set up and its eigenvalues and eigenfunctions calculated. These are given in table 4.2, which shows that one of the eigenvalues is 7-fold degenerate, one is 5-fold, and the other 3-fold degenerate.

This type of calculation using the complex d wave functions is both complicated and time consuming. A much simpler method of finding the eigenstates of spin-orbit interaction is to use the structural isomorphism of a $^{2S+1}T_i$ term to a ^{2s+1}P term [46]. This is justified by the previous assumption that there is no appreciable mixing of any of the excited states into the ground state. Here the $^5T_2$ term is considered equivalent to ^5P_J where J is 3, 2, 1. The wave functions may then be written in terms of $| M_L \; M_S \rangle$, where $M_S = \pm 2, \pm 1, 0$ and $M_L = \pm 1, 0$. This gives 15 basis wave functions, and it may be seen from table 4.1 that these are the terms given on the left hand side of the table.

The spin-orbit interaction is considered using the Hamiltonian

$$H'_s = \sum_i \nu \, l_i . s_i = \nu \, L.S$$

where ν is the spin-orbit coupling constant with respect to the new basis. The eigenfunctions are conveniently obtained using Wigner's formula [47],

$$|L\ S\ J\ M\rangle = \sum_{M_S, M_L} \langle L\ S\ M_L M_S | L\ S\ J\ M\rangle\ |L\ S\ M_L M_S\rangle$$

where $\langle L\ S\ M_L M_S | L\ S\ J\ M\rangle$ are the Clebsch-Gordon-Wigner coefficients and $|L\ S\ M_L M_S\rangle$ (or $|M_L M_S\rangle$ as L and S are constant throughout and can therefore be omitted) are the basis wave functions. The resulting eigenfunctions are the same as for the complex d case, as given in table 4.2.

The eigenvalues are then simply the diagonal elements of the spin-orbit interaction Hamiltonian, with respect to the appropriate eigenfunction:

$$\begin{aligned} E &= \langle J\ M | H'_s | J\ M\rangle = \langle J\ M | \nu\ L.S | J\ M\rangle \\ &= \langle J\ M | \frac{\nu}{2} [J^2 - L^2 - S^2] | J\ M\rangle \\ &= \langle J\ M | \frac{\nu}{2} [J(J+1) - L(L+1) - S(S+1)] | J\ M\rangle \\ &= \frac{\nu}{2} [J(J+1) - L(L+1) - S(S+1)]. \end{aligned}$$

In this case L = 1, S = 2 and J = 3, 2, 1, giving three eigenvalues,

$$\langle 3\ M | H'_s | 3\ M\rangle = 2\nu$$

$$\langle 2\ M | H'_s | 2\ M\rangle = -\nu$$

$$\langle 1\ M | H'_s | 1\ M\rangle = -3\nu\ .$$

Comparison with the previous results, given in table 4.2,

shows that ν is equivalent to $\zeta/4$.

4.4 Distortion Calculation

Having obtained the eigenstates for spin-orbit coupling interaction, the next effect to be considered is the lowering of the symmetry of the octahedral field, i.e. the "distortion" of the crystal field around the ion, as discussed in section 4.1. The appropriate Hamiltonian is taken as

$$H_d = \sum_i \delta \, l_{iz}^2 = \delta \, L_z^2$$

where δ is the distortion parameter. This is applied as a perturbation to the eigenfunctions ϕ_i of spin-orbit interaction.

Using this Hamiltonian, the 15x15 matrix whose elements are $\langle \phi_i | H_s + H_d | \phi_j \rangle$ is set up. This factorizes into three 1x1, three 2x2 and two 3x3 matrices, which are given in table 4.3. As it is not convenient to solve these matrices for the general case, numerical values were substituted for the ratio $x = \delta/\zeta$. The range of values considered for x was from -1.5 to +2.5.

Having obtained the matrix elements for the various x values, the eigenvalues and eigenfunctions were calculated using an ALGOL Jacobi eigenvalue procedure, on the Elliott 503 computer, of the Applied Mathematics Division, Department of Scientific and Industrial Research. A typical set of eigenstates for one value of x is given in table 4.4.

For cases when the distortion to the crystal field is much larger than the spin-orbit coupling interaction, the wave functions must first be diagonalized with respect to the distortion Hamiltonian H_d; then the spin-orbit coupling interaction Hamiltonian, H_s', is applied as a perturbation. The isomorphous p wave functions $|M_L M_S\rangle$ are taken as the basis, these already being eigenfunctions of H_d since L_z^2 does not alter the basis wave functions. The eigenvalues are then simply the diagonal matrix elements, $\langle M_L M_S | H_d | M_L M_S \rangle$, i.e.

$$\langle \pm 1 \; M_S | \delta L_z^2 | \pm 1 \; M_S \rangle = \delta$$

$$\langle 0 \; M_S | \delta L_z^2 | 0 \; M_S \rangle = 0 .$$

Under this reduction of symmetry, the ground state is split into two states, separated by an amount δ.

The spin-orbit coupling Hamiltonian, H_s', is now applied to the wave functions, and the matrix elements $\langle M_L M_S | H_d + H_s' | M_L' M_S' \rangle$ evaluated. The 15x15 matrix factorizes into two 1x1, two 2x2, and three 3x3 submatrices, these being given in table 4.5.

To find the limiting values of the matrix elements when δ/ζ tends to infinity, the ratio ζ/δ is given the value zero. The only non-zero terms in the matrices are then those arising solely from the distortion, i.e. the effect of spin-orbit coupling is negligible. Therefore the matrix elements

obtained are those for H_d, namely δ or 0.

As values of δ/ζ greater than 2.5 were not used in these calculations, matrices arising from large distortion were not needed for the remaining calculations.

4.5 Magnetic Moment Calculations

Having obtained the eigenvalues and eigenfunctions resulting from spin-orbit coupling and a distortion from octahedral symmetry, the effect of an external magnetic field is next considered. The magnetic interaction Hamiltonian to be applied to the eigenfunctions of spin-orbit and distortion interactions is

$$H'_m = \sum_i \beta(l_i + 2s_i).H$$

$$= \beta(L + 2S).H$$

$$= \beta H_z(L_z+2S_z) + \beta H_y(L_y+2S_y) + \beta H_x(L_x+2S_x)$$

where β is the Bohr magneton

H is the applied magnetic field.

When applied to the isomorphous p wave functions, this Hamiltonian is transformed to

$$H_m = \beta(\gamma L + 2S).H$$

$$= \beta H_z(\gamma L_z+2S_z) + \beta H_y(\gamma L_y+2S_y) + \beta H_x(\gamma L_x+2S_x)$$

$$= H_{//} + 2H_{\perp}$$

where γ is a constant to be determined, arising from the use of the isomorphous p wave functions

$$H_{//} = \beta H_z(\gamma L_z + 2S_z)$$

$$H_{\perp} = \beta H_y(\gamma L_y + 2S_y) = \beta H_x(\gamma L_x + 2S_x).$$

The constant γ is determined by evaluating one matrix element $\langle \phi_i | H_{//} | \phi_i \rangle$ using the complex d wave functions and comparing this with the corresponding element obtained using the isomorphous p wave functions:

$$\langle \phi_1 | H_{//} | \phi_1 \rangle = \langle 1\ 2 \mid \beta H(\gamma L_z + 2S_z) \mid 1\ 2 \rangle$$

$$= (\gamma + 4)\beta H$$

$$\langle {}^5T_2\ 1\ 2 | H'_{//} | {}^5T_2\ 1\ 2 \rangle = \langle 1^+ -1^2 \xi_1^+ \theta^+ \epsilon^+ | \beta H(L_z + 2S_z) | 1^+ -1^2 \xi_1^+ \theta^+ \epsilon^+ \rangle$$

$$= 3\ \beta H.$$

Hence $\gamma = -1$. The Hamiltonians can now be written

$$H_{//} = \beta H(-L_z + 2S_z)$$

$$H_{\perp} = \beta H(-L_x + 2S_x)$$

$$= \beta H\ [-\tfrac{1}{2}(L_+ + L_-) + (S_+ + S_-)].$$

The eigenfunctions ψ_i of the spin-orbit and distortion Hamiltonian, $H'_s + H_d$, have been determined as linear combinations of the eigenfunctions ϕ_i of the spin-orbit interaction Hamiltonian, H'_s. The effect of $H_{//}$ and $H_{\perp}$ on these spin-orbit eigenfunctions ϕ_i is therefore determined first. For $H_{//}$, e.g.

$$\langle \phi_2 | H_{//} | \phi_2 \rangle = \left\langle \sqrt{\tfrac{2}{3}}\ |1\ 1\rangle + \sqrt{\tfrac{1}{3}}\ |0\ 2\rangle \middle| \beta H(-L_z + 2S_z) \middle| \sqrt{\tfrac{2}{3}} |1\ 1\rangle + \sqrt{\tfrac{1}{3}} |0\ 2\rangle \right\rangle$$

$$= \left\langle \sqrt{\tfrac{2}{3}}\,|1\ 1\rangle + \sqrt{\tfrac{1}{3}}\,|0\ 2\rangle \,\middle|\, \sqrt{\tfrac{2}{3}}\,\beta H\,|1\ 1\rangle + \sqrt{\tfrac{1}{3}}\,4\beta H\,|0\ 2\rangle \right\rangle$$

$$= \tfrac{2}{3}\,\beta H \langle 1\ 1 \mid 1\ 1\rangle + \tfrac{4}{3}\,\beta H \langle 0\ 2 \mid 0\ 2\rangle$$

$$= 2\,\beta H$$

$$\langle \phi_2 | H_{\parallel} | \phi_8 \rangle = \left\langle \sqrt{\tfrac{2}{3}}\,|1\ 1\rangle + \sqrt{\tfrac{1}{3}}\,|0\ 2\rangle \,\middle|\, \beta H(-L_z + 2S_z) \,\middle|\, -\sqrt{\tfrac{1}{3}}\,|1\ 1\rangle + \sqrt{\tfrac{2}{3}}\,|0\ 2\rangle \right\rangle$$

$$= \left\langle \sqrt{\tfrac{2}{3}}\,|1\ 1\rangle + \sqrt{\tfrac{1}{3}}\,|0\ 2\rangle \,\middle|\, -\sqrt{\tfrac{1}{3}}\,\beta H\,|1\ 1\rangle + \sqrt{\tfrac{2}{3}}\,4\beta H\,|0\ 2\rangle \right\rangle$$

$$= -\tfrac{\sqrt{2}}{3}\,\beta H \langle 1\ 1 \mid 1\ 1\rangle + \tfrac{4}{3}\sqrt{2}\,\beta H \langle 0\ 2 \mid 0\ 2\rangle$$

$$= \sqrt{2}\,\beta H.$$

[Note that since $H_{\parallel}$ does not alter the M_S or M_L values of the wave functions, the only non-zero matrix elements will be between ϕ_i's containing linear combinations of basis functions with the same M_S and M_L values]. Similarly, for the $H_\perp$ case,

$$\langle \phi_1 | H_\perp | \phi_1 \rangle = \langle 1\ 2 \mid \beta H[-\tfrac{1}{2}(L_+ + L_-) + (S_+ + S_-)] \mid 1\ 2\rangle$$

$$= \left\langle 1\ 2 \,\middle|\, -\tfrac{\sqrt{2}}{2}\,\beta H\,|0\ 2\rangle + 2\,\beta H\,|1\ 1\rangle \right\rangle$$

$$= 0$$

$$\langle \phi_2 | H_\perp | \phi_1 \rangle = \left\langle \sqrt{\tfrac{2}{3}}\,|1\ 1\rangle + \sqrt{\tfrac{1}{3}}\,|0\ 2\rangle \,\middle|\, \beta H[-\tfrac{1}{2}(L_+ + L_-) + (S_+ + S_-)] \mid 1\ 2\rangle \right\rangle$$

$$= \left\langle \sqrt{\tfrac{2}{3}}\,|1\ 1\rangle + \sqrt{\tfrac{1}{3}}\,|0\ 2\rangle \,\middle|\, -\tfrac{\sqrt{2}}{2}\,\beta H\,|0\ 2\rangle + 2\,\beta H\,|1\ 1\rangle \right\rangle$$

$$= 2\sqrt{\tfrac{2}{3}}\,\beta H \langle 1\ 1 \mid 1\ 1\rangle - \tfrac{1}{2}\sqrt{\tfrac{2}{3}}\,\beta H \langle 0\ 2 \mid 0\ 2\rangle$$

$$= \sqrt{\tfrac{3}{2}}\,\beta H.$$

[Note that since $H_\perp$ contains only step-up and step-down angular momentum operators, it must alter either the M_S or the M_L values of the wave functions. Hence matrix elements between ϕ_i's containing linear combinations of the same basis wave functions must necessarily be zero, i.e. $\langle \phi_i | H_\perp | \phi_i \rangle = 0$ in particular].

These matrix elements with respect to the ϕ_i's, given in tables 4.6 and 4.7, are then used to find the matrix elements associated with the Hamiltonians H_1 and H_2, where

$$H_1 = H'_s + H_d + H_{//}$$

$$H_2 = H'_s + H_d + H_\perp \quad .$$

Two 15x15 matrices, with elements $\langle \psi_i | H_1 | \psi_j \rangle$ and $\langle \psi_i | H_2 | \psi_j \rangle$, are now set up. The first factorizes into two 1x1, two 2x2 and three 3x3 matrices; the second does not factorize. The off-diagonal elements contain terms in βH only, as the ψ_i have already been diagonalized with respect to $H'_s + H_d$. The diagonal elements are made up of the eigenvalues of $H'_s + H_d$ plus, in the case of H_1, a contribution from $H_{//}$. The diagonal elements for H_2 arising from $H_\perp$ have already been shown to be zero.

These off-diagonal elements are very much smaller than the diagonal elements, for values of the magnetic field H used experimentally:

$$\beta = 0.9273 \times 10^{-20} \text{ erg.gauss}^{-1} = 4.670 \times 10^{-5} \text{ cm}^{-1}\text{gss}^{-1}$$

and for H = 10,000 gauss, $\beta H \doteq 0.5\ cm^{-1}$, which is small compared with ζ ($\doteq 400\ cm^{-1}$ for the free Fe ion [48]).

To solve the matrices H_{ij} for their eigenvalues, E_i, second order perturbation theory was used [49]:

$$E_i = H_{ii} + \sum_{i \neq j}^{n} \frac{H_{ij} H_{ji}}{H_{ii} - H_{jj}} ,$$

where $H_{ij} = \langle \phi_i | H | \phi_j \rangle$.

Fifteen eigenvalues are obtained for each matrix, these being of the form

$$E_{\parallel i} = A_i \zeta + B_i \beta H + C_i \frac{\beta^2 H^2}{\zeta}$$

$$E_{\perp i} = A_i \zeta + D_i \frac{\beta^2 H^2}{\zeta}$$

where the A_i, B_i, C_i and D_i are numerical constants. It is found that for each value of δ/ζ there are 9 different values for A_i, C_i and D_i, while the B_i have 12 values (6 $\pm$ paired values), the other values being zero. The A_i values are the eigenvalues of the Hamiltonian $H_s' + H_d$. The constants are given for each value of δ/ζ in table 4.8.

Having obtained the eigenvalues, the magnetic susceptibility can be calculated from the formula [50]

$$\chi = \frac{N}{H} \frac{\sum_i \frac{-\partial E}{\partial H} i \exp(-E_i/kT)}{\sum_i \exp(-E_i/kT)}$$

where χ is the molar susceptibility

N is the Avogadro number

k is the Boltzmann constant

the E_i are the eigenvalues

and H is the applied magnetic field.

The formulae for $\chi_{//}$ and $\chi_{\perp}$ are defined similarly. In applying this formula, the mathematical approximation

$$\exp(b+a) \doteq (1+b)\exp(a) \qquad \text{if } a \gg b$$

is made. It has been shown previously that terms in βH are very much smaller than terms in ζ. Terms in higher powers of βH, i.e. $\beta^2 H^2$, are negligible and are omitted. Thus,

$$-\frac{\partial E_{//i}}{\partial H}\exp(-E_{//i}/kT) = [-B_i\beta - 2C_i\beta^2\frac{H}{\zeta}]\exp(-A_i\zeta/kT)[1-B_i\beta H/kT]$$

$$= [-B_i\beta + B_i^2\frac{\beta^2 H}{kT} - 2C_i\beta^2\frac{H}{\zeta}]\exp(-A_i\zeta/kT)$$

$$-\frac{\partial E_{\perp i}}{\partial H}\exp(-E_{\perp i}/kT) = [-2D_i\beta^2\frac{H}{\zeta}]\exp(-A_i\zeta/kT)$$

$$\chi_{//} = \frac{N\beta^2}{kT}\frac{\sum_{i=1}^{9}[B_i^2 - 2C_i\frac{kT}{\zeta}]\exp(-A_i\zeta/kT)}{\sum_{i=1}^{6}2\exp(-A_i\zeta/kT) + \sum_{i=7}^{9}\exp(-A_i\zeta/kT)}$$

$$\chi_{\perp} = \frac{N\beta^2}{kT}\frac{\sum_{i=1}^{9}[-2D_i\,kT/\zeta]\exp(-A_i\zeta/kT)}{\sum_{i=1}^{6}2\exp(-A_i\zeta/kT) + \sum_{i=7}^{9}\exp(-A_i\zeta/kT)}\ .$$

The terms in $B_i\beta$ cancel out on summation and are omitted.

Therefore the summation is over 9 eigenvalues, 6 of these being effectively doubly degenerate under this condition.

The magnetic moment is then found from the formula [50]

$$\chi = \frac{N\beta^2}{3kT}\mu^2.$$

The constants $N\beta^2/kT$ cancel on substituting the values for $\chi_{\parallel}$ and $\chi_{\perp}$ to obtain $\mu_{\parallel}$ and $\mu_{\perp}$. Initially ζ/kT was taken as 2.0, assuming that $\zeta \doteqdot 400$ cm^{-1} [47] ($kT \doteqdot 200$ cm^{-1} at room temperature). The temperature dependence was calculated by varying the value for kT/ζ.

The average magnetic moment [51]

$$\mu^2 = \frac{1}{3}\left(\mu_{\parallel}^2 + 2\mu_{\perp}^2\right)$$

is calculated for varying ratios of δ/ζ and kT/ζ. The values of $\mu_{\parallel}$, $\mu_{\perp}$ and μ, for various ratios of δ/ζ, for $\zeta/kT = 2.0$, are given in table 4.9 and figure 4.2. The variations of μ with kT/ζ and ζ/kT, for different values of δ/ζ, are given in table 4.10 and figures 4.3 and 4.4.

4.6 Quadrupole Splitting Calculations

The electrostatic interaction between electrons and nucleons gives rise to a nuclear quadrupole interaction, which is represented, for interactions with d electrons, by the Hamiltonian

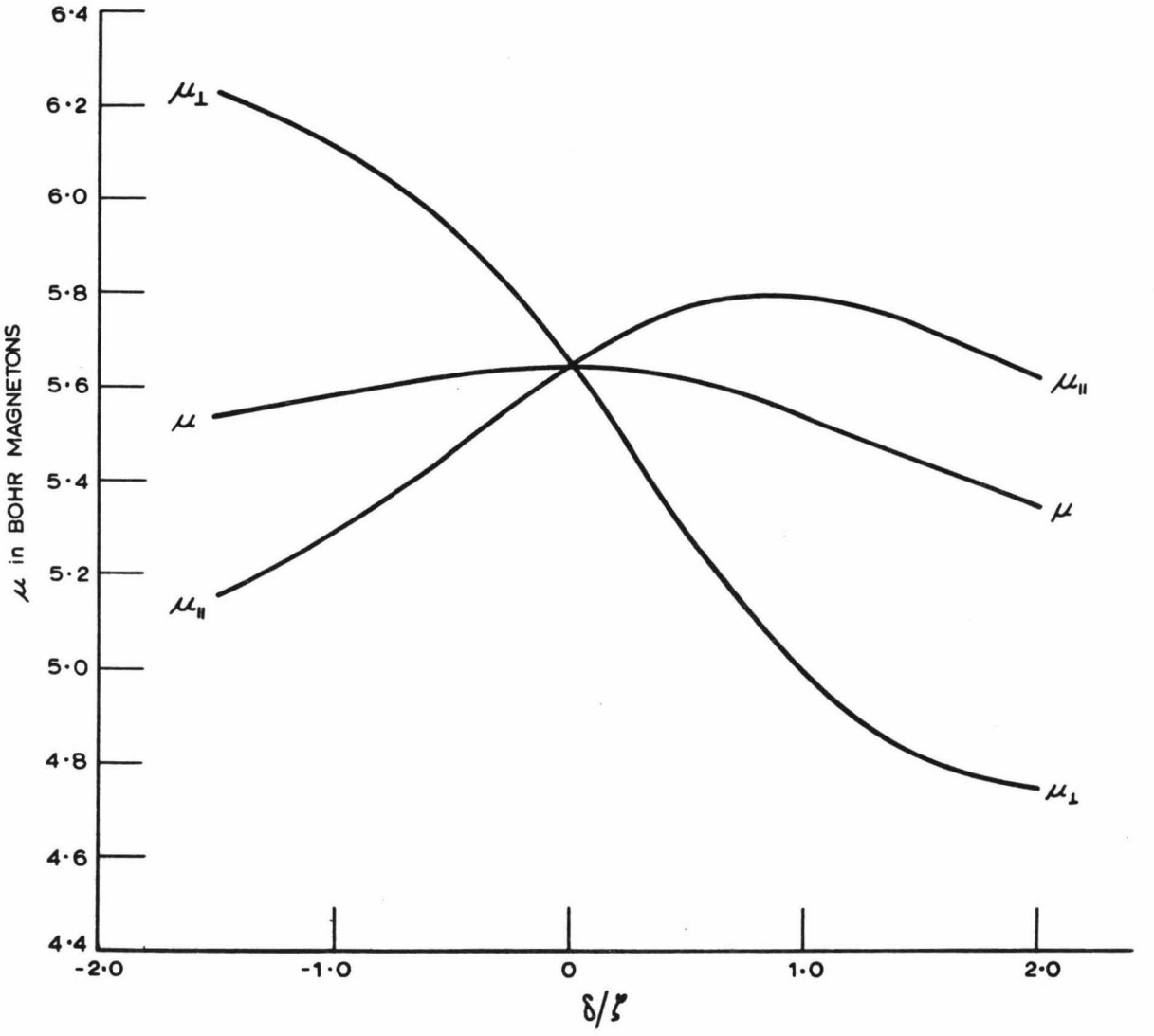

$\mu_\parallel, \mu_\perp, \mu$ AGAINST RATIOS δ/ζ AT $\zeta/kT = 2 \cdot 0$

FIGURE 4·2

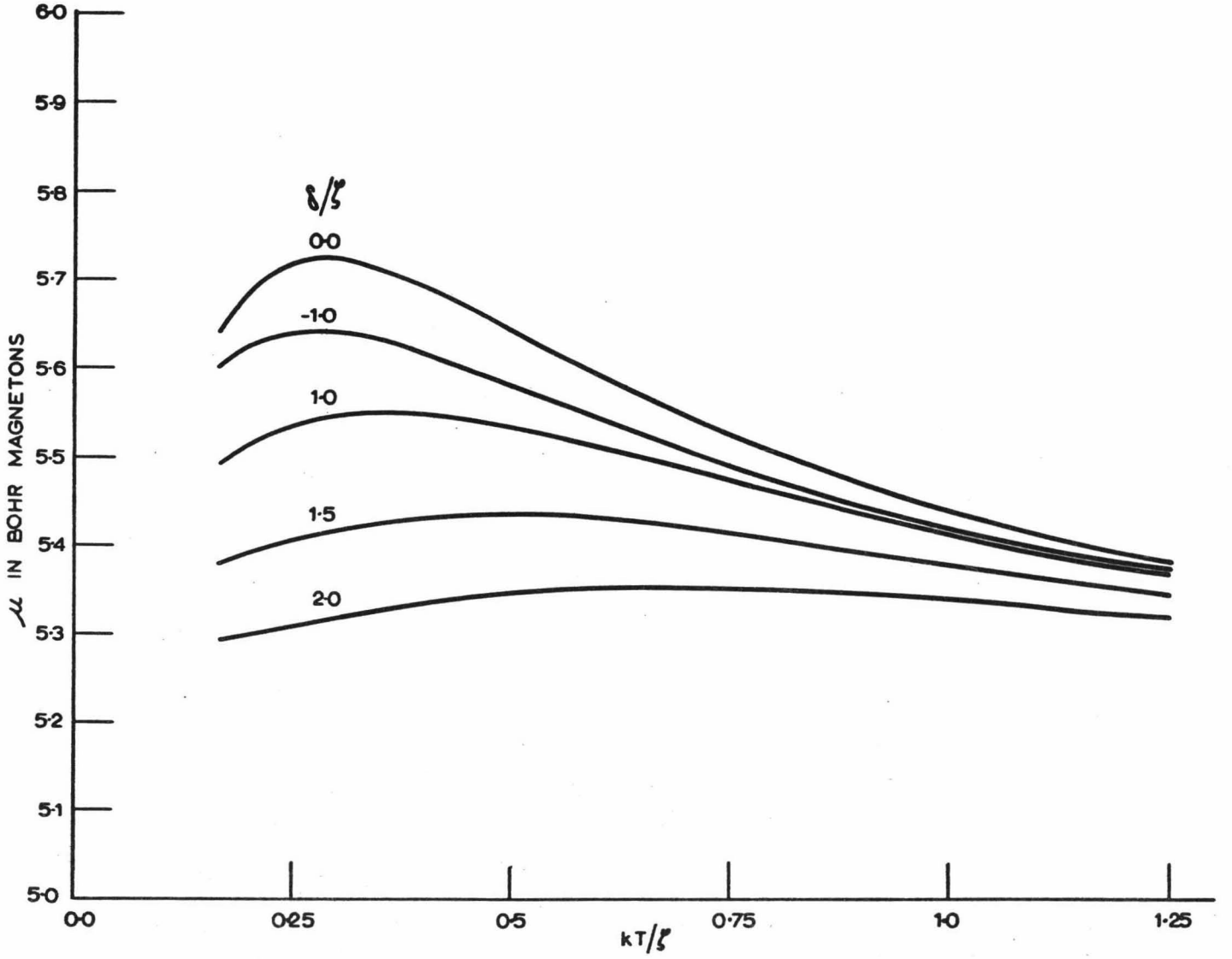

μ AGAINST kT/ζ FOR VARIOUS RATIOS OF δ/ζ

FIGURE 4·3

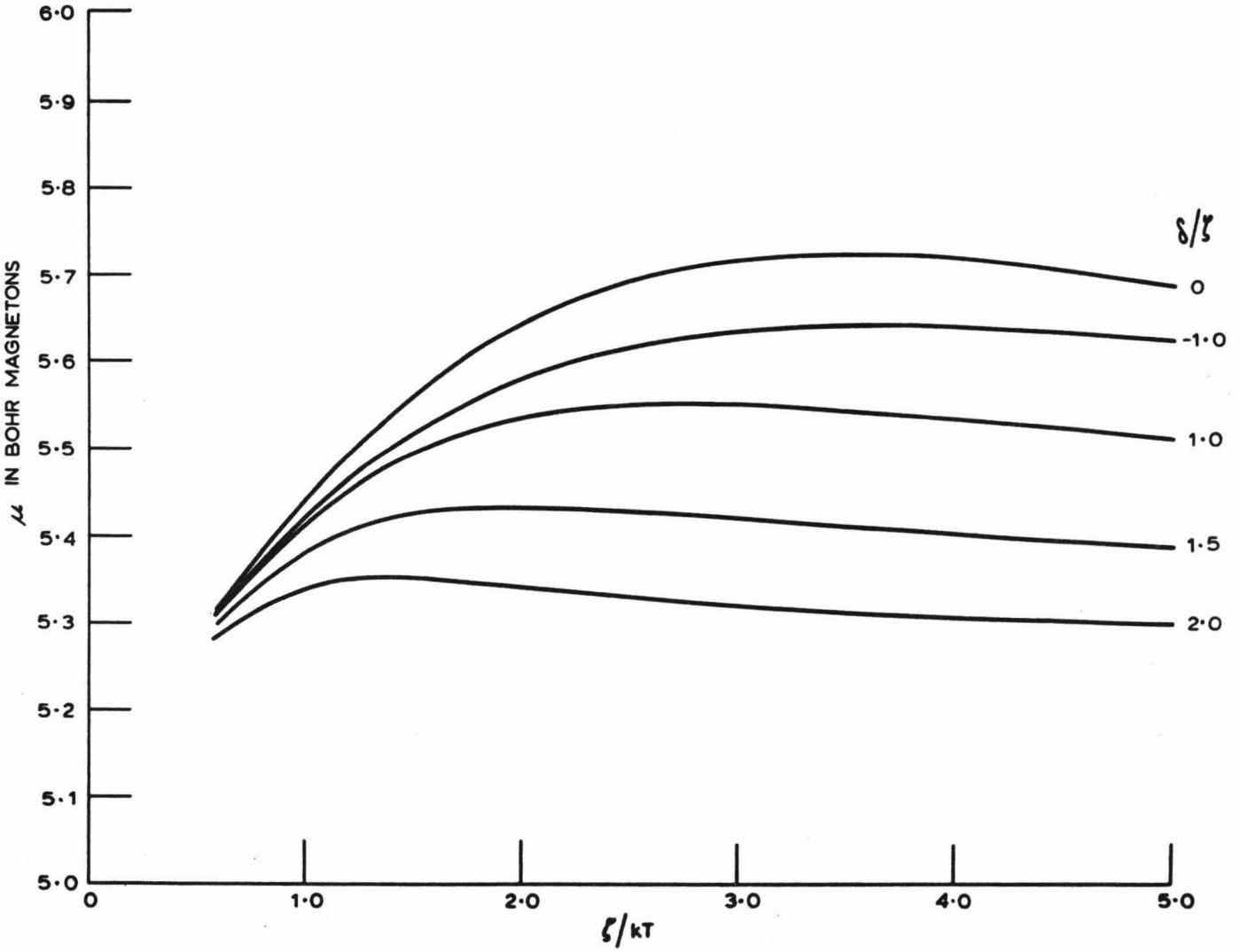

μ AGAINST RATIO ζ/kT FOR VARIOUS RATIOS OF δ/ζ

FIGURE 4·4

$$H_Q = \frac{e^2 Q' \langle r^{-3} \rangle}{7\ I(2I-1)} \sum_i \left[(l_i . I)^2 + \tfrac{1}{2}(l_i . I) - 2I(I+1) \right]$$

$$= P \sum_i \left[(l_i . I)^2 + \tfrac{1}{2}(l_i . I) - 2I(I+1) \right]$$

where I is the nuclear spin

Q' is the quadrupole moment including any shielding effects

$\langle r^{-3} \rangle$ is the average value of the inverse cube of the radial wave function of the d electrons.

In this calculation the basis wave functions employed are the complex d wave functions. The spin quantum number M_S no longer enters into the calculation and is omitted, but allowance must be made for the nuclear spin quantum number, M_I. Therefore the basis wave functions can be represented by

$$|1\ M_I\rangle \qquad |0\ M_I\rangle \qquad |-1\ M_I\rangle$$

in the $|M_L\ M_I\rangle$ notation. The Hamiltonian H_Q is applied to each of these and the matrix elements $\langle M_L\ M_I | H_Q | M'_L\ M'_I \rangle$ calculated, e.g.

$$\langle 1\ M | H_Q | 1\ M \rangle = \langle 1\ M \,|\, P \sum [(l_i I)^2 + \tfrac{1}{2}(I_i I) - 2I(I+1)] \,|\, 1\ M \rangle$$

$$= \langle 1\ M \,|\, [\, M^2 + \tfrac{M}{2} + K_-^2 + \tfrac{3}{2} K_+^2 - 2I(I+1) \,|\, 1\ M \rangle$$

$$+ \text{terms in } |0\ M+1\rangle\ ,\ |-1\ M+2\rangle, |2\ M-1\rangle]$$

$$= P \left[M^2 + \frac{M}{2} + K_-^2 + \frac{3}{2} K_+^2 - 2I(I+1) \right] \langle 1\ M \,|\, 1\ M \rangle$$

$$= - P[3M^2 - I(I+1)]$$

where $K_{\pm} = [I(I+1) - M(M\pm1)]^{\frac{1}{2}}$.

The only non-zero matrix elements are those between wave functions containing the same M_I and M_L values. Three elements are thus obtained,

$$\langle 1\ M \mid H_Q \mid 1\ M \rangle = - \frac{P'}{2}$$

$$\langle 0\ M \mid H_Q \mid 0\ M \rangle = P'$$

$$\langle -1\ M \mid H_Q \mid -1\ M \rangle = - \frac{P'}{2}$$

where $P' = P\,[3M^2 - I(I+1)]$.

The Hamiltonian can now be applied to the eigenfunctions ϕ_i of spin-orbit coupling interaction, obtained in section 4.3, e.g.

$$\langle \phi_3 | H_Q | \phi_3 \rangle = \left\langle \sqrt{\frac{2}{5}} \,|1\ 0\rangle + \sqrt{\frac{8}{15}} \,|0\ 1\rangle + \sqrt{\frac{1}{15}} \,|-1\ 2\rangle \right| H_Q \left| \sqrt{\frac{2}{5}} \,|1\ 0\rangle + \sqrt{\frac{8}{15}} \,|0\ 1\rangle + \sqrt{\frac{1}{15}} \,|-1\ 2\rangle \right\rangle$$

$$= \left[-\frac{2}{5} + 2x\,\frac{8}{15} - \frac{1}{15} \right] \frac{P'}{2}$$

$$= \frac{3}{10} P'.$$

These matrix elements, given in table 4.11, are now used to find the matrix elements associated with the Hamiltonian

$$H_3 = H'_s + H_d + H_Q.$$

Since H_Q is a very small perturbation to the crystal field, only the diagonal matrix elements $\langle \phi_i\ M \mid H_3 \mid \phi_i\ M \rangle$ need be

considered. For each value of δ/ζ, 9 eigenvalues are obtained, 6 of these being doubly degenerate. The eigenvalues are of the form

$$E_{Qi} = A_i \zeta + G_i P'$$

where A_i, G_i are numerical constants, the A_i being as defined before. These constants are given for each value of δ/ζ in table 4.8.

The nuclear quadrupole interaction energies, $G_i P'$, are now used to obtain the average E_Q values by taking a Boltzmann distribution over the eigenvalues $A_i\zeta$ obtained for the spin-orbit coupling and distortion Hamiltonian,

$$\langle E_Q \rangle = P' \frac{\sum_i G_i \exp(-A_i \zeta/kT)}{\sum_i \exp(-A_i \zeta/kT)} .$$

The quadrupole splitting for the ^{57}Fe nucleus with spin $I = 3/2$ is the difference between the average E_Q values for the nuclear spin states $M_I = \pm 1/2, \pm 3/2$:

$$\Delta E_Q = \langle E_Q(M_I = \pm 3/2) \rangle - \langle E_Q(M_I = \pm 1/2) \rangle$$

$$= \frac{2}{7} e^2 Q' \langle r^{-3} \rangle \frac{\sum_i G_i \exp(-A_i \zeta/kT)}{\sum_i \exp(-A_i \zeta/kT)}$$

$$= 3.70 \frac{\sum_i G_i \exp(-A_i \zeta/kT)}{\sum_i \exp(-A_i \zeta/kT)} .$$

For a discussion of the constant 3.70, see Golding [52].

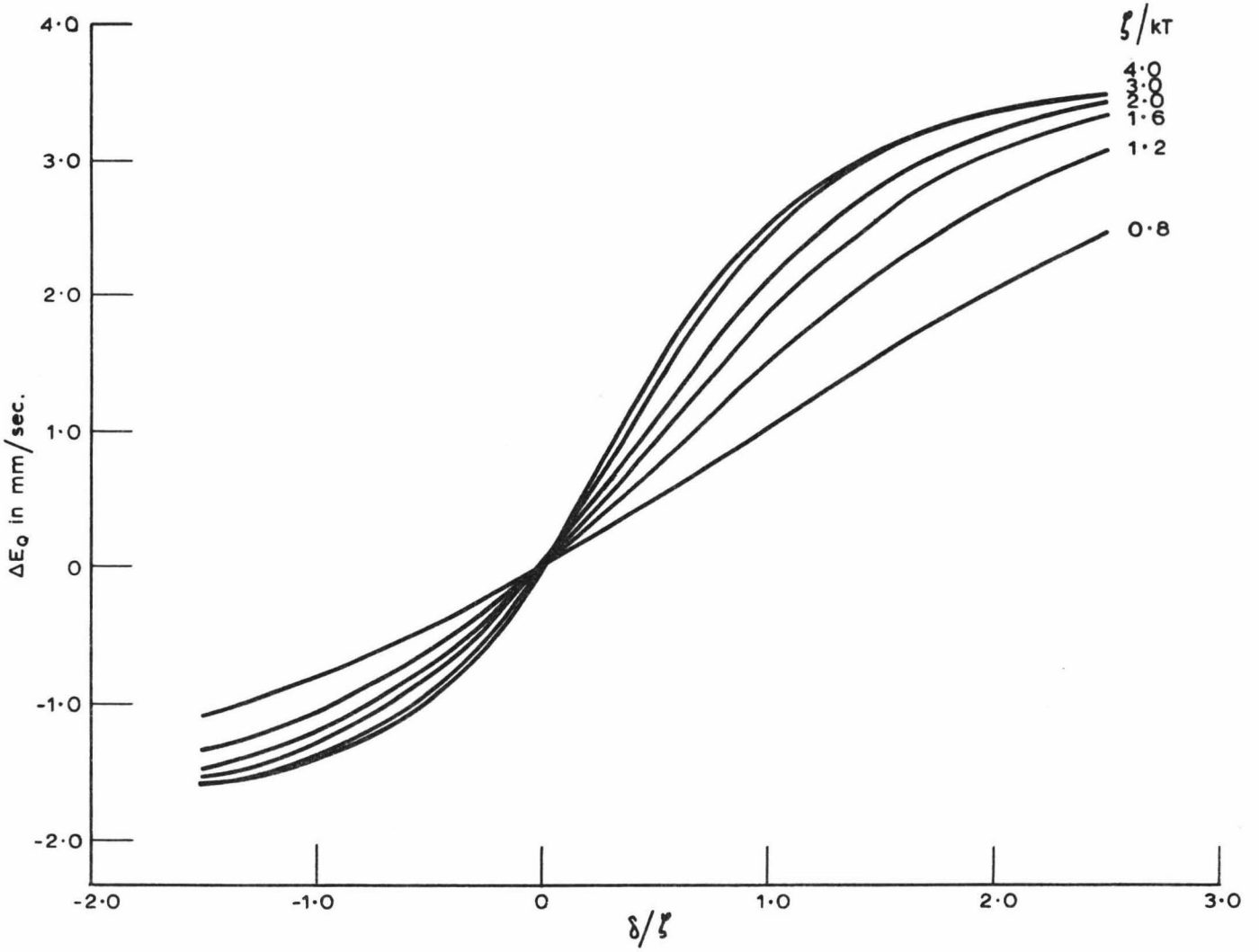

ΔEQ AGAINST RATIO δ/ζ FOR DIFFERENT RATIOS ζ/kT

FIGURE 4·5

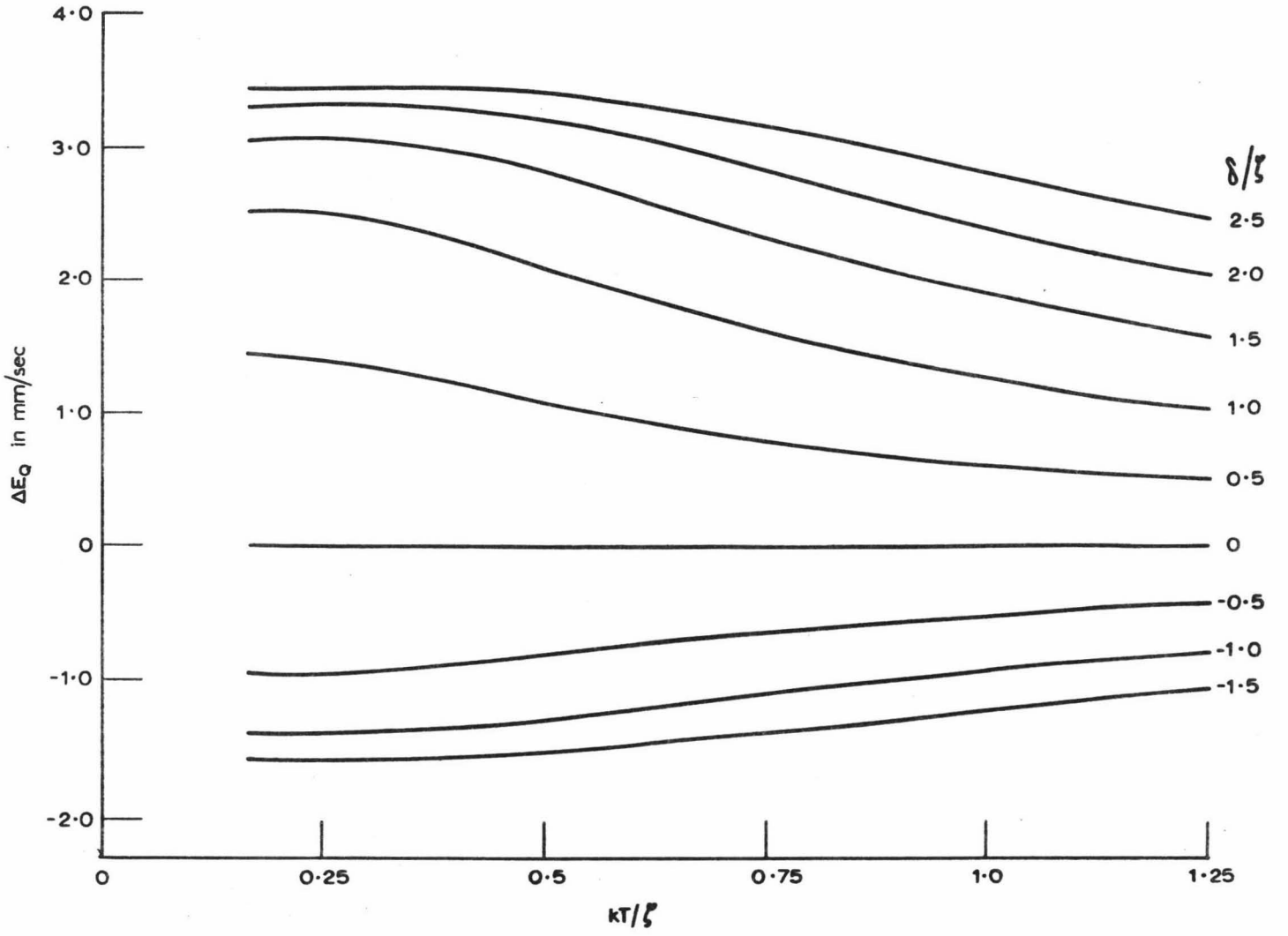

ΔE_Q AGAINST kT/ζ FOR DIFFERENT RATIOS δ/ζ

FIGURE 4·6

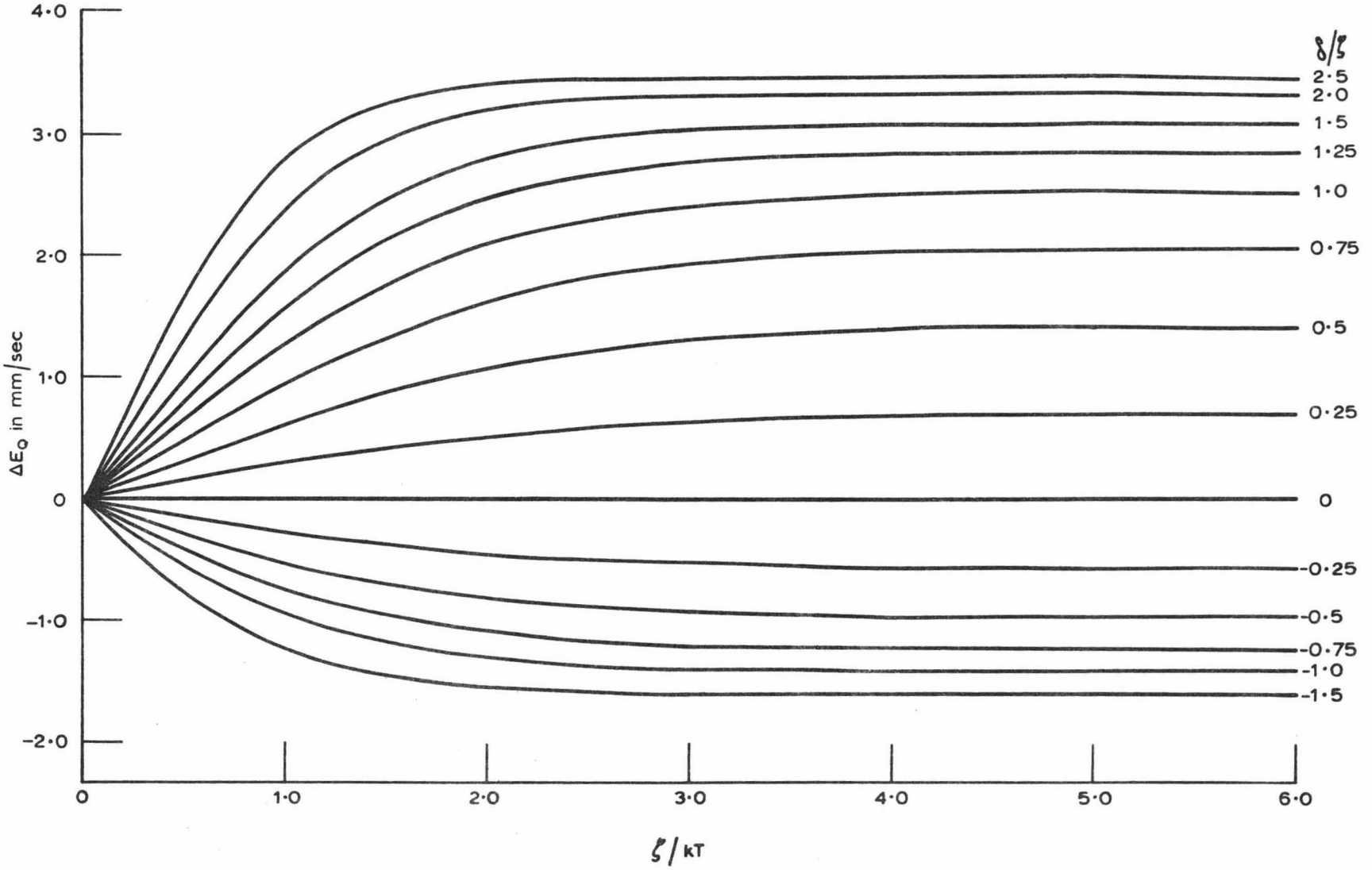

ΔE_Q AGAINST RATIO ζ/kT FOR DIFFERENT RATIOS δ/ζ

FIGURE 4·7

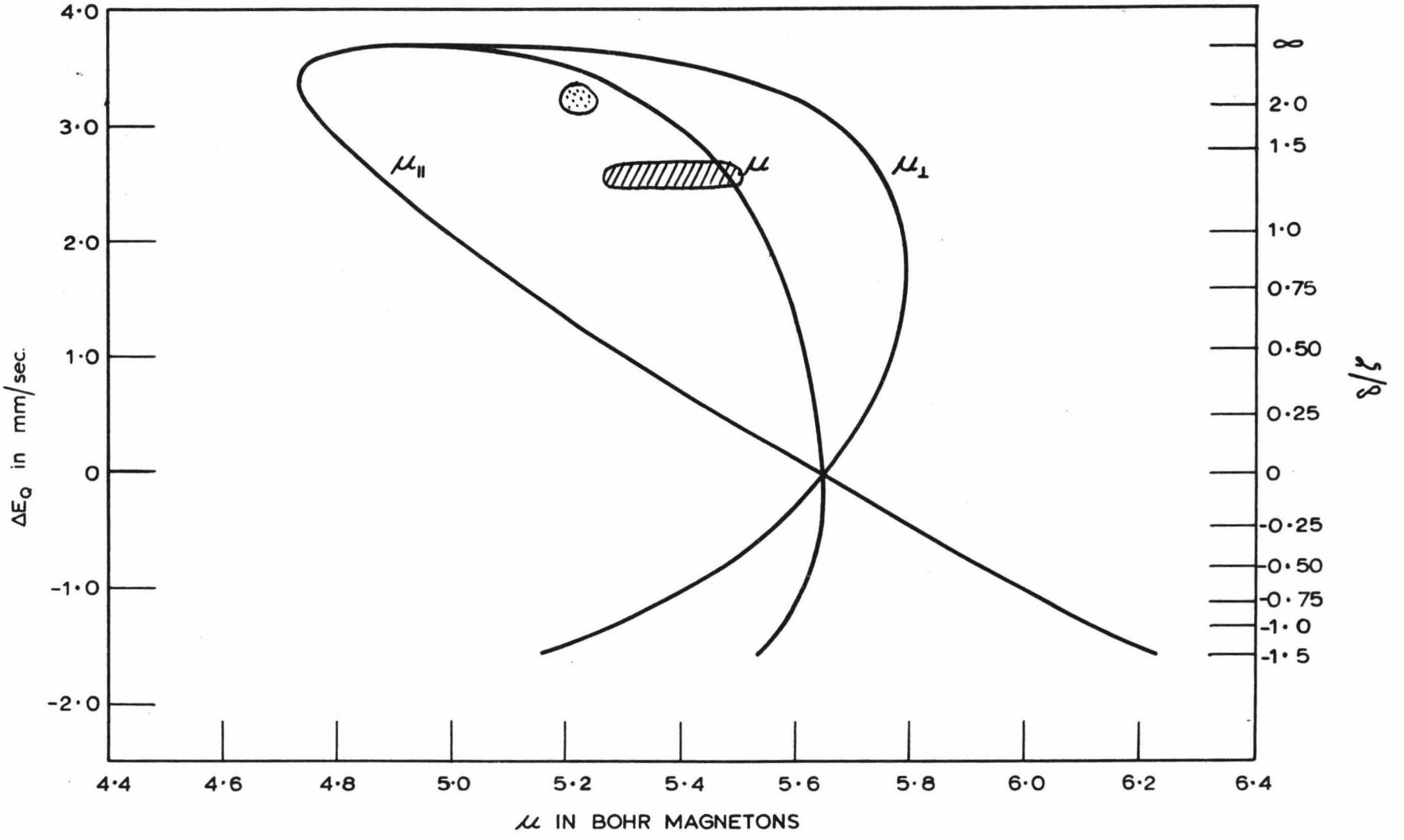

ΔE_Q AGAINST $\mu_{\parallel}$, $\mu_{\perp}$ AND μ FOR VARIOUS RATIOS δ/ζ AT $\zeta/kT = 2\cdot0$

FIGURE 4·8

The values of ΔE_Q for various ratios of δ/ζ are given in table 4.9 and figure 4.5, for $kT/\zeta = 0.5$. The temperature dependence of ΔE_Q was also calculated, by varying kT/ζ, and this is given in table 4.12 and figures 4.6 and 4.7.

The variation of ΔE_Q with μ is shown for varying ratios of δ/ζ at $\zeta/kT = 2.0$ in figure 4.8.

4.7 Discussion of Results

From calculations based on the "distorted" Crystal Field model for the ferrous/ascorbate complex, the variation of ΔE_Q and μ with various parameters has been obtained. Suitable values of these parameters can now be used to interpret the experimental results given in sections 3.7 and 3.8. The spin-orbit coupling constant, ζ, which is 400 cm^{-1} for the free ferrous ion [48], is usually taken to have 70-80 % of this value for ferrous in complex ions, so that a suitable value would be 300 cm^{-1}; both 400 and 300 cm^{-1} are considered for ζ. Thus only δ, the distortion parameter, remains to be determined from the experimental results.

As the Mössbauer results are not affected by the unknown factors in the nature of the solid complex, there is no problem in determining δ from the ΔE_Q values. From figure 4.9, the region of figure 4.5 in which the experimental

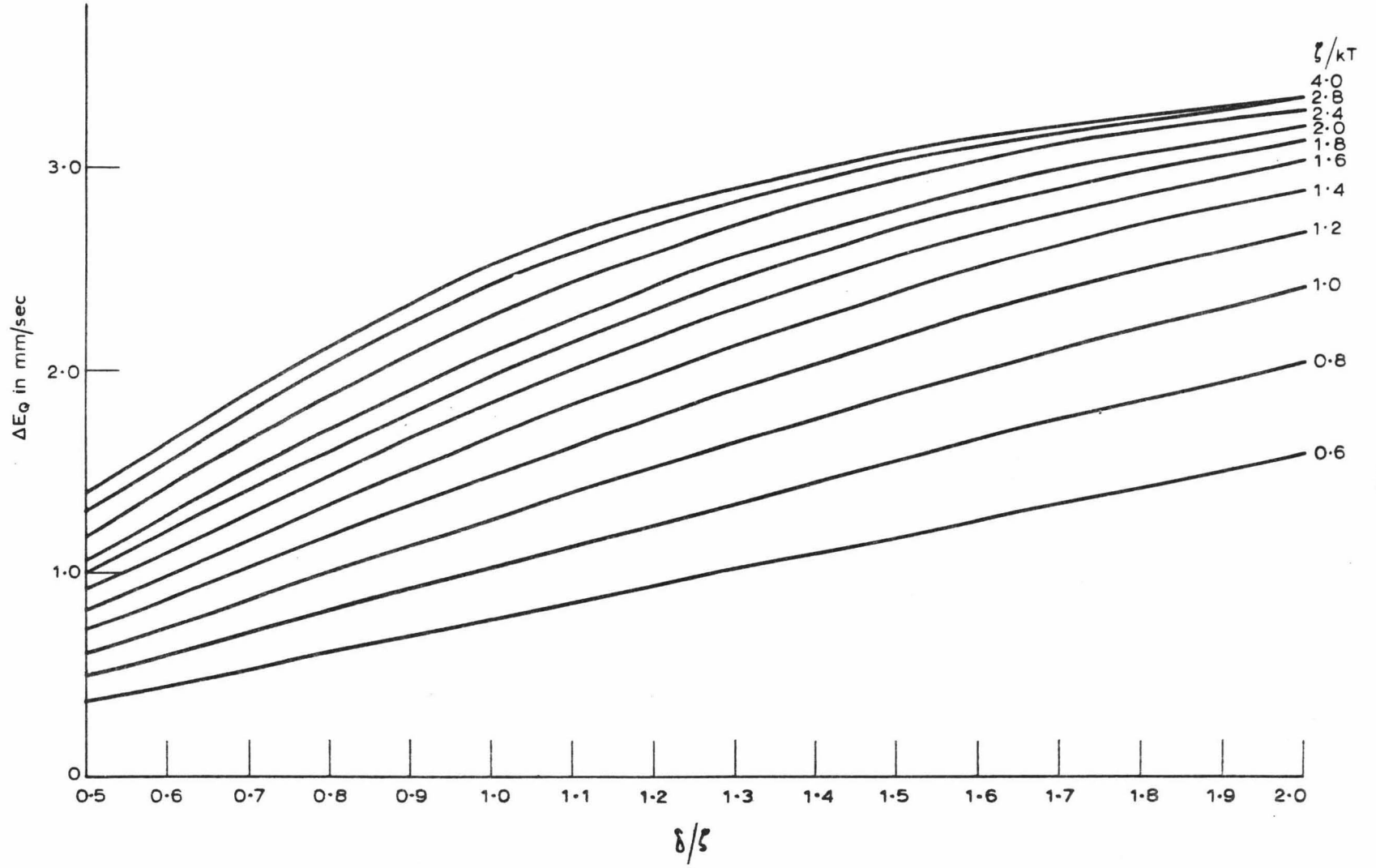

ΔE_Q AGAINST RATIO δ/ζ FOR DIFFERENT RATIOS ζ/kT IN EXPERIMENTAL REGION

FIGURE 4·9

results lie drawn to a larger scale, values of δ/ζ can be deduced from the appropriate values of ΔE_Q and kT determined experimentally:

ΔE_Q	T	kT	ζ/kT		δ/ζ (± 0.075)	
mm/sec	^oK	cm^{-1}	ζ=400	ζ=300	ζ=400	ζ=300
2.53	288	200	2.00	1.50	1.275	1.55
2.87	195	136	2.94	2.21	1.325	1.50

The value of δ obtained is approximately 500 cm^{-1} (± 50 cm^{-1}).

Using figure 4.7, the variation of ΔE_Q with ζ/kT can be determined from the curves for δ/ζ = 1.25 and 1.5, these being close to the deduced δ/ζ values. The experimental results fit the curve for δ/ζ = 1.5 very well, thus suggesting that the value of 300 cm^{-1} is a better estimate of ζ than 400 cm^{-1}. Hence, the temperature-dependence of ΔE_Q is taken from the curve for δ/ζ = 1.5 in figure 4.6.

From the deduced value of δ/ζ, it is now possible to predict a value of the magnetic moment and its variation with temperature, from figure 4.3. Using the experimental temperatures [see section 3.8], the values of μ are determined from the curve for δ/ζ = 1.5:

T	kT/ζ	μ
	ζ=300 cm^{-1}	(δ/ζ = 1.5)
84	0.195	5.38
96.5	0.224	5.40
112	0.260	5.41

134	0.311	5.42
166	0.385	5.43
222.5	0.514	5.435
288	0.667	5.425
295	0.684	5.42 .

The calculated magnetic moments are comparable with those obtained experimentally, especially those listed in the last column of table 3.2. However, the predicted variation with temperature is significantly less than that obtained experimentally, even for the results calculated assuming the Curie-Weiss Law.

The predicted magnetic moment at room temperature can be deduced from figure 4.2 using $\delta/\zeta = 1.55$, giving $\mu = 5.43 \pm 0.01$. Although figure 4.2 is calculated for $\zeta/kT = 2$, it is seen from figure 4.4 that μ is almost constant in the region $\zeta/kT = 1.5$ to 2, for $\delta/\zeta = 1.5$.

The experimental values of ΔE_Q and μ for both ferrous sulphate and the complex can now be compared using figure 4.8. The dotted circle gives the experimental results for ferrous sulphate, the lined oval those for the complex. Although both the values lie slightly below the curve, the agreement is at least as good as that obtained by Golding, Mok and Duncan [37] for similar results. This agreement is improved when the curve for $\zeta/kT = 1.5$ is used, since this lies slightly below and to the left of the curve for $\zeta/kT = 2$.

From these results, it would seem that crystal field calculations can be more profitably used in interpreting Mössbauer quadrupole splittings than magnetic moments, largely because of difficulty in correlating the experimental values of the magnetic moment with the calculated values. Mössbauer spectroscopy has the advantage of being insensitive to impurities and not requiring other data in the calculation of the results. In contrast, magnetic susceptibility measurements require a detailed knowledge of the composition and molecular weight of the substance studied, and assume that the diamagnetic correction can be calculated empirically using Pascal's constants, and that the Curie or Curie-Weiss Law is applicable. Thus it is not surprising that magnetic moments are difficult to interpret theoretically.

The "distortion" model has lead to a satisfactory explanation of the experimental results, a value of about 500 cm^{-1} having been deduced for the distortion parameter δ. Since this distortion of 500 cm^{-1} is negligible compared with the $^5T_2$ - ^5E transition energy, 18,100 cm^{-1}, this is indeed justification for using the Tanabe-Sugano diagram for octahedral symmetry to interpret the visible spectrum. Hence a value of 18,100 cm^{-1} was deduced for the crystal field parameter Δ. The calculated results have shown that the quadrupole splitting is highly sensitive to changes in

the symmetry of the environment of the iron atom; Mössbauer spectroscopy is therefore an ideal method of deducing the degree of distortion from octahedral symmetry of the environment of the iron atom in the ferrous/ascorbate complex.

Chapter 5 NMR SPECTRUM INTERPRETATION

5.1 Introduction

The proton NMR spectrum of ascorbic acid is complicated due to intricate interactions of the protons on C-4, C-5 and C-6 which form an AB_2C system. This spectrum, which has been discussed in section 3.5, is now interpreted by calculating the energies and intensities of the transitions. The method used follows that given by Pople, Schneider and Bernstein [53].

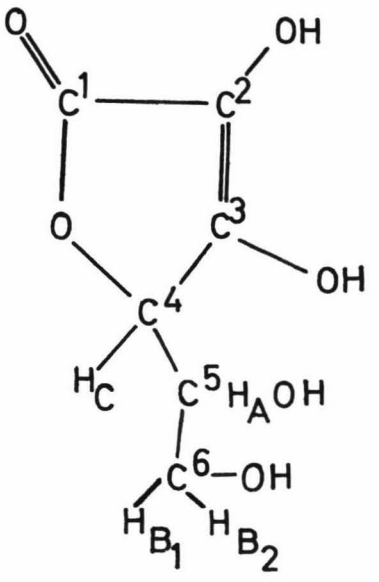

Sixteen basis spin wave functions are set up, classified according to their total spin component in the z-direction (the direction of the externally applied magnetic field), F_z; because the two protons on C-6 are assumed equivalent, a new set of basis functions can be constructed, using symmetry properties, by taking appropriate linear combinations of the basis wave functions. This choice of basis wave functions considerably simplifies the mathematics.

The matrix elements of the Hamiltonian representing interactions of the nucleus with the external magnetic field

and spin-spin coupling are then evaluated. The 16x16 matrix factorizes into smaller submatrices, since no matrix elements occur between functions with (i) different F_z values or (ii) different symmetry. At this stage, the system is approximated to an AB_2X system on the assumption that the chemical shift of the X proton is large compared with the spin-coupling constants. This further reduces the size of the matrices, giving only 2x2 and 1x1 submatrices, because to a high approximation no mixing occurs between functions which differ in their $M_I(X)$ values.

The eigenvalues and eigenfunctions are calculated for these submatrices, by substituting numerical values for the various parameters of chemical shift and spin-coupling constants, as suggested by observation of the experimental spectrum. From these eigenstates, the NMR spectrum is calculated.

The number of possible transitions is limited by the selection rule

$$\Delta F_z = \pm 1 \ .$$

Furthermore, transitions occur only between functions of the same symmetry and for functions differing by ± 1 in $M_I(X)$. The energies of the allowed transitions are obtained from the differences in the eigenvalues of the two eigenstates. The relative intensities are found from the squares of the

matrix elements of the total x component of the nuclear moment between the two eigenstates.

The NMR spectrum is drawn by plotting relative intensity against energy, for the various transitions, choosing an arbitrary zero. The graph is compared with the experimental spectrum, and hence by successive approximations, values are estimated for the various parameters.

5.2 The Wave Functions

In a magnetic field applied externally in the z-direction, each isolated proton (with spin I = ½) has two allowed states, with eigenvalues characterized by the spin quantum number M_I, and eigenfunctions represented by $|\alpha\rangle$ for $M_I = +½$, and $|\beta\rangle$ for $M_I = -½$.

The eigenfunctions of the 4 nuclei of an AB_2C system can be expanded in terms of the 2^4 basis product functions,

$$\psi_n = |M_I(A)\ M_I(B_1)\ M_I(B_2)\ M_I(C)\rangle \quad .$$

In a convenient shorthand notation, the basis product function $|\alpha(A)\ \beta(B_1)\ \alpha(B_2)\ \beta(C)\rangle$, for example, is written as $|\alpha\beta\alpha\beta\rangle$ where the i'th symbol refers to the i'th nucleus. The complete set of basis product functions is given in table 5.1. [tables 5.1-5.6 are given in appendix II].

The total spin operator in the z-direction,

$$F_z = \sum_{i=1}^{4} I_z(i) \quad ,$$

is then used to classify these basis functions, all of which are eigenfunctions of this operator, as shown in tables 5.1. This classification is most convenient as there are no off-diagonal elements of the NMR Hamiltonian, H_N, between basis product functions corresponding to different values of F_z.

Since the B_2 part of the AB_2C system represents two equivalent protons, symmetry theory may be employed to simplify the mathematics. An interchange of these two protons does not physically alter the system; consequently the eigenfunctions must transform as irreducible representations of the symmetry group. As the basis product functions do not belong to the irreducible representations, it is necessary to construct a new set of basis functions by taking appropriate linear combinations of the product functions. The functions $\alpha\alpha$ and $\beta\beta$ are symmetrical with respect to an interchange; the functions $\alpha\beta$ and $\beta\alpha$ are replaced by the linear combinations

$$\frac{1}{\sqrt{2}}(\alpha\beta + \beta\alpha) \qquad \text{(symmetrical)}$$

$$\frac{1}{\sqrt{2}}(\alpha\beta - \beta\alpha) \qquad \text{(antisymmetrical)}.$$

Using these, the complete set of basis symmetry functions are now evaluated. As a consequence of the properties of functions forming bases for irreducible representations of symmetry groups, all matrix elements of H_N between s

(symmetrical) and a (antisymmetrical) basis symmetry functions vanish. The basis symmetry functions are given in table 5.2, with the appropriate symmetry labels, and with the F_z value as a subscript.

This choice of basis wave functions makes the evaluation of the matrix elements much simpler than if the original product functions had been used.

5.3 The Hamiltonian

The NMR Hamiltonian, H_N, applied to the basis symmetry functions represents (i) the interaction of the nucleus with the external magnetic field, and (ii) the interaction of the nuclear spins, through spin-spin coupling:

$$H_N = H_N^{(0)} + H_N^{(1)}$$

$$= \frac{1}{2\pi} \sum_i \gamma_i H_i . I_z(i) + \sum_{i<j} J_{ij} \, I(i).I(j)$$

where γ_i is the magnetogyric ratio for nucleus i

H_i is the magnetic field at nucleus i

J_{ij} is the coupling constant between nuclei i and j

I(i) is the nuclear spin operator, with components $I_x(i)$, $I_y(i)$ and $I_z(i)$, for nucleus i.

For an AB_2C system, this becomes

$$H_N = \frac{1}{2\pi}\left[\gamma_A H_A . I_z(A) + \gamma_B H_B I_z(B_1) + \gamma_B H_B I_z(B_2) + \gamma_C H_C I_z(C)\right]$$

$$+ J_{AB} I(A).I(B_1) + J_{AB} I(A).I(B_2) + J_{AC} I(A).I(C)$$

$$+ J_{BB} I(B_1).I(B_2) + J_{BC} I(B_1).I(C) + J_{BC} I(B_2).I(C) \ .$$

The matrix elements, $\langle \psi_n | H_N | \psi_m \rangle$, of this Hamiltonian are now evaluated. Instead of tediously working through the calculation using this rather fearsome Hamiltonian, use was made of a set of rules devised to evaluate the diagonal and off-diagonal elements of $H_N^{(0)}$ and $H_N^{(1)}$ [54],

$$\langle \psi_n | H_N^{(0)} | \psi_n \rangle = \frac{1}{2\pi} \sum_{i=1}^{4} \gamma_i H_i \left[M_I(i)\right]_n$$

$$= \sum_{i=1}^{4} \nu_i \left[M_I(i)\right]_n$$

where $\nu_i = \gamma_i H_i / 2\pi$,

$$\langle \psi_n | H_N^{(0)} | \psi_m \rangle = 0 \ .$$

[Each product function is an eigenfunction of $H_N^{(0)}$ as the $I_z(i)$ operators do not alter the wave function, resulting in only diagonal elements].

$$\langle \psi_n | H_N^{(1)} | \psi_n \rangle = \frac{1}{4} \sum_{i<j} J_{ij} T_{ij}$$

where T_{ij} = 1 if spins i and j are parallel in ψ_n (i.e. have the same M_I value)

= -1 if spins i and j are antiparallel in ψ_n;

$$\langle \phi_n | H_N^{(1)} | \phi_m \rangle = \frac{1}{2} U J_{ij} , \quad m \neq n,$$

where U = 1 if ϕ_m differs from ϕ_n by an interchange of spins i and j

= 0 otherwise.

Matrix elements between linear combinations of basis product functions are evaluated by expansion. Some examples of these rules are now given:-

$$\langle \alpha\alpha\beta\alpha | H_N^{(0)} | \alpha\alpha\beta\alpha \rangle = \tfrac{1}{2}[-\nu_A + \nu_B - \nu_B + \nu_C] = \tfrac{1}{2}[\nu_A + \nu_C]$$

$$\langle \alpha\alpha\beta\alpha | H_N^{(1)} | \alpha\alpha\beta\alpha \rangle = \tfrac{1}{4}[J_{AB} - J_{AB} + J_{AC} - J_{BB} + J_{BC} - J_{BC}]$$

$$= \tfrac{1}{4}[J_{AC} - J_{BB}]$$

$$\langle \alpha\alpha\beta\alpha | H_N^{(1)} | \alpha\beta\alpha\alpha \rangle = \tfrac{1}{2} J_{BB}$$

$$\langle a_1 | H_N | a_1 \rangle = \nu_A/2 + \nu_C/2 - 3J_{BB}/4 + J_{AC}/4$$

$$\langle s_2 | H_N | s_2 \rangle = \nu_A/2 + \nu_B + \nu_C/2 + J_{AB}/2 + J_{BB}/4 + J_{AC}/4 + J_{BC}/2 .$$

$$\langle 1s_1 | H_N | 2s_1 \rangle = J_{BC}/\sqrt{2} .$$

The complete set of matrix elements is given in table 5.3 Because the basis symmetry functions are used, it is seen that there are no matrix elements between functions of different F_z value or different symmetry. Hence one 4x4, two 3x3, one 2x2 and four 1x1 matrices are obtained.

When the chemical shift ν_C is large compared with the spin coupling constants, the AB_2C system can be approximated

to an AB_2X system, all C labels being replaced by X labels. This is later shown to be a reasonable approximation since excellent agreement is obtained between the theoretical and experimental spectra. Since there are no matrix elements between product functions with different X spins, the above matrices factorize into eight 1x1 and four 2x2 matrices, these being given in table 5.4.

Consequently, eight of the basis symmetry functions are eigenfunctions of H_N, the corresponding eigenvalues being given by the appropriate diagonal matrix elements in table 5.3. The remaining eight eigenfunctions and eigenvalues are found from the four 2x2 matrices.

A convenient general solution could not be found for these 2x2 matrices, so numerical values were substituted to solve the problem. These values were suggested from the experimental spectrum [see section 5.5]. Hence the complete set of 16 eigenvalues and eigenfunctions are obtained, a typical set being given in table 5.5.

5.4 Transition Probabilities and Spectrum

Having obtained the complete set of eigenfunctions, the number of allowed transitions, and their probabilities are determined. The number of possible transitions is determined by the selection rule [55] $\Delta F_z = \pm 1$. Symmetry

requirements allow transitions only between eigenfunctions of the same symmetry; the X approximation allows transitions only between functions differing by $\pm$ 1 in either $F_z(X)$ or $F_z(AB_2)$. This reduces the number of transitions to 4 antisymmetrical and 26 symmetrical.

The relative transition probability is found from the square of the matrix element of the nuclear-moment component in the x-direction, between the two eigenfunctions:

$$\text{T.P.}_{m\to n} \sim \left|\langle \psi_m | \sum_i I_x(i) | \psi_n \rangle\right|^2 .$$

In calculating the effect of $I_x(i)$ on the basic symmetry functions, use is made of the step operators

$$I_+ = I_x + i\, I_y$$

$$I_- = I_x - i\, I_y \qquad [\text{where } i^2 = -1]$$

and hence $I_x = \tfrac{1}{2}(I_+ + I_-)$. For example,

$$\sum_i I_x(i) \,|\alpha\beta\alpha\alpha\rangle = \tfrac{1}{2}\,[\,\beta\beta\alpha\alpha + \alpha\alpha\alpha\alpha + \alpha\beta\beta\alpha + \alpha\beta\alpha\beta\,]$$

and so $\langle \alpha\alpha\alpha\alpha | \sum I_x(i) | \alpha\beta\alpha\alpha \rangle = \tfrac{1}{2}$.

The matrix elements between the basis symmetry functions are given in table 5.6. The transition probabilities for the 16 eigenfunctions are then evaluated by taking the appropriate linear combinations. The energies are calculated from the eigenvalues.

The spectrum is drawn by plotting relative transition

probability against transition energy, the zero being chosen arbitrarily at $\nu_B = 0$.

5.5 Discussion of Results

The values of the parameters used to calculate the NMR spectrum of ascorbic acid were deduced from the experimental spectrum. The position of the low-field doublet depends only on the chemical shift ν_X, from the X approximation, and its splitting on the coupling constants J_{AX} and J_{BX}. From the peak positions given in table 3.1, ν_X was taken as 70 c/s, relative to the high-field singlet peak. The coupling constants were taken as $J_{AX} = 2$ and $J_{BX} = 0$ from the 2 c/s splitting of this doublet. As J_{BX} is the coupling constant between the protons on C-4 and C-6, its value can be expected to be fairly small.

Both the transition energies and intensities are independent of the coupling constant J_{BB}, so this cannot be obtained from the spectrum. This is a particular case of a general result given by Pople, Schneider and Bernstein [56], namely that the spectrum due to two equivalent sets of nuclei, with all coupling constants between nuclei in different sets equal, is independent of the coupling constants within the sets. This statement was checked by substituting two different values for J_{BB}, other parameters remaining constant;

the transition energies and intensities were identical.

The values of J_{AB} and ν_A were more difficult to assign. The calculation showed that one doublet of the spectrum depends solely on ν_A and J_{AX}. Experimentally, several doublets occur close to the singlet peak. Values of ν_A = 10 and 15 c/s were deduced to be reasonable, together with J_{AB} = 6 and 10 c/s. This gave a total of four spectra to be calculated. These are given in figures 5.1-5.4.

The spectrum in figure 5.4 is found to be closest to the experimental spectrum. The values of the coupling constants and chemical shifts (relative to the high-field singlet peak) are thus:

$$\nu_X = 69 \text{ c/s} \qquad \nu_A = 14 \text{ c/s}$$

$$\nu_B = -1 \text{ c/s} \qquad J_{AX} = 2 \text{ c/s}$$

$$J_{AB} = 6 \text{ c/s} \qquad J_{BX} = 0 \text{ c/s} .$$

The X-approximation is shown to be valid, as the difference between the chemical shifts of the hydrogens on C-4 and C-5 is 55 c/s.

Not all of the lines calculated theoretically will be observed, both because of small transition probabilities and because some of the lines are so close that they will coalesce to form a single peak. For example, the doublet at low field arises from eight transitions grouped into two lots of four, with almost identical transition energies.

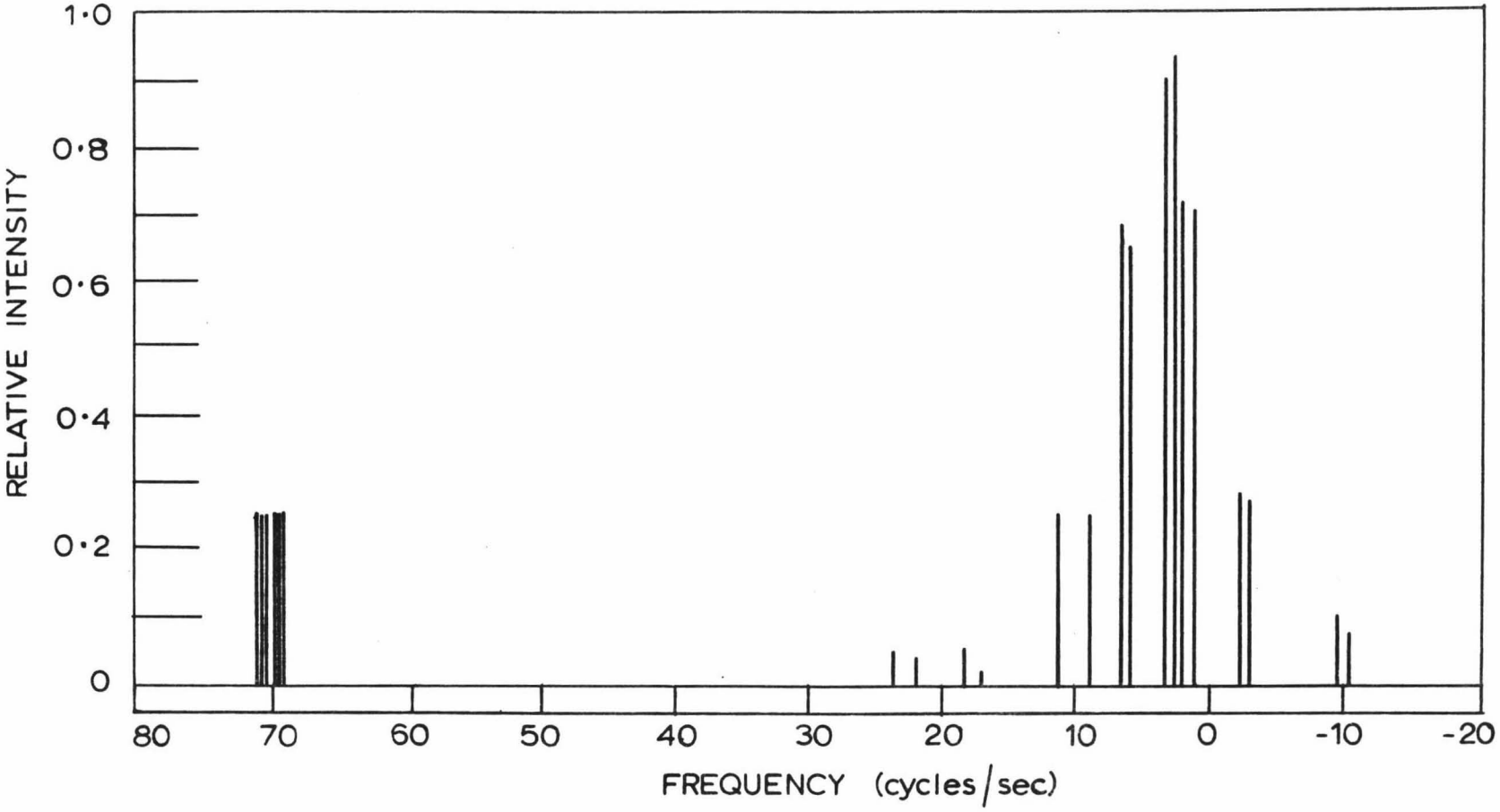

PREDICTED NMR SPECTRUM OF ASCORBIC ACID

FOR $\nu_A = 10$, $\nu_B = 0$, $\nu_X = 70$, $J_{AB} = 10$, $J_{BB} = 0$, $J_{AX} = 2$, $J_{BX} = 0$

FIGURE 5·1

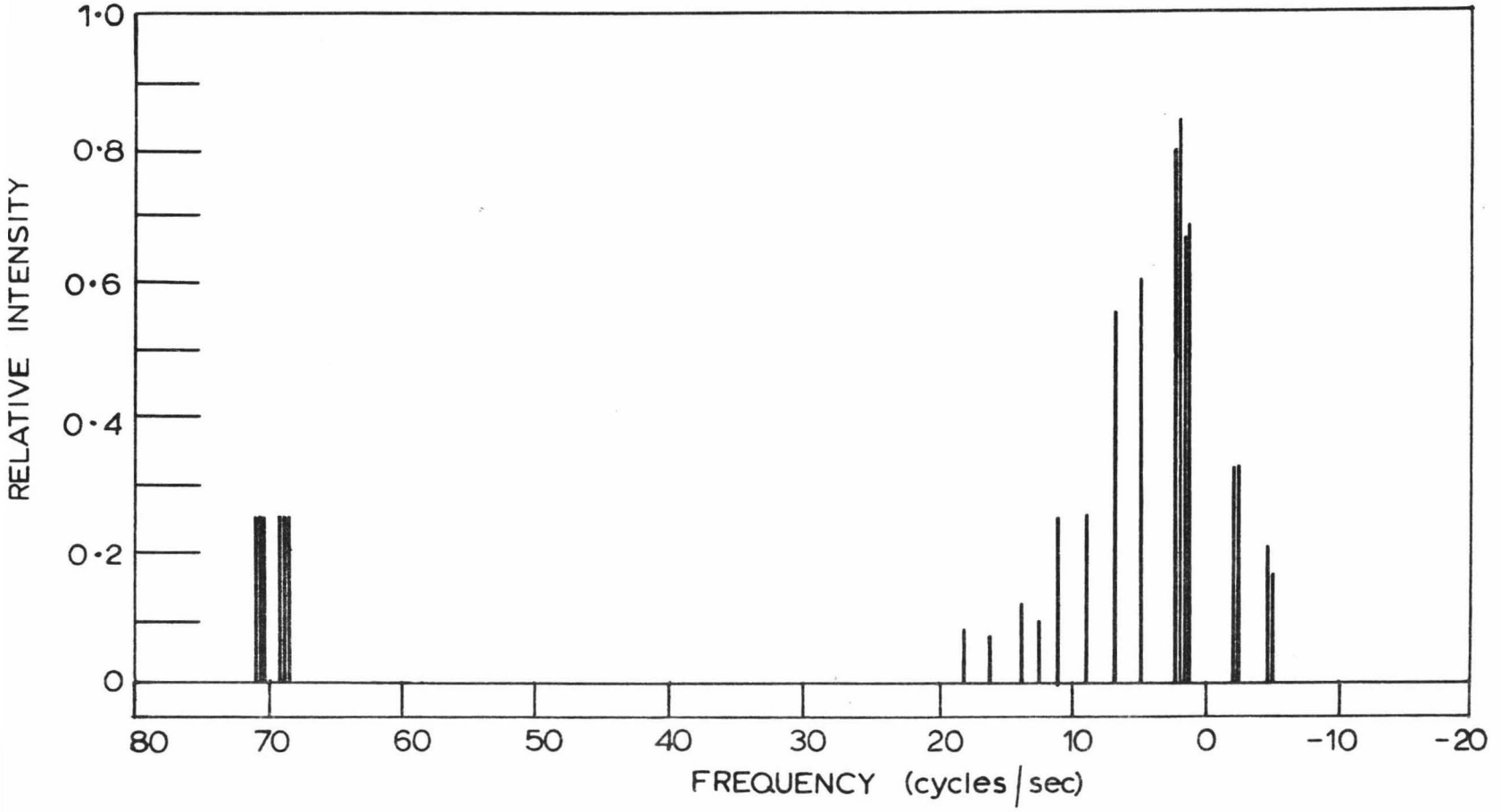

PREDICTED NMR SPECTRUM OF ASCORBIC ACID

FOR $\nu_A = 10$, $\nu_B = 0$, $\nu_X = 70$, $J_{AX} = 6$, $J_{BB} = 0$, $J_{AX} = 2$, $J_{BX} = 0$

FIGURE 5·2

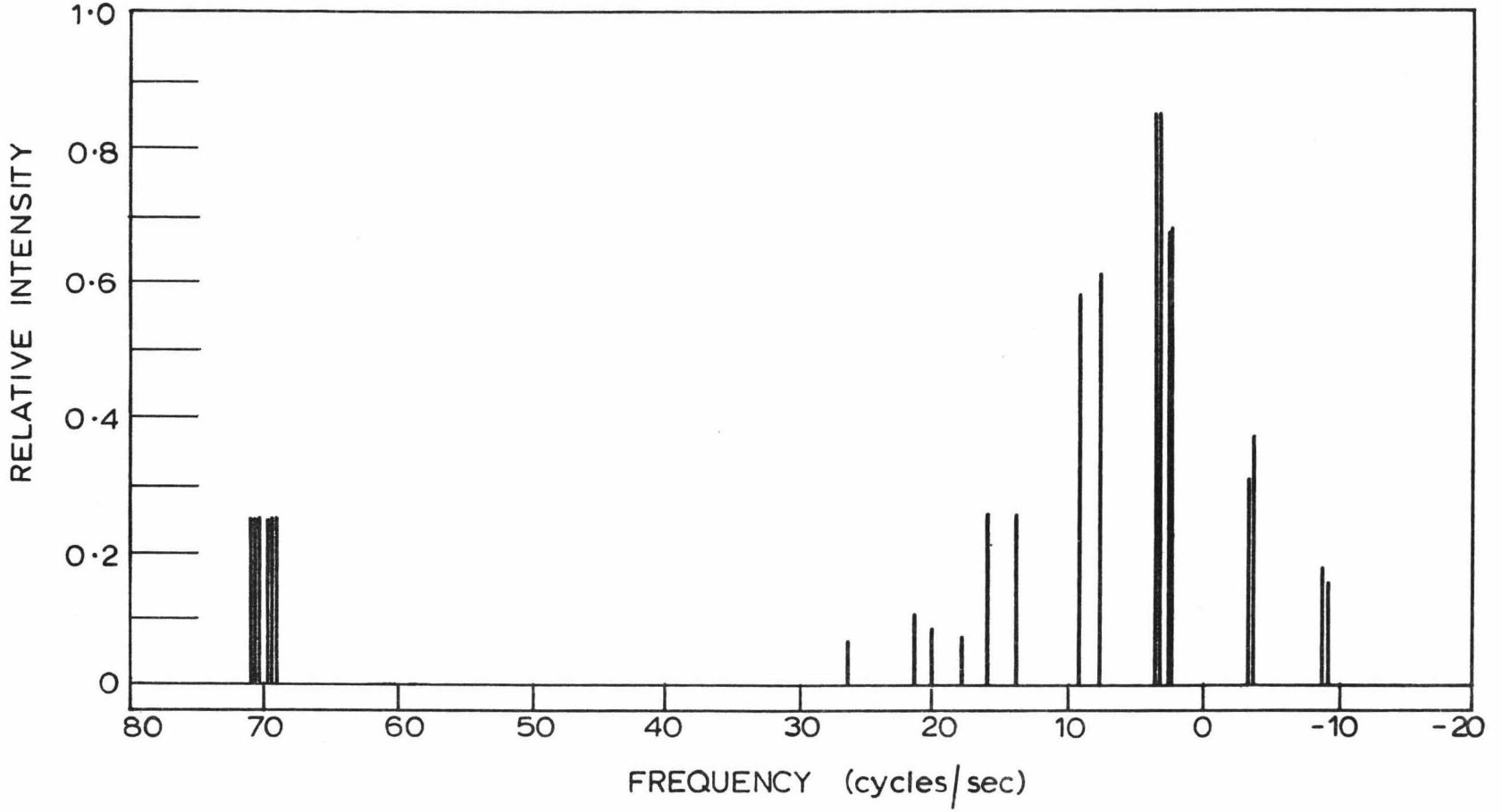

PREDICTED NMR SPECTRUM OF ASCORBIC ACID

FOR $\nu_A = 15$, $\nu_B = 0$, $\nu_X = 70$, $J_{AB} = 10$, $J_{BB} = 0$, $J_{AX} = 2$, $J_{BX} = 0$

FIGURE 5·3

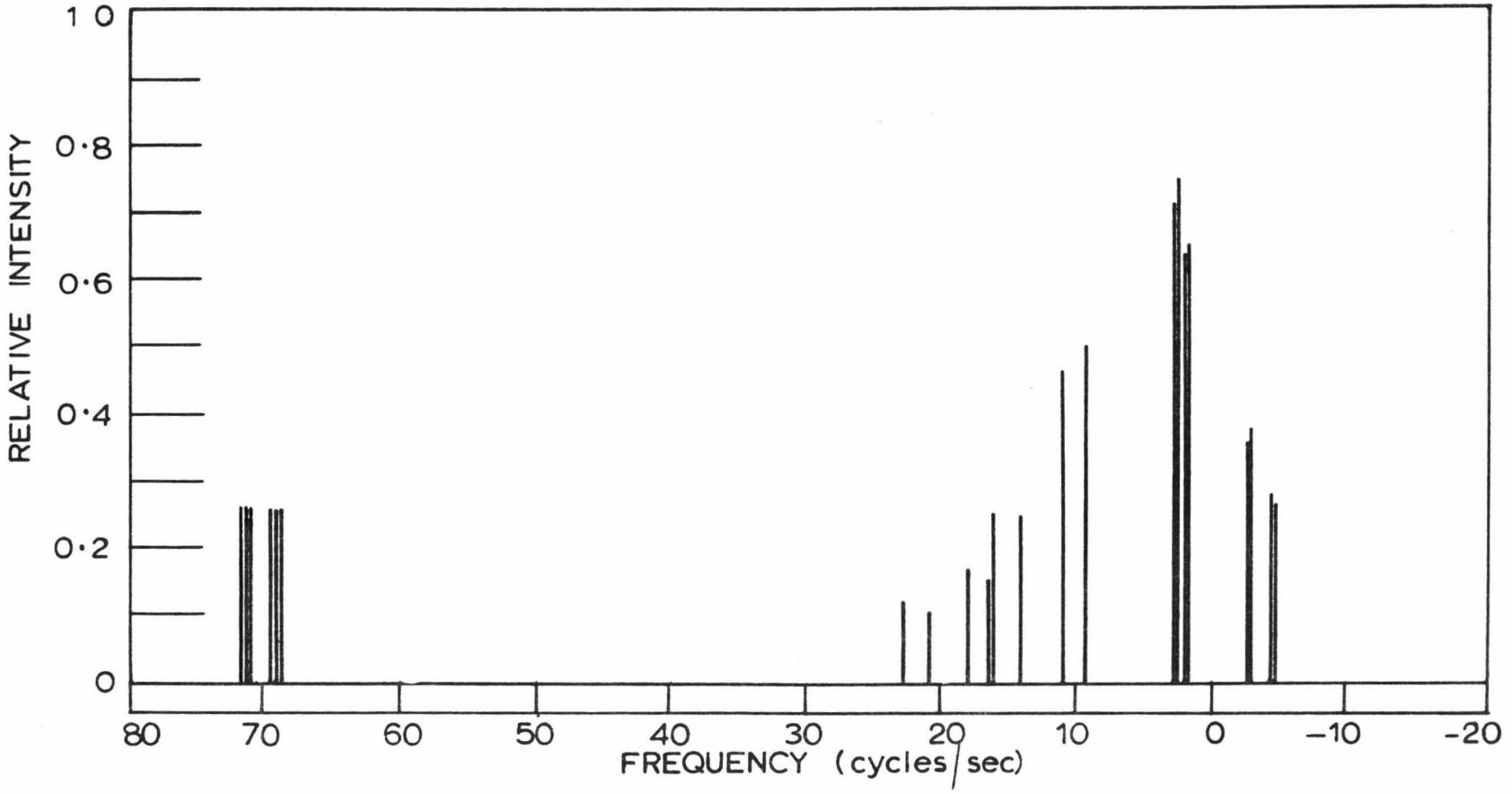

PREDICTED NMR SPECTRUM OF ASCORBIC ACID

FOR $\nu_A = 15$, $\nu_B = 0$, $\nu_X = 70$, $J_{AB} = 6$, $J_{BB} = 0$, $J_{AX} = 2$, $J_{BX} = 0$

FIGURE 5·4

The presence of several lines close together will increase the intensity of the resulting peak relative to that from a single line, as can be seen on comparing the experimental and calculated spectra.

For the spectrum of sodium ascorbate, the calculation will be exactly the same, except that the value of ν_X is decreased by 27 c/s. Although this decreases the chemical shift difference between the A and X protons, the X approximation still gives an adequate interpretation. The change in the chemical shift ν_X is due to the altered environment of the X proton, presumably arising from the presence of the ionized hydroxyl group on C-3.

The spectrum of the complex would be expected to arise from the sodium ascorbate spectrum, but, as has already been discussed in section 3.5, its broad peaks do not lend themselves to the calculation of a satisfactory spectrum.

Chapter 6 MOLECULAR ORBITAL CALCULATIONS

6.1 Introduction

In section 1.1, it was mentioned that ascorbic acid and 2,4,5-triamino, 6-hydroxy-pyrimidine (hereafter referred to as pyrimidine) could both be used as model systems for the phenylalanine hydroxylase cofactor, tetrahydropteridine. As this use as a model system was attributed to similar structural features, it was decided to perform molecular orbital (MO) calculations for both ascorbic acid and pyrimidine to compare their electronic properties. In this way, it was hoped to gain an insight into why these two different species act as a model system for the same cofactor.

Some suitable form of MO calculation had to be chosen. The lack of any symmetry elements in the ascorbic acid molecule prevents a separation of the electronic states of ascorbic acid into π- and σ-type MOs; instead, all of the high energy (i.e. valence shell) electrons had to be considered. Furthermore, although π-electron methods such as simple Hückel theory or the Pariser-Pople-Parr methods are applicable to pyrimidine, the σ-electrons are probably as important as the π-electrons in considering co-ordination properties. Pyrimidine, which can be regarded as having symmetry elements for certain assumed configurations, can have its electronic

states separated into π- and σ-type MOs, by the use of group theory. The size of the ascorbic acid molecule (20 atoms, 56 high energy electrons) is such that at the present time only a semi-empirical type MO calculation could be performed. The order of the secular equation, 56, could not be reduced by factorization by group theory. This led to the choice of the Extended Hückel method, as being a suitable method. It was also an advantage that calculations of this type had already been carried out at Victoria University and the required computer programs were available.

Having performed the calculation, various properties of the two molecules were calculated: the electronic energy levels, the net atomic charges and the atomic overlap populations (which are related to bond strengths between atoms). From a comparison of these properties, and an appreciation of the limitations of the method, some correlation of the experimental details is given.

6.2 The Extended Hückel Method

This method, developed by Hoffmann [57], is based on a one-electron MO approach. The eigenfunctions (MOs) for a single electron in the field of all the nuclei are approximated as a linear combination of atomic orbitals (LCAO).

The basis set of AOs consists of all the carbon, nitrogen, and oxygen 2s, $2p_x$, $2p_y$ and $2p_z$ AOs and all the hydrogen 1s AOs. In accordance with the Aufbau principle, the total number of electrons is then fed into these MOs in order of increasing energy, placing two electrons in each non-degenerate orbital. Any electron-electron interactions are neglected in this method, since the Hamiltonian used to calculate the MOs is a one-electron Hamiltonian.

Expansion of the one-electron MOs in terms of a LCAO, followed by a minimization of the energy of each one-electron eigenfunction using the variation principle, gives the secular equation in matrix form:

$$H\,C = S\,C\,E \qquad C^{\dagger}\,S\,C = 1$$

where H is the Hückel matrix, with elements $H_{ij} = \langle \phi_i | H_{eff} | \phi_j \rangle$

S is the overlap matrix, with elements $S_{ij} = \langle \phi_i | \phi_j \rangle$

C is the MO matrix, whose column vectors give the coefficients of the AOs in the LCAO-MOs

E is the energy matrix, giving the energies of the MOs

$C^{\dagger}$ is the Hermitian transpose of C

the $|\phi_i\rangle$ are the basis AOs

H_{eff} is the effective one-electron Hamiltonian.

The order of the secular equation is $4n+m$ where n is the number of carbon, nitrogen and/or oxygen atoms, and m is the number of hydrogen atoms.

The secular equation may be transformed [58] to a standard eigenvalue equation, namely

$$H' C' = C' E$$

by taking $H' = S^{-\frac{1}{2}} H S^{-\frac{1}{2}}$ and $C = S^{-\frac{1}{2}} C'$. To ensure that the matrix $S^{-\frac{1}{2}}$ exists in real form, the matrix S must be positive definite [59]. If all the overlap matrix elements are considered, this condition will be rigorously fulfilled [59]. This consideration of overlap means that the basis AOs do not form an orthogonal set.

For this calculation, the overlap integrals are evaluated with Slater AOs using the appropriate exponents, given in table 6.1, from Slater's rules. The input for the program

Table 6.1 Parameters for MO Calculations

	Slater exponent	Coulomb Integrals (e.v.)	
atom	for 2s, 2p AOs	2s	2p
C	1.625	-21.4	-11.4
N	1.95	-26.0	-13.4
O	2.275	-35.6	-18.0

used for computing the overlap matrices [60] consists of simply the atomic number and x,y and z co-ordinates of each atom. The specification of atomic number enables the computer to assign values to the Slater exponents and diagonal matrix elements H_{ii} for the s and p AOs.

These H_{ii} (coulomb integrals) are estimated from atomic

emission spectral data, being taken as the negative of the valence state ionization energies. The values used are given in table 6.1. The off-diagonal matrix elements, H_{ij}, are evaluated from the assumed relation

$$H_{ij} = 0.5\ k\ (H_{ii} + H_{jj})\ S_{ij}$$

where k, a constant, is taken as 1.75 by Hoffmann [57]. Once the overlap matrix has been computed from the supplied cartesian co-ordinates, the Hückel matrix H is constructed by the computer, using the above formula. Two matrix diagonalizations, i.e. eigenvalue extractions, are required to give the desired matrices C and E. The program used for this MO calculation is a modification (to include the Mulliken population analysis discussed in the next section) of the one given by Bailey [61].

If the molecule being studied contains any symmetry elements, it is desirable to reduce the order of the matrices by factorization as this considerably decreases the total time required for the above computations. Using group theory, sets of symmetry adapted linear combinations of the basis AOs may be found which transform as irreducible representations of the point group of the molecule; hence the secular equation may be factorized. In this case, the formulae used for setting up the calculation must be modified; this has been allowed for in the programs used.

6.3 Mulliken Population Analysis

From the MO coefficients, i.e. the C matrix, a Mulliken population analysis [62] can be performed. A study of overlap populations gives a measure of the bonding and antibonding strengths between atoms. From the statistics of the distribution of electronic population among the atoms in the molecule and among the different orbitals of each atom, values of net atomic charges can be obtained.

A summary of the definitions and formulae on which the computer program for performing the population analysis is based, is now given:

Let the number of basis AOs $|\phi_i\rangle$ be n. This will give rise to n energy levels E_i, and n MOs $\psi_i = \sum_{j=1}^{n} C_{ji}\,\phi_j$ where the C_{ji} are the MO coefficients. Following the Aufbau principle, two electrons are fed into each E_i until the total number of electrons has been used, so that energy levels E_1 through E_h are now occupied. The following quantities are then defined in terms of the MO coefficients and the overlap matrix elements:

the net atomic population in AO ϕ_i = $NAP_i = \sum_{r=1}^{h} 2\,C_{ir}^{2}$;

the overlap population between AOs ϕ_i and ϕ_j

$= OP_{ij} = OP_{ji} = 4\,S_{ij} \sum_{r=1}^{h} C_{ir}\,C_{jr}$;

the net overlap population in AO ϕ_i = $NOP_i = \sum_{j=1}^{n} \tfrac{1}{2}\,OP_{ij}$;

the gross atomic population in AO ϕ_i = GAP_i = NAP_i+NOP_i. From these quantities, the overlap populations between atoms and the net atomic charges can be calculated, as shown in section 6.5.

6.4 The Model Used

In this calculation the cartesian co-ordinates of the atoms in the molecule are used to compute the MOs. These co-ordinates are calculated from the assumed geometry of the molecules. For ascorbic acid, no x-ray data of bond lengths and bond angles was found, so these were calculated by comparison with other similar molecules. The 5-membered ring was assumed planar, this being supported by crystallographic studies [63]. The $-CH(OH)-CH_2OH$ portion was assumed to have the normal bond lengths and angles for an aliphatic hydroxyl system. The bond lengths used are shown in figure 6.1.

For pyrimidine, the bond lengths and bond angles were taken as the average values of the x-ray data for various substituted pyrimidines given in the "Tables of Interatomic Distances" [64], the 6-membered ring being considered as planar. As there would be an infinite number of conformations for the amino groups, two extreme cases were considered:

(i) the NH_2 group lying completely in the plane of the ring, so that the whole molecule is planar,

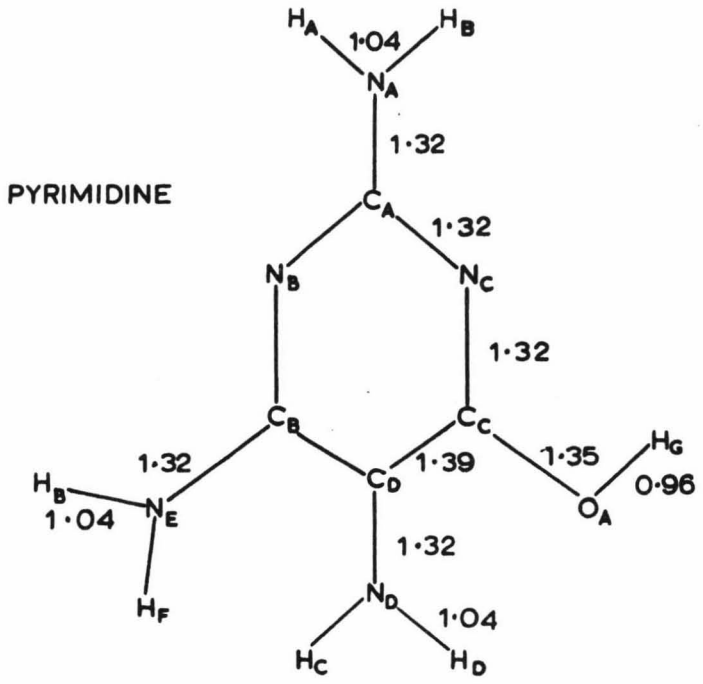

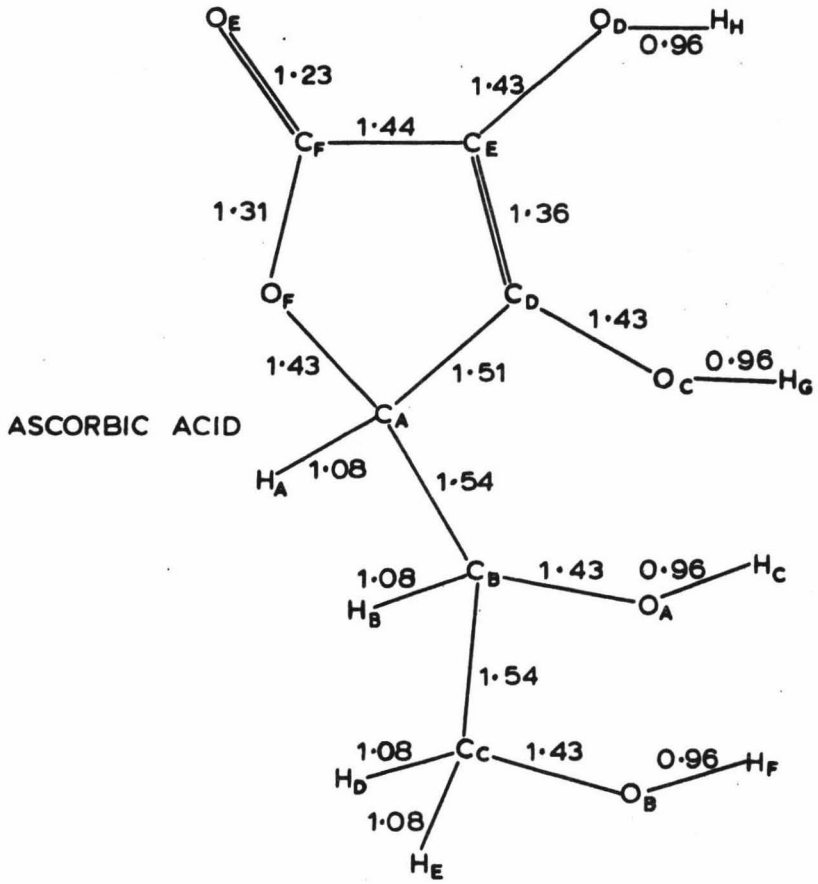

BOND LENGTHS USED IN MO CALCULATION

FIGURE 6·1

(ii) the NH_2 being at right angles to the plane of the ring, so that the two hydrogens lay above and below the plane of the ring.

The bond lengths used are shown in figure 6.1.

From these bond lengths and the corresponding bond angles, the cartesian co-ordinates were calculated by trigonometry, and then checked by a computer program. These then formed the input for the MO calculation, together with certain symmetry information in the case of pyrimidine.

From the assumed geometries of the pyrimidine molecule, factorization of the secular equation was achieved because the π- and σ-type AOs belong to different irreducible representations of the point group (C_s) of the molecule. Hence separate calculations were performed for the π and σ orbitals of pyrimidine, thus saving an appreciable amount of computer time.

This part of the calculation was set up by John Bailey, with the computations carried out on the Elliott 503 computer of the Applied Mathematics Division of the Department of Scientific and Industrial Research. The original computer programs were written by Mr Keith Morris of the Applied Mathematics Division, and the modifications, to include the Mulliken population analysis, were made by John Bailey.

6.5 Calculations

The computer output consisted of the energy levels, MO coefficients, the OP_{ij}, NAP_i, NOP_i and GAP_i as defined in section 6.3. All of the occupied energy levels, and the first few unoccupied levels, are shown in figure 6.2. Those MOs for pyrimidine which are marked with an asterisk are the π MOs, arising from the π AOs.

The net charge on atom k is $N_k^o - \sum_i GAP_i$ where N_k^o is the total number of high energy electrons in the ground state of the free neutral atom k (e.g. 1 for H, 4 for C, 5 for N, 6 for O), and the i summation is over all of the AOs ϕ_i centred on atom k.

The overlap population between atoms k and m is $\sum_i \sum_j OP_{ij}$ where the i summation is over all of the AOs ϕ_i centred on atom k, and the j summation is over all of the AOs ϕ_j centred on atom m.

The values of the net atomic charges and overlap populations are shown in figures 6.3, 6.4 and 6.5 for ascorbic acid and the two conformations of pyrimidine.

6.6 Discussion of Results

The energy level diagrams given in figure 6.2 are fairly similar with regard to the location of the highest occupied level and lowest unoccupied levels. The energy

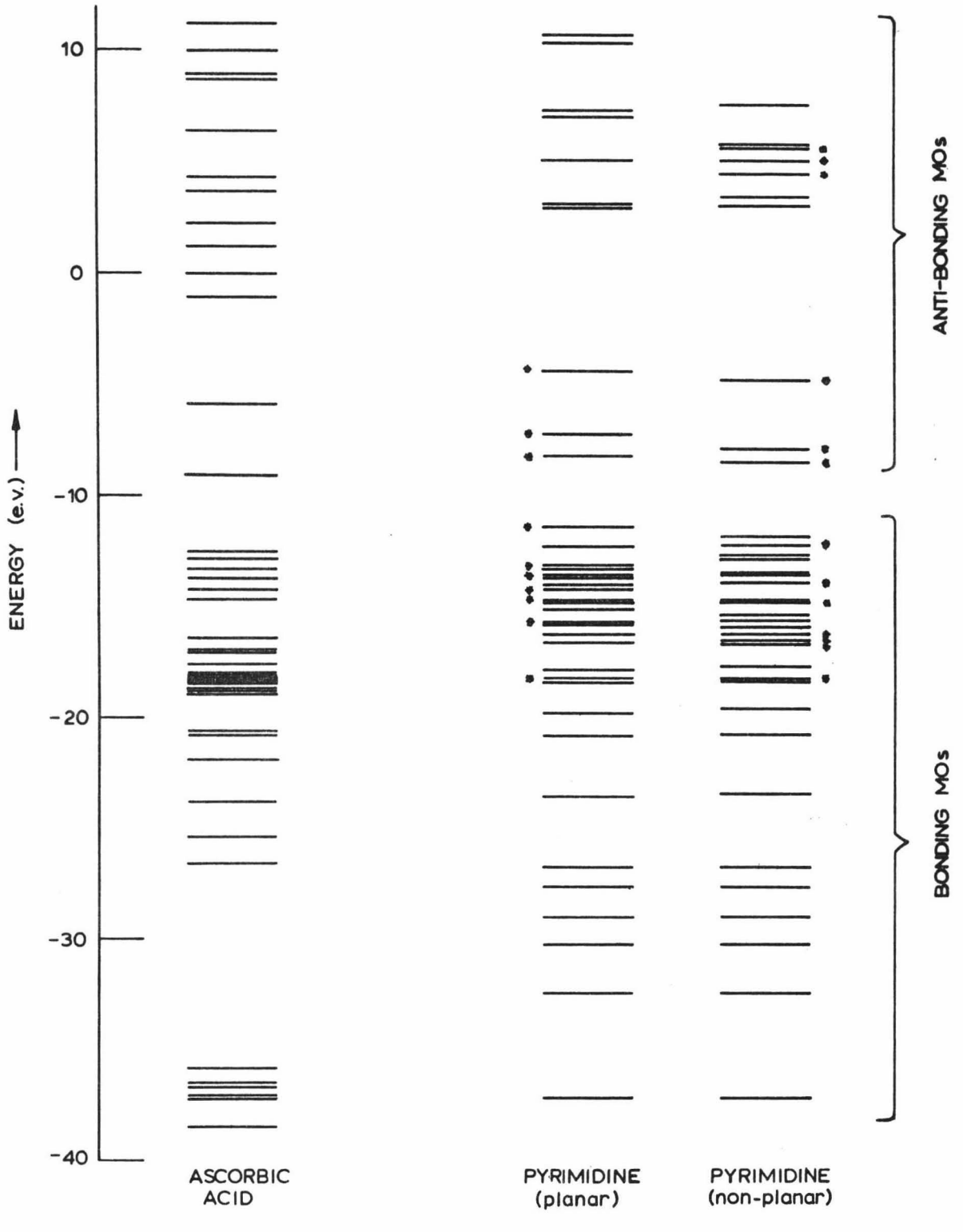

ENERGY LEVEL DIAGRAMS FOR ASCORBIC ACID AND PYRIMIDINE

FIGURE 6·2

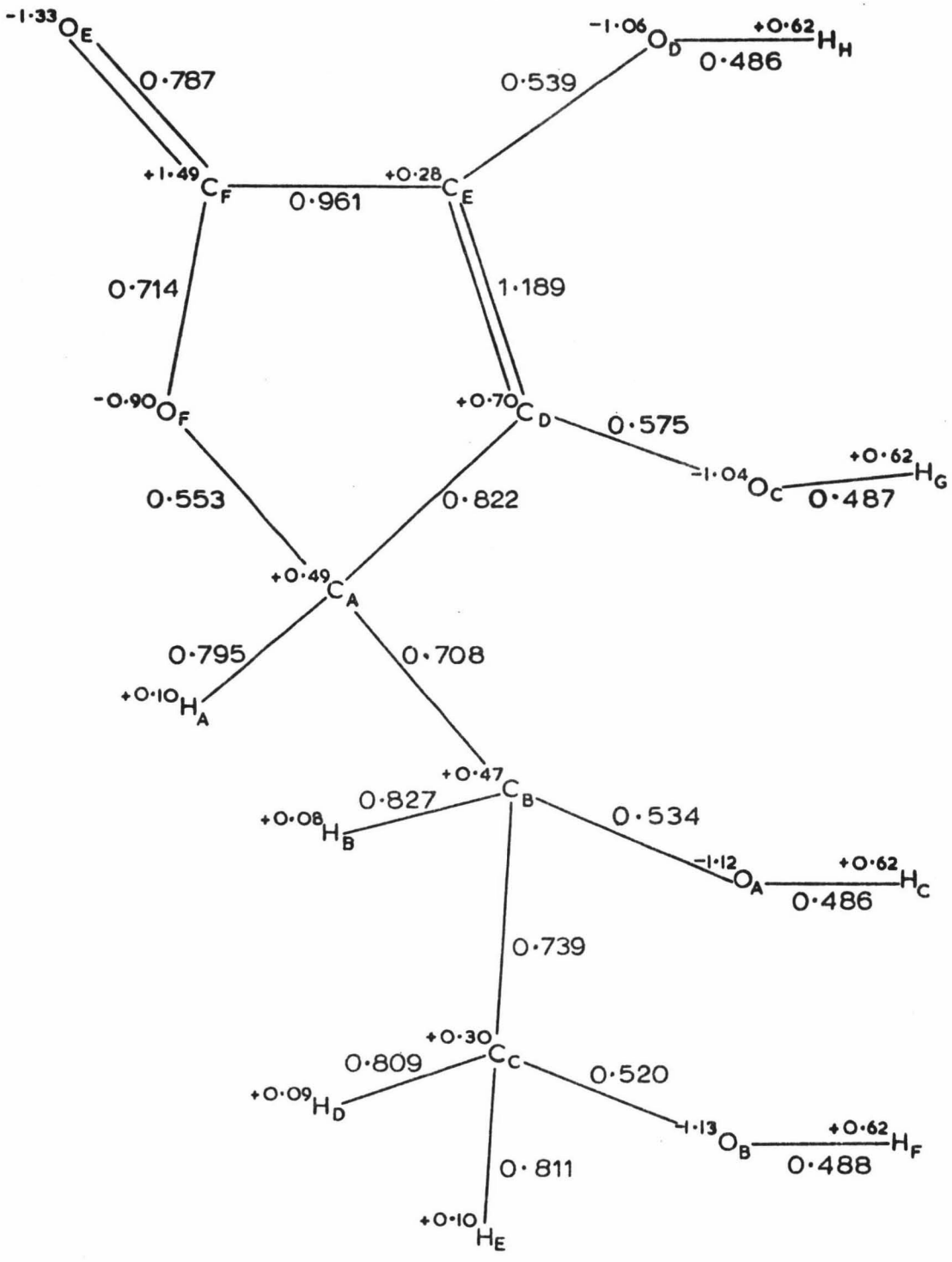

Signed quantities are net atomic charges.
Unsigned quantities are overlap populations.

NET ATOMIC CHARGES AND OVERLAP POPULATIONS FOR ASCORBIC ACID

FIGURE 6·3

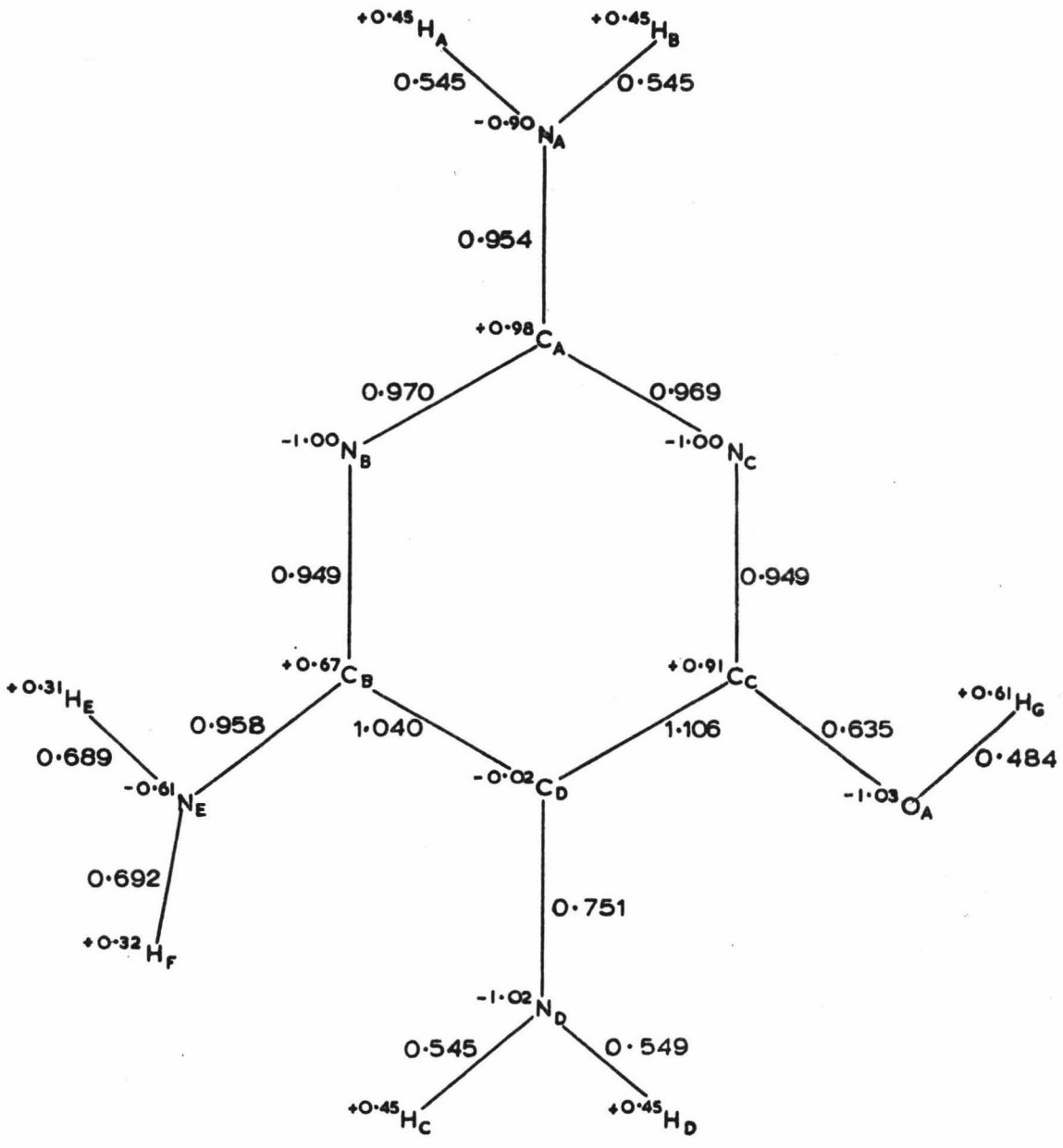

Signed quantities are net atomic charges.
Unsigned quantities are overlap populations.

NET ATOMIC CHARGES AND OVERLAP POPULATIONS FOR PYRIMIDINE (planar)

FIGURE 6·4

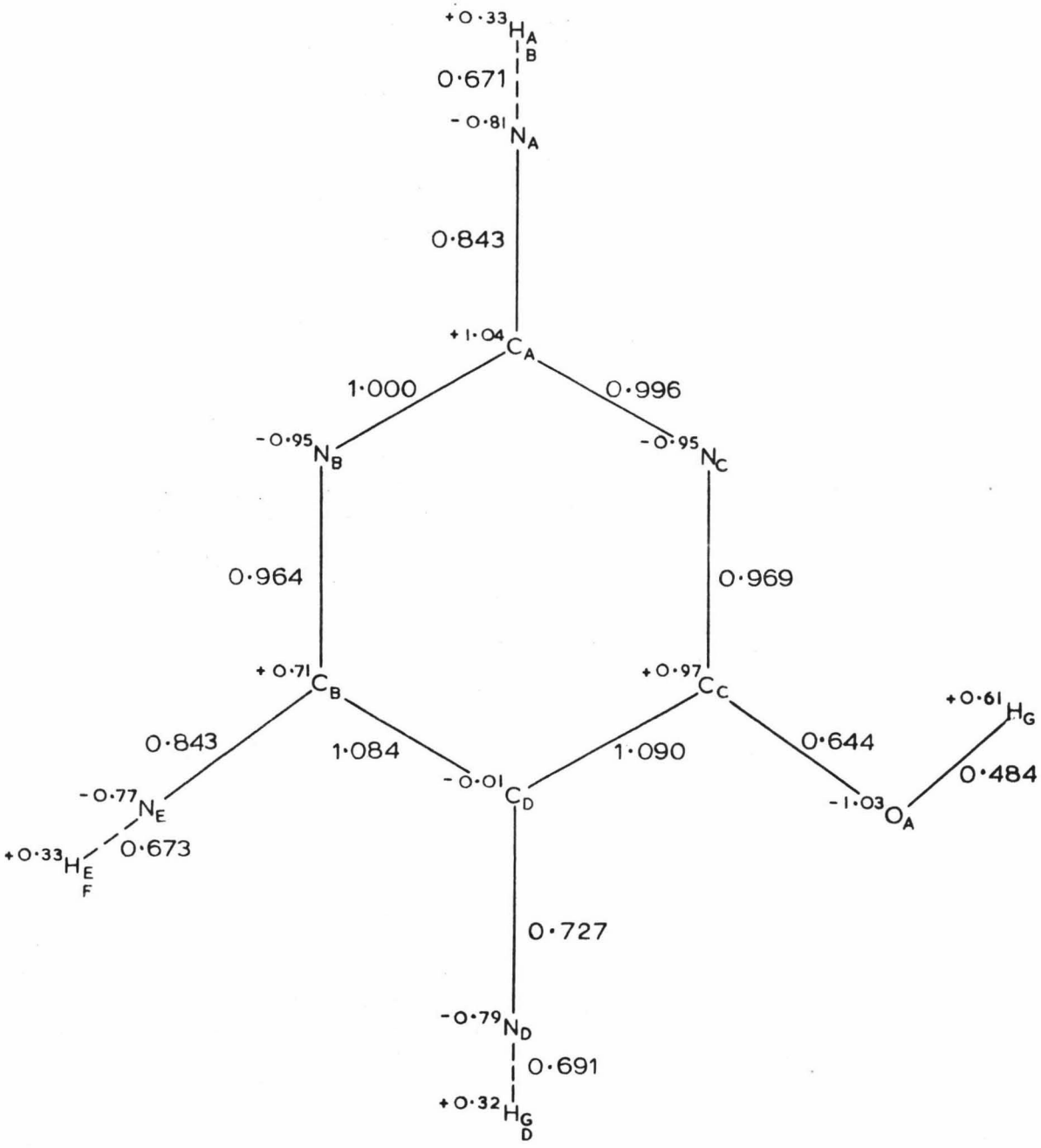

Signed quantities are net atomic charges.
Unsigned quantities are overlap populations.

NET ATOMIC CHARGES AND OVERLAP POPULATIONS FOR PYRIMIDINE (non-planar)

FIGURE 6·5

differences between these two levels are 3.4 e.v. for ascorbic acid, 3.2 e.v. for pyrimidine (planar) and 3.3 e.v. for pyrimidine (non-planar), which are very similar.

The energy of the highest occupied level is expected to be related to the ionization potential for the molecule. Hence the calculated ionization potential for ascorbic acid is about one e.v. higher than for pyrimidine. From the energy differences between the one-electron MOs, the UV spectrum can be predicted, although one-electron MO methods do not usually give very good predictions. For ascorbic acid, the computed energy difference is 3.425 e.v. = 27,600 cm^{-1}, compared with the experimental value of 265 mμ = 37,700 cm^{-1}. The theoretical value is, however, of the right magnitude.

From the net atomic charges (figures 6.3, 6.4), the pyrimidines have about the same charge distributions except for the NH_2 groups. In ascorbic acid, the hydroxyl groups O_D-H_H and O_C-H_G have almost the same overlap populations and net atomic charges. This cannot account for one hydrogen being more acidic than the other.

On comparing the pyrimidines and ascorbic acid, it is seen that the hydroxyl groups mentioned above and the hydroxyl group O_A-H_G and amino group N_D-$H_C H_D$ have almost the same net atomic charge on the oxygen or nitrogen atom for

the planar pyrimidine. Apart from this similarity, there does not seem to be much correlation in their electronic properties.

Three problems arise in MO calculations such as this. The method of calculating the MOs depends on certain assumptions, which may limit the significance of the calculated results. Even if reasonable MOs are obtained, it is often difficult to know what properties to calculate from the MOs to explain reactivity, co-ordinating ability and other experimental features. Having obtained these calculated properties the correlation with experimental results also requires knowledge of what property the experiment is determining.

CONCLUSION

As indicated in chapter 1, previous biochemical research had suggested that the Udenfriend model system of ferrous ions and ascorbic acid was of importance in certain biological reactions in vivo. On studying this system, Hamilton postulated a mechanism for these reactions which included an intermediate consisting of a complex formed between the ferrous ions and ascorbate ions. In this thesis, a complex formed from ferrous and ascorbate ions has been isolated. Although it cannot definitely be said that the complex studied is that postulated by Hamilton as being of importance in these biological reactions, the repetition of the experiments performed by Hamilton (but using this isolated ferrous/ascorbate complex) did lead to the same results.

Having obtained a complex, which could have interesting biochemical properties, the techniques typical of physical chemistry used to study transition-metal ion complexes were employed to characterize it. In other words, the usual chemical techniques were used on this biochemical complex. The experimental work was rather difficult because of the unusual properties of the complex including its gradual oxidation in solution open to the atmosphere and the inability

to obtain a pure crystalline solid. Such difficulties typify the chemical problems inherent in studying biochemical reactions.

Even so, enough experimental information was obtained to enable theoretical studies to be done on both the complex and its component species. Once again, the techniques used were limited by the nature of the complex, mainly because of its size. For molecules containing more than a few atoms or those of low symmetry, only semi-empirical type calculations can be employed and these are necessarily limited in accuracy by the assumptions of the methods. The component species lent themselves more readily to calculation and interesting chemical information was deduced about ascorbic acid from these theoretical studies.

The theoretical and experimental investigations of the complex system fall into two catagories:

(i) those concerned with a solid complex, and

(ii) those concerned with a complex in solution.

In each of these catagories, as indicated in the relevant sections of the thesis, the theoretical results were consistent with those obtained from experiment.

It is important to stress that the answer to the initial biological problem of whether this complex is that actually involved in biological reactions in vivo is a very

difficult matter. Physiological conditions in the body would be quite different from those used in laboratory experiments. However it is considered that the work done in this thesis is an attempt to investigate a biochemical problem from a purely chemical viewpoint, which may prove a useful aid in further work of this type.

REFERENCES

[1] Schubert, J., 1966, Scientific American, 214, no. 5, 40.

[2] Udenfriend, S., Clark, C.T., Axelrod, J. and Brodie, B.B., 1954, J. Biol. Chem., 208, 731.

[3] Brodie, B.B., and Axelrod, J., 1948, J. Pharmacol. and Exp. Therap., 94, 29;
Smith, J.N., and Williams, R.T., 1949, Biochem. J., 44, 242.

[4] Novak, L., and Brodie, B.B., 1950, J.Biol.Chem.,187, 787.

[5] Brodie, B.B., Axelrod, J., Shore, P.A., and Udenfriend,S., 1954, J.Biol.Chem., 208, 741.

[6] Mason, H.S., 1957, Advan. Enzymol., 19, 128.

[7] Hamilton, G.A. and Friedman,J.P.,1963,J.Am.Chem.Soc., 85, 1008.

[8] Hamilton, G.A., Workman, R.J. and Woo, L., 1964, J.Am.Chem.Soc., 86, 3390.

[9] Kaufman, S., 1962, J.Biol.Chem., 237, P.C. 2712;
Kaufman, S., 1964, J.Biol.Chem., 239, 332.

[10] Hamilton, G.A., 1964, J.Am.Chem.Soc., 86, 3391.

[11] Hine, J., 1964, "Divalent Carbon", Ronald Press,New York.

[12] Weissburger,A. and Linvalle,J.E.,1944, J.Am.Chem.Soc., 66, 700.

[13] Martell, A.E. and Calvin, M., 1952, "Chemistry of Metal Chelate Compounds", Prentice-Hall,New York,p.389.

[14] Hawk, P.B., Oser, B.L. and Summerson, W.H., 1954, "Practical Physiological Chemistry", McGraw-Hill, New York, p.1226;
Roe, J.H., 1954, "Methods of Biochemical Analysis", vol. 1, Gluck, D., Ed., Interscience, New York, p.115.

[15] Kirk, R.E. and Othmer, D.F., 1963, "Encyclopaedia of Chemical Technology", vol.8, Interscience, New York,p.63; Mellor, J.W.,1947, "A Comprehensive Treatise in Inorganic and Theoretical Chemistry", vol. 14, Longmans, London, p.242.

[16] Sadtler Standard Spectra, Sadtler Research Laboratories, Philadelphia.

[17] Cole, A.R.H., 1963, "Technique of Organic Chemistry", vol 11, Weissberger, A., Ed., Interscience,New York,p.143; Brugel, W., 1962, "An Introduction to Infrared Spectroscopy", Methuen, London, p.368.

[18] Figgis, B.N., 1966, "Introduction to Ligand Fields", Interscience, New York, p.208.

[19] Job, 1928, Ann. Chim, 9, 113;
Vosburgh, W.C. and Cooper, G.R., 1941, J.Am.Chem.Soc., 63, 437.

[20] King, J.F., 1963, "Technique of Organic Chemistry", vol 11, part 1, Weissberger, A., Ed., Interscience, New York, p.322.

[21] Ref. 13, chapter 3.

[22] Bjerrum, J., 1941, "Metal Ammine Formation in Aqueous Solution", P. Haase and Son, Copenhagen; Rosotti, F.J.C, and Rosotti, H., 1961, "The Determination of Stability Constants", McGraw-Hill, New York.

[23] Stothers, J.B., 1963, "Technique of Organic Chemistry", vol 11, part 1, Weissberger, A., Ed., Interscience, New York, p.184.

[24] NMR Spectra Catalog, 1963, compiled by Bhacca, N.S., Hollis, D.P., Johnson, L.F. and Pier, E.A., Varian Associates, U.S.A.

[25] Pople, J.A., Schneider, W.G. and Bernstein, H.J., 1959, "High Resolution Nuclear Magnetic Resonance", McGraw-Hill, New York, p.207.

[26] Ref. 23, p.210.

[27] Bleaney, B. and Ingram, D.J.E.,1951, Proc.Roy.Soc. (London), A205, 336.

[28] Ref. 18, chapter 11.

[29] Duncan, J.F., and Golding, R.M., 1965, Quart.Rev.,14, 36.

[30] Figgis, B.N. and Lewis, J.,1960, "Modern Co-ordination Chemistry", Lewis, J. and Wilkins, R.G., Ed., Interscience, New York, chapter 6.

[31] Ref. 30, p.403.

[32] Figgis, B.N. and Lewis, J., 1964, Prog. In Inorg.Chem., 6,177.

[33] Ref. 18, p.129.

[34] Griffith, J.S., 1961, "The Theory of Transition-Metal Ions", Cambridge University Press, Cambridge, p.202.

[35] Bleaney, B. and Stevens, K.W.H., 1953, Rep.Prog.Phys., 16, 132.

[36] Cotton, F.A., 1963, "Chemical Applications of Group Theory", Interscience, New York, p.285.

[37] Golding, R.M., Mok, K.F. and Duncan, J.F., 1966, Inorg. Chem., 5, 774.

[38] Ref. 34, chapters 8, 9.

[39] Tanabe, Y. and Sugano, S., 1954, J.Phys.Soc.Japan, 9, 753.

[40] Ref. 18, p.163.

[41] Ref. 18, chapter 9.

[42] Ref. 18, p.225.

[43] Ref. 18, p.228.

[44] Ref. 34, p.271.

[45] Ref. 34, Table A24.

[46] Ref. 34, p.238.

[47] Ref. 34, p.19.

[48] Ref. 18, p.60.

[49] Landau, L.D. and Lifshitz, E.M., 1958, "Quantum Mechanics", Permagon, London, chapter 6.

[50] Ref. 34, p.270.

[51] Mok, K.F., 1965, Ph.D. Thesis, Victoria University of Wellington.

[52] Golding, R.M., 1965, International Atomic Energy Agency, Report no. 50, Vienna, p.26.

[53] Ref. 25, chapter 6.

[54] Ref. 25, p.114.

[55] Ref. 25, p.109.

[56] Ref. 25, p.117.

[57] Hoffman, R., 1963, J.Chem.Phys., 31, 1397.

[58] Lowdin, P.O., 1950, J.Chem.Phys., 18, 365.

[59] Lohr, L.L. and Lipscomb, W.N., 1963, J.Chem.Phys., 38, 1607.

[60] Bailey, J.P.M., 1965, M.Sc. Thesis, Victoria University of Wellington, appendix 7.

[61] Ref. 60, appendix 6.

[62] Mulliken, R.S., 1955, J.Chem.Phys., 23, 1833.

[63] Hvoslef, J., 1964, Acta Chem. Scand., 18, 841.

[64] "Tables of Interatomic Distances and Configuration in Molecules and Ions", 1958, Chem. Soc. Special Publication no. 11, Sutton, L.E., Ed., Chemical Society, London.

APPENDIX I

Table 4.1 BASIS WAVE FUNCTIONS FOR CRYSTAL FIELD CALCULATIONS

$\lvert M_L \; M_S \rangle$	complex d orbitals
$\lvert 1 \; 2 \rangle$	$= - \lvert 1^+ -1^2 \xi_1^+ \theta^+ \epsilon^+ \rangle$
$\lvert 1 \; 1 \rangle$	$= -\frac{1}{2} [\lvert 1^- -1^2 \xi_1^+ \theta^+ \epsilon^+ \rangle + \lvert 1^+ -1^2 \xi_1^- \theta^+ \epsilon^+ \rangle + \lvert 1^+ -1^2 \xi_1^+ \theta^- \epsilon^+ \rangle + \lvert 1^+ -1^2 \xi_1^+ \theta^+ \epsilon^- \rangle]$
$\lvert 1 \; 0 \rangle$	$= -\frac{1}{\sqrt{6}} [\lvert 1^- -1^2 \xi_1^- \theta^+ \epsilon^+ \rangle + \lvert 1^- -1^2 \xi_1^+ \theta^- \epsilon^+ \rangle + \lvert 1^- -1^2 \xi_1^+ \theta^+ \epsilon^- \rangle + \lvert 1^+ -1^2 \xi_1^- \theta^- \epsilon^+ \rangle + \lvert 1^+ -1^2 \xi_1^- \theta^+ \epsilon^- \rangle + \lvert 1^+ -1^2 \xi_1^+ \theta^- \epsilon^- \rangle]$
$\lvert 1 \; -1 \rangle$	$= -\frac{1}{2} [\lvert 1^- -1^2 \xi_1^- \theta^- \epsilon^+ \rangle + \lvert 1^- -1^2 \xi_1^- \theta^+ \epsilon^- \rangle + \lvert 1^- -1^2 \xi_1^+ \theta^- \epsilon^- \rangle + \lvert 1^+ -1^2 \xi_1^- \theta^- \epsilon^- \rangle]$
$\lvert 1 \; -2 \rangle$	$= - \lvert 1^- -1^2 \xi_1^- \theta^- \epsilon^- \rangle$
$\lvert 0 \; 2 \rangle$	$= \lvert 1^+ -1^+ \xi_1^2 \theta^+ \epsilon^+ \rangle$
$\lvert 0 \; 1 \rangle$	$= \frac{1}{2} [\lvert 1^- -1^+ \xi_1^2 \theta^+ \epsilon^+ \rangle + \lvert 1^+ -1^- \xi_1^2 \theta^+ \epsilon^+ \rangle + \lvert 1^+ -1^+ \xi_1^2 \theta^- \epsilon^+ \rangle + \lvert 1^+ -1^+ \xi_1^2 \theta^+ \epsilon^- \rangle]$

$$|0\ \ 0\rangle = \frac{1}{\sqrt{6}}\left[|1^{-}-1^{-}\xi_1^{2}\theta^{+}\epsilon^{+}\rangle + |1^{-}-1^{+}\xi_1^{2}\theta^{-}\epsilon^{+}\rangle + |1^{-}-1^{+}\xi_1^{2}\theta^{+}\epsilon^{-}\rangle + |1^{+}-1^{-}\xi_1^{2}\theta^{-}\epsilon^{+}\rangle + |1^{+}-1^{-}\xi_1^{2}\theta^{+}\epsilon^{-}\rangle + |1^{+}-1^{+}\xi_1^{2}\theta^{-}\epsilon^{-}\rangle\right]$$

$$|0\ -1\rangle = \frac{1}{2}\left[|1^{-}-1^{-}\xi_1^{2}\theta^{-}\epsilon^{+}\rangle + |1^{-}-1^{-}\xi_1^{2}\theta^{+}\epsilon^{-}\rangle + |1^{-}-1^{+}\xi_1^{2}\theta^{-}\epsilon^{-}\rangle + |1^{+}-1^{-}\xi_1^{2}\theta^{-}\epsilon^{-}\rangle\right]$$

$$|0\ -2\rangle = |1^{-}-1^{-}\xi_1^{2}\theta^{-}\epsilon^{-}\rangle$$

$$|-1\ \ 2\rangle = -|1^{2}-1^{+}\xi_1^{+}\theta^{+}\epsilon^{+}\rangle$$

$$|-1\ \ 1\rangle = -\frac{1}{2}\left[|1^{2}-1^{-}\xi_1^{+}\theta^{+}\epsilon^{+}\rangle + |1^{2}-1^{+}\xi_1^{-}\theta^{+}\epsilon^{+}\rangle + |1^{2}-1^{+}\xi_1^{+}\theta^{-}\epsilon^{+}\rangle + |1^{2}-1^{+}\xi_1^{+}\theta^{+}\epsilon^{-}\rangle\right]$$

$$|-1\ \ 0\rangle = -\frac{1}{\sqrt{6}}\left[|1^{2}-1^{-}\xi_1^{-}\theta^{+}\epsilon^{+}\rangle + |1^{2}-1^{-}\xi_1^{+}\theta^{-}\epsilon^{+}\rangle + |1^{2}-1^{-}\xi_1^{+}\theta^{+}\epsilon^{-}\rangle + |1^{2}-1^{+}\xi_1^{-}\theta^{-}\epsilon^{+}\rangle + |1^{2}-1^{+}\xi_1^{-}\theta^{+}\epsilon^{-}\rangle + |1^{2}-1^{+}\xi_1^{+}\theta^{-}\epsilon^{-}\rangle\right]$$

$$|-1\ -1\rangle = -\frac{1}{2}\left[|1^{2}-1^{-}\xi_1^{-}\theta^{-}\epsilon^{+}\rangle + |1^{2}-1^{-}\xi_1^{+}\theta^{-}\epsilon^{-}\rangle + |1^{2}-1^{-}\xi_1^{-}\theta^{+}\epsilon^{-}\rangle + |1^{2}-1^{+}\xi_1^{-}\theta^{-}\epsilon^{-}\rangle\right]$$

$$|-1\ -2\rangle = -|1^{2}-1^{-}\xi_1^{-}\theta^{-}\epsilon^{-}\rangle$$

Table 4.2 EIGENSTATES OF SPIN-ORBIT HAMILTONIAN

Eigenvalue H_s	Eigenvalue H'_s	Eigenfunction $\phi_i(J\ M)$
$\zeta/2$	2ν	$\phi_1(3\ \ 3) = \lvert 1\ 2\rangle$
		$\phi_2(3\ \ 2) = \sqrt{\frac{2}{3}}\lvert 1\ 1\rangle + \sqrt{\frac{1}{3}}\lvert 0\ 2\rangle$
		$\phi_3(3\ \ 1) = \sqrt{\frac{2}{5}}\lvert 1\ 0\rangle + \sqrt{\frac{8}{15}}\lvert 0\ 1\rangle + \sqrt{\frac{1}{15}}\lvert -1\ 2\rangle$
		$\phi_4(3\ \ 0) = \sqrt{\frac{1}{5}}\lvert 1\ -1\rangle + \sqrt{\frac{3}{5}}\lvert 0\ 0\rangle + \sqrt{\frac{1}{5}}\lvert -1\ 1\rangle$
		$\phi_5(3\ -1) = \sqrt{\frac{1}{15}}\lvert 1\ -2\rangle + \sqrt{\frac{8}{15}}\lvert 0\ -1\rangle + \sqrt{\frac{2}{5}}\lvert -1\ 0\rangle$
		$\phi_6(3\ -2) = \sqrt{\frac{1}{3}}\lvert 0\ -2\rangle + \sqrt{\frac{2}{3}}\lvert -1\ -1\rangle$
		$\phi_7(3\ -3) = \lvert -1\ -2\rangle$
$-\zeta/4$	$-\nu$	$\phi_8(2\ \ 2) = -\sqrt{\frac{1}{3}}\lvert 1\ 1\rangle + \sqrt{\frac{2}{3}}\lvert 0\ 2\rangle$
		$\phi_9(2\ \ 1) = -\sqrt{\frac{1}{2}}\lvert 1\ 0\rangle + \sqrt{\frac{1}{6}}\lvert 0\ 1\rangle + \sqrt{\frac{1}{3}}\lvert -1\ 2\rangle$
		$\phi_{10}(2\ 0) = -\sqrt{\frac{1}{2}}\lvert 1\ -1\rangle + \sqrt{\frac{1}{2}}\lvert -1\ 1\rangle$
		$\phi_{11}(2\ -1) = -\sqrt{\frac{1}{3}}\lvert 1\ -2\rangle - \sqrt{\frac{1}{6}}\lvert 0\ -1\rangle + \sqrt{\frac{1}{2}}\lvert -1\ 0\rangle$
		$\phi_{12}(2\ -2) = -\sqrt{\frac{2}{3}}\lvert 0\ -2\rangle + \sqrt{\frac{1}{3}}\lvert -1\ -1\rangle$
$-3\zeta/4$	-3ν	$\phi_{13}(1\ \ 1) = \sqrt{\frac{1}{10}}\lvert 1\ 0\rangle - \sqrt{\frac{3}{10}}\lvert 0\ 1\rangle + \sqrt{\frac{3}{5}}\lvert -1\ 2\rangle$
		$\phi_{14}(1\ 0) = \sqrt{\frac{3}{10}}\lvert 1\ -1\rangle - \sqrt{\frac{2}{5}}\lvert 0\ 0\rangle + \sqrt{\frac{3}{10}}\lvert -1\ 1\rangle$
		$\phi_{15}(1\ -1) = \sqrt{\frac{3}{5}}\lvert 1\ -2\rangle - \sqrt{\frac{3}{10}}\lvert 0\ -1\rangle + \sqrt{\frac{1}{10}}\lvert -1\ 0\rangle$

Table 4.3 MATRICES OF SPIN-ORBIT AND DISTORTION INTERACTION

	ϕ_1
ϕ_1	$\frac{1}{2} + x$

	ϕ_7
ϕ_7	$\frac{1}{2} + x$

	ϕ_{10}
ϕ_{10}	$-\frac{1}{4} + x$

	ϕ_2	ϕ_8
ϕ_2	$\frac{1}{2} + \frac{2}{3}x$	$-\frac{\sqrt{2}}{3}x$
ϕ_8	$-\frac{\sqrt{2}}{3}x$	$-\frac{1}{4} + \frac{1}{3}x$

	ϕ_6	ϕ_{12}
ϕ_6	$\frac{1}{2} + \frac{2}{3}x$	$\frac{\sqrt{2}}{3}x$
ϕ_{12}	$\frac{\sqrt{2}}{3}x$	$-\frac{1}{4} + \frac{1}{3}x$

	ϕ_4	ϕ_{14}
ϕ_4	$\frac{1}{2} + \frac{2}{5}x$	$\frac{\sqrt{6}}{5}x$
ϕ_{14}	$\frac{\sqrt{6}}{5}x$	$-\frac{3}{4} + \frac{3}{5}x$

	ϕ_3	ϕ_9	ϕ_{13}
ϕ_3	$\frac{1}{2} + \frac{7}{15}x$	$-\frac{2\sqrt{5}}{15}x$	$\frac{2}{5}x$
ϕ_9	$-\frac{2\sqrt{5}}{15}x$	$-\frac{1}{4} + \frac{5}{6}x$	$-\frac{\sqrt{5}}{10}x$
ϕ_{13}	$\frac{2}{5}x$	$-\frac{\sqrt{5}}{10}x$	$-\frac{3}{4} + \frac{7}{10}x$

	ϕ_5	ϕ_{11}	ϕ_{15}
ϕ_5	$\frac{1}{2} + \frac{7}{15}x$	$\frac{2\sqrt{5}}{15}x$	$\frac{2}{5}x$
ϕ_{11}	$\frac{2\sqrt{5}}{15}x$	$-\frac{1}{4} + \frac{5}{6}x$	$-\frac{\sqrt{5}}{10}x$
ϕ_{15}	$\frac{2}{5}x$	$-\frac{\sqrt{5}}{10}x$	$-\frac{3}{4} + \frac{7}{10}x$

Table 4.4 SPIN-ORBIT AND DISTORTION EIGENFUNCTIONS FOR $\delta/\zeta = 1.5$

Eigenvalue E_i	Eigenfunction ψ_i
2.0	ϕ_1
2.0	ϕ_7
1.81873	$0.911665\ \phi_2 - 0.410934\ \phi_8$
1.81873	$0.911665\ \phi_6 + 0.410934\ \phi_{12}$
1.63087	$0.847484\ \phi_3 - 0.451957\ \phi_9 + 0.266356\ \phi_{13}$
1.63087	$0.847484\ \phi_5 + 0.459157\ \phi_{11} + 0.266356\ \phi_{15}$
1.08170	$0.269578\ \phi_3 + 0.797869\ \phi_9 + 0.543123\ \phi_{13}$
1.08170	$0.261578\ \phi_5 - 0.797869\ \phi_{11} + 0.543123\ \phi_{15}$
-0.06873	$0.410934\ \phi_2 + 0.911665\ \phi_8$
-0.06873	$-0.410934\ \phi_6 + 0.911665\ \phi_{12}$
-0.21257	$0.461896\ \phi_3 + 0.390615\ \phi_9 - 0.796287\ \phi_{13}$
-0.21257	$-0.461896\ \phi_5 + 0.390615\ \phi_{11} + 0.796287\ \phi_{15}$
1.5	$0.878310\ \phi_4 + 0.478091\ \phi_{14}$
1.25	ϕ_{10}
-0.25	$0.478091\ \phi_4 - 0.878310\ \phi_{14}$

Table 4.5 MATRICES OF SPIN-ORBIT AND DISTORTION INTERACTION FOR LARGE DISTORTIONS

	$\|1\ 2\rangle$
$\langle 1\ 2\|$	$\frac{\zeta}{2} + \delta$

	$\|-1\ -2\rangle$
$\langle -1\ -2\|$	$\frac{\zeta}{2} + \delta$

	$\|1\ 1\rangle$	$\|0\ 2\rangle$
$\langle 1\ 1\|$	$\frac{\zeta}{4} + \delta$	$\frac{\sqrt{2}}{4}\zeta$
$\langle 0\ 2\|$	$\frac{\sqrt{2}}{4}\zeta$	0

	$\|-1\ -1\rangle$	$\|0\ -2\rangle$
$\langle -1\ -1\|$	$\frac{\zeta}{4} + \delta$	$\frac{\sqrt{2}}{4}\zeta$
$\langle 0\ -2\|$	$\frac{\sqrt{2}}{4}\zeta$	0

	$\|1\ 0\rangle$	$\|0\ 1\rangle$	$\|-1\ 2\rangle$
$\langle 1\ 0\|$	δ	$\frac{\sqrt{3}}{4}\zeta$	0
$\langle 0\ 1\|$	$\frac{\sqrt{3}}{4}\zeta$	0	$\frac{\sqrt{2}}{4}\zeta$
$\langle -1\ 2\|$	0	$\frac{\sqrt{2}}{4}\zeta$	$-\frac{\zeta}{2} + \delta$

	$\|-1\ 0\rangle$	$\|0\ -1\rangle$	$\|1\ -2\rangle$
$\langle -1\ 0\|$	δ	$\frac{\sqrt{2}}{4}\zeta$	0
$\langle 0\ -1\|$	$\frac{\sqrt{2}}{4}\zeta$	0	$\frac{\sqrt{3}}{4}\zeta$
$\langle 1\ -2\|$	0	$\frac{\sqrt{3}}{4}\zeta$	$-\frac{\zeta}{2}+\delta$

	$\|1\ -1\rangle$	$\|0\ 0\rangle$	$\|-1\ 1\rangle$
$\langle 1\ -1\|$	$-\frac{\zeta}{4}+\delta$	$\frac{\sqrt{3}}{4}\zeta$	0
$\langle 0\ \ 0\|$	$\frac{\sqrt{3}}{4}\zeta$	0	$\frac{\sqrt{3}}{4}\zeta$
$\langle -1\ \ 1\|$	0	$\frac{\sqrt{3}}{4}\zeta$	$-\frac{\zeta}{4}+\delta$

Table 4.6 NON-ZERO MATRIX ELEMENTS OF $H_{//}$

$\langle \phi_1 \mid H_{//} \mid \phi_1 \rangle$	$= -\langle \phi_7 \mid H_{//} \mid \phi_7 \rangle$	$= 3\ \beta H$
$\langle \phi_2 \mid H_{//} \mid \phi_2 \rangle$	$= -\langle \phi_6 \mid H_{//} \mid \phi_6 \rangle$	$= 2\ \beta H$
$\langle \phi_8 \mid H_{//} \mid \phi_8 \rangle$	$= -\langle \phi_{12} \mid H_{//} \mid \phi_{12} \rangle$	$= 3\ \beta H$
$\langle \phi_2 \mid H_{//} \mid \phi_8 \rangle$	$= \langle \phi_6 \mid H_{//} \mid \phi_{12} \rangle$	$= 1.414214\ \beta H$
$\langle \phi_3 \mid H_{//} \mid \phi_3 \rangle$	$= -\langle \phi_5 \mid H_{//} \mid \phi_5 \rangle$	$= \beta H$
$\langle \phi_9 \mid H_{//} \mid \phi_9 \rangle$	$= -\langle \phi_{11} \mid H_{//} \mid \phi_{11} \rangle$	$= 1.5\ \beta H$
$\langle \phi_{13} \mid H_{//} \mid \phi_{13} \rangle$	$= -\langle \phi_{15} \mid H_{//} \mid \phi_{15} \rangle$	$= 3.5\ \beta H$
$\langle \phi_3 \mid H_{//} \mid \phi_9 \rangle$	$= \langle \phi_5 \mid H_{//} \mid \phi_{11} \rangle$	$= 1.788854\ \beta H$
$\langle \phi_9 \mid H_{//} \mid \phi_{13} \rangle$	$= \langle \phi_{11} \mid H_{//} \mid \phi_{15} \rangle$	$= 2.012461\ \beta H$
$\langle \phi_4 \mid H_{//} \mid \phi_{10} \rangle$		$= 1.897367\ \beta H$
$\langle \phi_{10} \mid H_{//} \mid \phi_{14} \rangle$		$= 2.323790\ \beta H$

Table 4.7 NON-ZERO MATRIX ELEMENTS OF $H_\perp$

$\langle \phi_1 \mid H_\perp \mid \phi_2 \rangle$	$= \langle \phi_6 \mid H_\perp \mid \phi_7 \rangle$	$= 1.224745\ \beta H$
$\langle \phi_1 \mid H_\perp \mid \phi_8 \rangle$	$= -\langle \phi_7 \mid H_\perp \mid \phi_{12} \rangle$	$= -1.732051\ \beta H$
$\langle \phi_2 \mid H_\perp \mid \phi_3 \rangle$	$= \langle \phi_5 \mid H_\perp \mid \phi_6 \rangle$	$= 1.581139\ \beta H$
$\langle \phi_2 \mid H_\perp \mid \phi_9 \rangle$	$= -\langle \phi_6 \mid H_\perp \mid \phi_{11} \rangle$	$= -1.414214\ \beta H$
$\langle \phi_3 \mid H_\perp \mid \phi_4 \rangle$	$= \langle \phi_4 \mid H_\perp \mid \phi_5 \rangle$	$= 1.732051\ \beta H$
$\langle \phi_3 \mid H_\perp \mid \phi_8 \rangle$	$= -\langle \phi_5 \mid H_\perp \mid \phi_{12} \rangle$	$= 0.447214\ \beta H$
$\langle \phi_3 \mid H_\perp \mid \phi_{10} \rangle$	$= -\langle \phi_5 \mid H_\perp \mid \phi_{10} \rangle$	$= -1.095445\ \beta H$
$\langle \phi_4 \mid H_\perp \mid \phi_9 \rangle$	$= -\langle \phi_4 \mid H_\perp \mid \phi_{11} \rangle$	$= 0.774597\ \beta H$
$\langle \phi_8 \mid H_\perp \mid \phi_9 \rangle$	$= \langle \phi_{11} \mid H_\perp \mid \phi_{12} \rangle$	$= 1.5\ \beta H$
$\langle \phi_8 \mid H_\perp \mid \phi_{13} \rangle$	$= -\langle \phi_{12} \mid H_\perp \mid \phi_{15} \rangle$	$= -2.012461\ \beta H$
$\langle \phi_9 \mid H_\perp \mid \phi_{10} \rangle$	$= \langle \phi_{10} \mid H_\perp \mid \phi_{11} \rangle$	$= 1.837117\ \beta H$
$\langle \phi_9 \mid H_\perp \mid \phi_{14} \rangle$	$= -\langle \phi_{11} \mid H_\perp \mid \phi_{14} \rangle$	$= -1.423025\ \beta H$
$\langle \phi_{10} \mid H_\perp \mid \phi_{13} \rangle$	$= -\langle \phi_{10} \mid H_\perp \mid \phi_{15} \rangle$	$= 0.821584\ \beta H$
$\langle \phi_{13} \mid H_\perp \mid \phi_{14} \rangle$	$= \langle \phi_{14} \mid H_\perp \mid \phi_{15} \rangle$	$= 2.474874\ \beta H$

Table 4.8 VALUES OF A_i, B_i, C_i, D_i, G_i AS FUNCTIONS OF δ/ζ

	A_i	B_i	C_i	D_i	G_i
$\delta/\zeta = 0.25$					
1	0.75	3.0	0.0	33.99874	-0.5
2	0.68301	1.63398	1.73207	26.95061	-0.18301
3	0.63223	0.62179	5.04120	86.27394	0.11376
4	-0.04186	2.33729	2.34858	-71.23944	-0.25355
5	-0.18301	3.36603	-1.73207	0.38741	0.68301
6	-0.59037	3.04093	-7.38978	29.96779	0.13980
7	0.61237	0.0	7.34850	-276.59459	0.25
8	0.0	0.0	0.00001	154.00855	-0.5
9	-0.61237	0.0	-7.34850	-628.51231	0.25
$\delta/\zeta = 0.5$					
1	1.0	3.0	0.0	25.00037	-0.5
2	0.89039	1.40859	1.02720	13.27614	-0.29571
3	0.79435	0.24581	5.07034	28.31697	-0.05386
4	0.16959	3.11642	0.40234	-39.75422	-0.28764
5	-0.14039	3.59141	-1.02720	12.38890	0.79571
6	-0.46394	2.63777	-5.47268	188.75728	0.34150
7	0.75	0.0	10.80001	-115.40665	0.1
8	0.25	0.0	-6.00001	72.99942	-0.5
9	-0.5	0.0	-4.80000	-413.56364	0.4

$\delta/\zeta = 0.75$

1	1.25	3.0	0.0	21.99964	-0.5
2	1.11237	1.27525	0.61238	9.70835	-0.36237
3	0.98136	0.07062	4.49546	12.26749	-0.18333
4	0.38798	3.71233	-0.98499	-29.12200	-0.33326
5	-0.11237	3.72474	-0.61238	18.95978	0.86237
6	-0.36934	2.35830	-3.51047	160.85161	0.51658
7	0.91144	0.0	15.07108	-69.62838	-0.03347
8	0.5	0.0	-11.99995	45.99887	-0.5
9	-0.41144	0.0	-3.07114	-365.70024	0.53347

$\delta/\zeta = 1.0$

1	1.5	3.0	0.0	20.49999	-0.5
2	1.34307	1.19442	0.37981	8.36535	-0.40279
3	1.18664	0.30941	3.70633	5.88652	-0.27435
4	0.61373	4.11588	-1.57013	-23.83311	-0.37418
5	-0.09307	3.80559	-0.37981	24.46750	0.90279
6	-0.30037	2.19352	-2.13620	154.62291	0.64853
7	1.09307	0.0	19.96690	-50.23399	-0.14167
8	0.75	0.0	-18.00001	32.50119	-0.5
9	-0.34307	0.0	-1.96689	-362.28552	0.64167

$\delta/\zeta = 1.5$

1	2.0	3.0	0.0	19.00007	-0.5
2	1.81873	1.10924	0.16731	7.50189	-0.44538
3	1.63087	0.60165	2.35654	1.34652	-0.37767
4	1.08170	4.54661	-1.52406	-18.94644	-0.42788
5	-0.06873	3.89076	-0.16731	34.83193	0.94538
6	-0.21257	2.05506	-0.83248	165.59292	0.80555
7	1.5	0.0	30.85711	-34.09493	-0.28571
8	1.25	0.0	-29.99997	18.99970	-0.5
9	-0.25	0.0	-0.85714	-403.55853	0.78571

$\delta/\zeta = 2.0$

1	2.5	3.0	0.0	18.25023	-0.5
2	2.30425	1.06900	0.08575	7.30925	-0.46550
3	2.09918	0.75067	1.52692	-0.00956	-0.42651
4	1.56276	4.73647	-1.14793	-16.97647	-0.45551
5	-0.05425	3.93100	-0.08575	45.10863	0.96550
6	-0.16194	2.01421	-0.37899	189.31444	0.88202
7	1.94300	0.0	42.41861	-27.25817	-0.36447
8	1.75	0.0	-42.00008	12.24953	-0.5
9	-0.19300	0.0	0.41853	-470.98441	0.86447

$\delta/\zeta = -0.25$

1	0.25	3.0	0.0	-2.00023	-0.5
2	0.35355	2.5	3.18202	-43.37923	0.25
3	0.39815	1.32305	3.12355	-192.19714	0.47331
4	-0.46027	0.77337	4.21844	55.88082	-0.27711
5	-0.35355	2.5	-3.18202	31.92402	0.25
6	-0.93788	3.91085	-7.34199	-209.99037	-0.19619
7	0.41144	0.0	3.07114	495.80866	0.53347
8	-0.5	0.0	11.99992	-169.99686	-0.5
9	-0.91144	0.0	-15.07106	393.71244	-0.03347

$\delta/\zeta = -0.5$

1	0.0	3.0	0.0	6.99999	-0.5
2	0.25	3.0	2.66667	-30.99824	0.5
3	0.32249	1.54243	2.09422	-139.33298	0.61223
4	-0.67643	0.23681	3.83183	25.17244	-0.31746
5	-0.5	2.00000	-2.66667	21.33331	0.0
6	-1.14606	4.22076	-5.92605	-95.20253	-0.29477
7	0.34307	0.0	1.96690	349.26592	0.64167
8	-0.75	0.0	18.00002	-89.00016	-0.5
9	-1.09307	0.0	-19.96692	163.79025	-0.14167

$\delta/\zeta = -0.75$

1	-0.25	3.0	0.0	10.00007	-0.5
2	0.18301	3.36603	1.73206	-29.61881	0.68301
3	0.26681	1.69162	1.36297	-130.86877	0.71391
4	-0.89931	0.12738	3.19438	15.38949	-0.35614
5	-0.68301	1.63397	-1.73206	16.95303	-0.18301
6	-1.36750	4.43577	-4.55735	-60.51694	-0.35777
7	0.29057	0.0	1.28157	325.81922	0.72434
8	-1.0	0.0	23.99995	-61.99831	-0.5
9	-1.29057	0.0	-25.28152	93.50294	-0.22434

$\delta/\zeta = -1.0$

1	-0.5	3.0	0.0	11.49997	-0.5
2	0.14039	3.59141	1.02721	-31.31678	0.79571
3	0.22545	1.78694	0.89349	-134.43520	0.78552
4	-1.12806	0.36854	2.58085	10.74651	-0.38753
5	-0.89039	1.40859	-1.02721	14.48317	-0.29570
6	-1.59739	4.58161	-3.47434	-44.97807	-0.39799
7	0.25	0.0	0.85714	335.07297	0.78571
8	-1.25	0.0	29.99999	-48.49930	-0.5
9	-0.5	0.0	-30.85714	61.42714	-0.28571

$\delta/\zeta = -1.5$

1	-1.0	3.0	0.0	13.00003	-0.5
2	0.09307	3.80559	0.37981	-38.26256	0.90279
3	0.16989	1.88839	0.41542	-154.85945	0.87138
4	-1.59820	0.63963	1.67699	6.41960	-0.42930
5	-1.34307	1.19442	-0.37981	11.92980	-0.40279
6	-2.07169	4.75125	-2.09242	-31.56864	-0.44208
7	0.19300	0.0	0.41853	388.84979	0.88515
8	-1.75	0.0	42.00011	-34.99918	-0.5
9	-1.94300	0.0	-42.41864	32.83185	-0.36447

$\delta/\zeta = 0.0$

1	0.5	3.0	0.0
2	0.5	2.0	2.66667
3	0.5	1.0	4.26667
4	-0.25	1.5	3.83333
5	-0.25	3.0	-2.66667
6	-0.75	3.5	-8.1
7	0.5	0.0	4.8
8	-0.25	0.0	6.0
9	-0.75	0.0	-10.8

Table 4.9 VALUES OF $\mu_{\parallel}$, $\mu_{\perp}$, μ AND ΔE_Q FOR $\zeta/kT = 2$ AND VARIOUS VALUES OF δ/ζ

δ/ζ	$\mu_{\parallel}$	$\mu_{\perp}$	μ	ΔE_Q
2.0	4.748	5.618	5.343	3.203
1.5	4.818	5.718	5.434	2.803
1.0	4.994	5.786	5.535	2.094
0.75	5.132	5.791	5.580	1.613
0.5	5.295	5.768	5.615	1.074
0.25	5.471	5.717	5.637	0.520
0.0	5.644	5.644	5.644	0.0
-0.25	5.799	5.562	5.642	-0.450
-0.5	5.929	5.463	5.623	-0.812
-0.75	6.034	5.373	5.602	-1.089
-1.0	6.116	5.292	5.580	-1.292
-1.5	6.226	5.158	5.537	-1.541

Table 4.10 AVERAGE MAGNETIC MOMENT μ AS A FUNCTION OF ζ/kT AND δ/ζ

ζ/kT	δ/ζ 2.0	1.5	1.0	0.0	-1.0
6.0	5.293	5.381	5.492	5.640	5.599
5.0	5.299	5.391	5.514	5.687	5.625
4.0	5.308	5.405	5.535	5.720	5.641
3.6	5.313	5.411	5.542	5.725	5.642
3.2	5.318	5.418	5.547	5.722	5.638
3.0	5.322	5.421	5.549	5.718	5.634
2.8	5.326	5.425	5.550	5.710	5.628
2.4	5.334	5.431	5.547	5.685	5.610
2.0	5.345	5.434	5.535	5.644	5.580
1.8	5.348	5.433	5.523	5.615	5.559
1.6	5.352	5.429	5.507	5.581	5.534
1.4	5.353	5.420	5.482	5.541	5.502
1.2	5.350	5.405	5.453	5.495	5.465
1.0	5.341	5.381	5.415	5.442	5.422
0.8	5.320	5.346	5.368	5.384	5.372
0.6	5.286	5.301	5.311	5.320	5.312

Table 4.11 MATRIX ELEMENTS OF QUADRUPOLE HAMILTONIAN WITH RESPECT TO SPIN-ORBIT EIGENFUNCTIONS

$\langle \phi_1 | H_Q | \phi_1 \rangle = \langle \phi_7 | H_Q | \phi_7 \rangle = -0.5\ P'$

$\langle \phi_2 | H_Q | \phi_2 \rangle = \langle \phi_6 | H_Q | \phi_6 \rangle = 0$

$\langle \phi_3 | H_Q | \phi_3 \rangle = \langle \phi_5 | H_Q | \phi_5 \rangle = 0.3\ P'$

$\langle \phi_4 | H_Q | \phi_4 \rangle = 0.4\ P'$

$\langle \phi_8 | H_Q | \phi_8 \rangle = \langle \phi_{12} | H_Q | \phi_{12} \rangle = 0.5\ P'$

$\langle \phi_9 | H_Q | \phi_9 \rangle = \langle \phi_{11} | H_Q | \phi_{11} \rangle = -0.25\ P'$

$\langle \phi_{10} | H_Q | \phi_{10} \rangle = -0.5\ P'$

$\langle \phi_{13} | H_Q | \phi_{13} \rangle = \langle \phi_{15} | H_Q | \phi_{15} \rangle = -0.05\ P'$

$\langle \phi_{14} | H_Q | \phi_{14} \rangle = 0.1\ P'$

$\langle \phi_2 | H_Q | \phi_8 \rangle = -\langle \phi_6 | H_Q | \phi_{12} \rangle = 0.707107\ P'$

$\langle \phi_3 | H_Q | \phi_9 \rangle = -\langle \phi_5 | H_Q | \phi_{11} \rangle = 0.447214\ P'$

$\langle \phi_3 | H_Q | \phi_{13} \rangle = \langle \phi_5 | H_Q | \phi_{15} \rangle = -0.6\ P'$

$\langle \phi_4 | H_Q | \phi_{14} \rangle = -0.734847\ P'$

$\langle \phi_9 | H_Q | \phi_{13} \rangle = -\langle \phi_{11} | H_Q | \phi_{15} \rangle = -0.335410\ P'$

All other matrix elements are zero.

Table 4.12 ΔE_Q AS A FUNCTION OF δ/ζ AND ζ/kT

δ/ζ ζ/kT:	6.0	5.0	4.0	3.0	2.8
2.5	3.454	3.458	3.462	3.462	3.459
2.0	3.321	3.329	3.334	3.324	3.315
1.75	3.215	3.224	3.229	3.224	3.193
1.5	3.063	3.075	3.077	3.036	3.014
1.25	2.843	2.856	2.852	2.784	2.752
1.0	2.520	2.532	2.517	2.421	2.381
0.75	2.055	2.061	2.036	1.925	1.884
0.5	1.431	1.432	1.405	1.310	1.277
0.25	0.703	0.702	0.686	0.637	0.621
0.0	0.0	0.0	0.0	0.0	0.0
-0.25	-0.565	-0.564	-0.556	-0.528	-0.518
-0.5	-0.964	-0.963	-0.955	-0.922	-0.908
-0.75	-1.229	-1.228	-1.222	-1.196	-1.184
-1.0	-1.402	-1.401	-1.398	-1.381	-1.372
-1.5	-1.596	-1.594	-1.593	-1.588	-1.585

δ/ζ ζ/kT:	2.4	2.0	1.8	1.6	1.4
2.5	3.446	3.409	3.370	3.307	3.206
2.0	3.281	3.203	3.134	3.032	2.886
1.75	3.141	3.025	2.947	2.825	2.650
1.5	2.940	2.803	2.698	2.560	2.382
1.25	2.656	2.493	2.376	2.230	2.051
1.0	2.268	2.094	1.977	1.838	1.673
0.75	1.772	1.613	1.511	1.393	1.259
0.5	1.191	1.074	1.001	0.920	0.828
0.25	0.578	0.520	0.485	0.445	0.401
0.0	0.0	0.0	0.0	0.0	0.0
-0.25	-0.490	-0.450	-0.424	-0.394	-0.360

-0.5	-0.871	-0.812	-0.773	-0.726	-0.669
-0.75	-1.149	-1.089	-1.046	-0.992	-0.926
-1.0	-1.344	-1.292	-1.250	-1.200	-1.132
-1.5	-1.571	-1.541	-1.515	-1.476	-1.420

δ/ζ ζ/kT:	1.2	1.0	0.8	0.6	0.2
2.5	3.046	2.801	2.441	1.948	0.656
2.0	2.680	2.399	2.031	1.579	0.520
1.75	2.439	2.153	1.800	1.384	0.452
1.5	2.156	1.880	1.553	1.184	0.385
1.25	1.835	1.582	1.295	0.981	0.319
1.0	1.482	1.267	1.031	0.778	0.254
0.75	1.108	0.943	0.764	0.576	0.189
0.5	0.727	0.617	0.500	0.378	0.125
0.25	0.353	0.300	0.244	0.185	0.062
0.0	0.0	0.0	0.0	0.0	0.0
-0.25	-0.321	-0.277	-0.229	-0.176	-0.061
-0.5	-0.603	-0.527	-0.439	-0.342	-0.121
-0.75	-0.844	-0.746	-0.631	-0.497	-0.180
-1.0	-1.046	-0.937	-0.803	-0.641	-0.237
-1.5	-1.342	-1.233	-1.086	-0.892	-0.345

APPENDIX II

Table 5.1 BASIS PRODUCT FUNCTIONS

F_z	function
2	$\alpha\alpha\alpha\alpha$
1	$\beta\alpha\alpha\alpha$
	$\alpha\beta\alpha\alpha$
	$\alpha\alpha\beta\alpha$
	$\alpha\alpha\alpha\beta$
0	$\beta\beta\alpha\alpha$
	$\beta\alpha\beta\alpha$
	$\beta\alpha\alpha\beta$
	$\alpha\beta\beta\alpha$
	$\alpha\beta\alpha\beta$
	$\alpha\alpha\beta\beta$
-1	$\alpha\beta\beta\beta$
	$\beta\alpha\beta\beta$
	$\beta\beta\alpha\beta$
	$\beta\beta\beta\alpha$
-2	$\beta\beta\beta\beta$

Table 5.2 BASIS SYMMETRY FUNCTIONS

Label	Basis symmetry function
$^{s}_{2}$	$\alpha\alpha\alpha\alpha$
$^{1s}_{1}$	$\alpha\alpha\alpha\beta$
$^{2s}_{1}$	$\frac{1}{\sqrt{2}}[\alpha\alpha\beta\alpha + \alpha\beta\alpha\alpha]$
$^{3s}_{1}$	$\beta\alpha\alpha\alpha$
$^{a}_{1}$	$\frac{1}{\sqrt{2}}[\alpha\alpha\beta\alpha - \alpha\beta\alpha\alpha]$
$^{1s}_{0}$	$\frac{1}{\sqrt{2}}[\alpha\alpha\beta\beta + \alpha\beta\alpha\beta]$
$^{2s}_{0}$	$\frac{1}{\sqrt{2}}[\beta\alpha\beta\alpha + \beta\beta\alpha\alpha]$
$^{3s}_{0}$	$\beta\alpha\alpha\beta$
$^{4s}_{0}$	$\alpha\beta\beta\alpha$
$^{1a}_{0}$	$\frac{1}{\sqrt{2}}[\alpha\alpha\beta\beta - \alpha\beta\alpha\beta]$
$^{2a}_{0}$	$\frac{1}{\sqrt{2}}[\beta\alpha\beta\alpha - \beta\beta\alpha\alpha]$
$^{1s}_{-1}$	$\beta\beta\beta\alpha$
$^{2s}_{-1}$	$\frac{1}{\sqrt{2}}[\beta\beta\alpha\beta + \beta\alpha\beta\beta]$
$^{3s}_{-1}$	$\alpha\beta\beta\beta$
$^{s}_{-2}$	$\beta\beta\beta\beta$
$^{a}_{-1}$	$\frac{1}{\sqrt{2}}[\beta\beta\alpha\beta - \beta\alpha\beta\beta]$

Table 5.3 MATRIX ELEMENTS OF NMR HAMILTONIAN

Diagonal matrix elements

$\langle s_2 | H_N | s_2 \rangle = \frac{1}{2}[\nu_A + 2\nu_B + \nu_C] + \frac{1}{4}[2J_{AB} + J_{BB} + J_{AC} + 2J_{BC}]$

$\langle 1s_1 | H_N | 1s_1 \rangle = \frac{1}{2}[\nu_A + 2\nu_B - \nu_C] + \frac{1}{4}[2J_{AB} + J_{BB} - J_{AC} - 2J_{BC}]$

$\langle 2s_1 | H_N | 2s_1 \rangle = \frac{1}{2}[\nu_A + \nu_C] + \frac{1}{4}[J_{BB} + J_{AC}]$

$\langle 3s_1 | H_N | 3s_1 \rangle = \frac{1}{2}[-\nu_A + 2\nu_B + \nu_C] + \frac{1}{4}[-2J_{AB} + J_{BB} - J_{AC} + 2J_{BC}]$

$\langle 1s_0 | H_N | 1s_0 \rangle = \frac{1}{2}[\nu_A - \nu_C] + \frac{1}{4}[J_{BB} - J_{AC}]$

$\langle 2s_0 | H_N | 2s_0 \rangle = \frac{1}{2}[-\nu_A + \nu_C] + \frac{1}{4}[J_{BB} - J_{AC}]$

$\langle 3s_0 | H_N | 3s_0 \rangle = \frac{1}{2}[-\nu_A + 2\nu_B - \nu_C] + \frac{1}{4}[-2J_{AB} + J_{BB} + J_{AC} - 2J_{BC}]$

$\langle 4s_0 | H_N | 4s_0 \rangle = \frac{1}{2}[\nu_A - 2\nu_B + \nu_C] + \frac{1}{4}[2J_{AB} + J_{BB} + J_{AC} - 2J_{BC}]$

$\langle 1s_{-1} | H_N | 1s_{-1} \rangle = \frac{1}{2}[-\nu_A - 2\nu_B + \nu_C] + \frac{1}{4}[2J_{AB} + J_{BB} - J_{AC} - 2J_{BC}]$

$\langle 2s_{-1} | H_N | 2s_{-1} \rangle = \frac{1}{2}[-\nu_A - \nu_C] + \frac{1}{4}[J_{BB} + J_{AC}]$

$\langle 3s_{-1} | H_N | 3s_{-1} \rangle = \frac{1}{2}[\nu_A - 2\nu_B - \nu_C] + \frac{1}{4}[-2J_{AB} + J_{BB} - J_{AC} + J_{BC}]$

$\langle s_{-2} | H_N | s_{-2} \rangle = \frac{1}{2}[-\nu_A - 2\nu_B - \nu_C] + \frac{1}{4}[2J_{AB} + J_{BB} + J_{AC} + 2J_{BC}]$

$\langle a_1 | H_N | a_1 \rangle = \frac{1}{2}[\nu_A + \nu_C] + \frac{1}{4}[-3J_{BB} + J_{AC}]$

$\langle 1a_0 | H_N | 1a_0 \rangle = \frac{1}{2}[\nu_A - \nu_C] + \frac{1}{4}[-3J_{BB} - J_{AC}]$

$\langle 2a_0 | H_N | 2a_0 \rangle = \frac{1}{2}[-\nu_A + \nu_C] + \frac{1}{4}[-3J_{BB} - J_{AC}]$

$\langle a_{-1} | H_N | a_{-1} \rangle = \frac{1}{2}[-\nu_A - \nu_C] + \frac{1}{4}[-3J_{BB} + J_{AC}]$

Off-diagonal matrix elements

$$\langle 1s_1|H_N|2s_1\rangle = \langle 1s_{-1}|H_N|2s_{-1}\rangle = J_{BC}/\sqrt{2}$$

$$\langle 2s_1|H_N|3s_1\rangle = \langle 2s_{-1}|H_N|3s_{-1}\rangle = J_{AB}/\sqrt{2}$$

$$\langle 3s_1|H_N|1s_1\rangle = \langle 3s_{-1}|H_N|1s_{-1}\rangle = J_{AC}/2$$

$$\langle 1s_0|H_N|2s_0\rangle = \langle 1a_0|H_N|2a_0\rangle = J_{AC}/2$$

$$\langle 1s_0|H_N|3s_0\rangle = \langle 2s_0|H_N|4s_0\rangle = J_{AB}/\sqrt{2}$$

$$\langle 1s_0|H_N|4s_0\rangle = \langle 2s_0|H_N|3s_0\rangle = J_{BC}/\sqrt{2}$$

All other matrix elements are zero.

Table 5.4 2x2 MATRICES OF NMR HAMILTONIAN

	$2s_1$	$3s_1$
$2s_1$	$\frac{1}{2}[\nu_A+\nu_X]+\frac{1}{4}[J_{BB}+J_{AX}]$	$J_{AB}/\sqrt{2}$
$3s_1$	$J_{AB}/\sqrt{2}$	$\frac{1}{2}[-\nu_A+2\nu_B+\nu_X]+\frac{1}{4}[-2J_{AB}+J_{BB}-J_{AX}-2J_{BX}]$

	$1s_0$	$3s_0$
$1s_0$	$\frac{1}{2}[\nu_A-\nu_X]+\frac{1}{4}[J_{BB}-J_{AX}]$	$J_{AB}/\sqrt{2}$
$3s_0$	$J_{AB}/\sqrt{2}$	$\frac{1}{2}[-\nu_A+2\nu_B-\nu_X]+\frac{1}{4}[-2J_{AB}+J_{BB}+J_{AX}-2J_{BX}]$

	$2s_0$	$4s_0$
$2s_0$	$\frac{1}{2}[-\nu_A+\nu_X]+\frac{1}{4}[J_{BB}-J_{AX}]$	$J_{AB}/\sqrt{2}$
$4s_0$	$J_{AB}/\sqrt{2}$	$\frac{1}{2}[\nu_A-2\nu_B+\nu_X]+\frac{1}{4}[-2J_{AB}+J_{BB}+J_{AX}-2J_{BX}]$

	$2s_{-1}$	$3s_{-1}$
$2s_{-1}$	$\frac{1}{2}[-\nu_A-\nu_X]+\frac{1}{4}[J_{BB}+J_{AX}]$	$J_{AB}/\sqrt{2}$
$3s_{-1}$	$J_{AB}/\sqrt{2}$	$\frac{1}{2}[\nu_A-2\nu_B-\nu_X]+\frac{1}{4}[-2J_{AB}+J_{BB}-J_{AX}+2J_{BX}]$

Table 5.5 EIGENSTATES OF AB_2X SYSTEM FOR PARAMETER VALUES $\nu_A = 15, \nu_B = 0, \nu_X = 70, J_{AB} = 6, J_{BB} = 0, J_{AX} = 2, J_{BX} = 0$

	Eigenvalue		Eigenfunction
E_{s_2}	47.50	s_2	s_2
E_{1s_1}	-23.50	$1s_1$	$1s_1$
E_{2s_1}	45.40	$2s_1$	$0.97803\ 2s_1 + 0.20847\ 3s_1$
E_{3s_1}	24.60	$3s_1$	$-0.20847\ 2s_1 + 0.97803\ 3s_1$
E_{1s_0}	-25.50	$1s_0$	$0.97333\ 1s_0 + 0.22942\ 3s_0$
E_{2s_0}	-27.24	$2s_0$	$0.95849\ 2s_0 - 0.28513\ 4s_0$
E_{3s_0}	-44.50	$3s_0$	$-0.22942\ 1s_0 + 0.97333\ 3s_0$
E_{4s_0}	42.76	$4s_0$	$0.28513\ 2s_0 + 0.95849\ 4s_0$
$E_{1s_{-1}}$	31.50	$1s_{-1}$	$1s_{-1}$
$E_{2s_{-1}}$	-41.95	$2s_{-1}$	$0.94652\ 2s_{-1} - 0.32265\ 3s_{-1}$
$E_{3s_{-1}}$	-28.05	$3s_{-1}$	$0.32265\ 2s_{-1} + 0.94652\ 3s_{-1}$
$E_{s_{-2}}$	-37.50	s_{-2}	s_{-2}
E_{a_1}	38.50	a_1	a_1
E_{1a_0}	-32.50	$1a_0$	$1a_0$
E_{2a_0}	22.50	$2a_0$	$2a_0$
$E_{a_{-1}}$	-46.50	a_{-1}	a_{-1}

Table 5.6 MATRIX ELEMENTS OF I_x BETWEEN BASIS SYMMETRY FUNCTIONS

Matrix elements with value 1/2 :

$\langle 1s_1 | I_x | s_2 \rangle$ $\langle 3s_1 | I_x | s_2 \rangle$ $\langle 3s_0 | I_x | 1s_1 \rangle$

$\langle 1s_0 | I_x | 2s_1 \rangle$ $\langle 2s_0 | I_x | 2s_1 \rangle$ $\langle 3s_0 | I_x | 3s_1 \rangle$

$\langle 2s_{-1} | I_x | 1s_0 \rangle$ $\langle 2s_{-1} | I_x | 2s_0 \rangle$ $\langle 1s_{-1} | I_x | 4s_0 \rangle$

$\langle 3s_{-1} | I_x | 4s_0 \rangle$ $\langle s_{-2} | I_x | 1s_{-1} \rangle$ $\langle 1a_0 | I_x | a_1 \rangle$

$\langle 2a_0 | I_x | a_1 \rangle$

Matrix elements with value $1/\sqrt{2}$:

$\langle 2s_1 | I_x | s_2 \rangle$ $\langle 1s_0 | I_x | 1s_1 \rangle$ $\langle 4s_0 | I_x | 2s_1 \rangle$

$\langle 2s_0 | I_x | 3s_1 \rangle$ $\langle 3s_{-1} | I_x | 1s_0 \rangle$ $\langle 1s_{-1} | I_x | 2s_0 \rangle$

$\langle 2s_{-1} | I_x | 3s_0 \rangle$ $\langle s_{-2} | I_x | 2s_{-1} \rangle$

Matrix elements with value -1/2 :

$\langle a_{-1} | I_x | 1a_0 \rangle$ $\langle a_{-1} | I_x | 2a_0 \rangle$

All other matrix elements are zero.